The Mechanisms of the Fuel Cell Oxygen Reduction Reaction on Pt and Other 8–11 Column Metal Surfaces

Thesis by

Yao Sha

In Partial Fulfillment of the Requirements

For the Degree of

Doctor of Philosophy

CALIFORNIA INSTITUTE OF TECHNOLOGY

Pasadena, California

April 2011

Defended April 22nd, 2011

Acknowledgements

I owe my deepest gratitude to my advisor Professor William A Goddard III for his guidance throughout my six years here at Caltech. He has been supportive in showing me the way to do theoretical research gracefully and effectively. I learned from him how to choose a promising approach to tackle my research projects and how to generalize solid and useful implications that matter to the understanding of the science behind the subject. His enthusiasm and immense knowledge make the PhD study an enjoyable and stimulating experience.

I would like to thank my other committee members—Professor Aron Kuppermann, Professor Jack Beauchamp, and Professor Sosinna Haile—for advice. It is a great honor to have such a group of brilliant scientists on my committee. I appreciate their comments and advice on my exams.

I would like to acknowledge my colleges at the Materials and Process Simulation Center for the discussions and help that made this thesis possible. Dr Boris Merinov has been a great manager in keeping my research on the right track. I appreciate Ted Yu for the valuable time we spend together in all the beneficial discussions about fuel cells. De Yuki Matsuda taught me how to carry out density functional theory calculations on periodic systems and made it possible for me to get a good start on my research. Many thanks to Mu-jeng Cheng, Adri van Duin, Seung Soon Jiang, Julius Su, Dan Fisher, Amos Anderson, and many other members for the help on my research projects.

Thanks for Dr. Peter A. Schultz at Sandia National Laboratories for the instant responses whenever I had problems with the calculations. Thanks for my collaborators Debbie Myers at Argonne National Laboratory, John R. Regalbuto at University of Illinois-Chicago, Clemens Heske at University of Nevada-Las Vegas, Karren More at Oak Ridge National Laboratory, and Piotr Zelenay at Los Alamos National Laboratory for the discussions and help.

Last but not least, I would like to thank my family and friends. I would like to thank my parents and my wife for their love and support in my down times. Many thanks to Tao Liu, Bolin Lin, and Jigang Wu for helping me get accustomed to the life here at Caltech. My life here would be a lot more difficult without your help. Thanks to Mulin Cheng, Yuebin Liu, and Yan Xia for the fun we had together. Thanks to Jiaqi Jin, Yizhou Liu and Jie Cheng for giving me inspiration and support to keep improving myself. Thanks to Tong Chen, Jinghao Huang, Xin Hu, and all my other friends here for making my six years here a joyful experience.

Abstract

To better understand and improve the cathode process for low-temperature (85°C) hydrogen fuel cells, we have used quantum mechanical (QM) calculations aimed at discovering the mechanism of oxygen reduction reaction on group 8–11 metals and their alloys. Our first principles QM used the PBE flavor of density functional theory (DFT) to study the binding site preference, unit reaction pathways, and overall mechanisms on the closest packed surface of various metal surfaces.

In order to describe the reaction kinetics in aqueous solution we developed a practical implicit solvation model based on the Poisson-Boltzmann equation. We also carried out the QM calculations for a vacuum, which we consider approximates the situation in which the O_2 accesses the Pt surface through the Teflon part of the Nafion membrane. We find that without solvation, Pd would have better performance than Pt, but Pt is a much better catalyst for solvation. With solvation, direct formation of OH_{ad} from O_{ad} and H_{ad} becomes prohibitive on Pt surface. In addition to the two previously discussed ORR mechanisms, we discovered three novel mechanisms that could be important for ORR under various conditions, especially in solvent.

Particularly important is that that hydrolysis of O_{ad} by H_2O_{ad} to form two OH_{ad} is much more favorable than the direct process, $O_{ad} + H_{ad} \rightarrow OH_{ad}$, for Pt and other metals.

We showed that without solvation, the dissociation of O_2 into adsorbed atoms on Pt goes through a mechanism in which H_{ad} reacts with O_{2ad} to form OOH_{ad}, which subsequently decomposes to form O_{ad} and OH_{ad}. However in solvent, the direct dissociation of O_{2ad} into $O_{ad} + O_{ad}$ becomes the dominant mechanism.

We also developed a method to determine how the electron transfer affects the barrier for $(H_3O)^+$ to react with surface species. These calculations show that H_3O^+ attack on O_{ad} does not compete with O_{ad} hydration for Pt.

Using the same approach we studied the ORR on eleven metals in 8–11 column including Pt, Pd, Co, Ni, Au, Ag, Cu, Os, Ir, Ru, and Rh (Fe was excluded because the bulk phase is ferromagnetic BCC). We examined binding site preferences, reaction barriers, and the preferred ORR mechanisms. We showed that for all the metals except for Au and Pt, H_2O formation via $OH_{ad} + H_{ad}$ is the step with highest barrier and hence is the RDS. For Au the major problem is weak binding Oad leading to a high barrier for dissociating O_2. Among these eleven metals, only Au, Ir, Os, Pd, and Pt have a H_2O formation barrier lower than 0.80eV. This suggests two approaches for improved ORR catalyst: one possible solution is to combine a metal with strong OH binding with another with weaker OH binding to shift the OH binding energy to a better range. Another approach is to develop systems that lead to an inhomogeneous catalyst on which different ORR steps can occur on different metals. This might be possible since OH generally has large mobility.

We also studied the ORR on Pt_3Ni alloy surface at the atomic level and found for the first time that the sublayer Ni dramatically changed the property surface. The (111) surface becomes inhomogeneous and leads to a coverage dependence in binding energies, reaction barriers, and mechanisms. We find that the Pt_3Ni alloy is less active than pure Pt at low coverage. At steady state we expect higher coverage, where we find that Pt_3Ni becomes a better catalyst than Pt, as observed in experiments.

We also demonstrated a general way for handling new alloying system. Taking the Pd-Cu system as an example, we studied the structural preference of the PdCu alloy at various atomic concentrations. We found that for the 1:1 PdCu alloy, the B_2 (CsCl type) structure is preferred to FCC types, as known experimentally. We then developed an approach to predict the preferred surface for an alloy by calculating the surface energy. We found that the (110) surface is the most stable surface for the B_2 phase of PdCu alloy. We then studied the ORR property for five possible surfaces that the PdCu alloy could possess. We found out that the layered $L1_1$ variation of FCC leads to a surface showing the best performance in catalyzing ORR among the five surfaces studied. This implies that one should try to maximize layered $L1_1$ surface in PdCu alloy catalyst. This agrees with the experimental observations that acid and heat treatment gives the best catalyst.

Table of Contents

Acknowledgements iii

Abstract v

Table of Contents viii

List of Tables xii

List of Figures xiv

Abbreviations xviii

Chapter 1 Overview 1

Chapter 2 Theoretical Study of Solvent Effects on the Platinum Catalyzed Oxygen Reduction Reaction 3

- Abstract 3
- Introduction 3
- Methodology 5
- Results and Discussion 7
- Conclusion 12
- Tables and Figures 14

Chapter 3 The Oxygen Hydration Mechanism for the Oxygen Reduction Reaction at Pt and Pd Fuel Cell Catalysts 18

- Abstract 18
- Introduction 19
- Methodology 20
- Results and Discussion 21

Conclusion 27

Tables and Figures 28

Chapter 4 Prediction of Optimum Operating Voltage for the Fuel Cell Oxygen Reduction Reaction from DFT Calculations 31

Abstract 31

Introduction 31

Methodology 33

Results and Discussion 35

Conclusion 42

Tables and Figures 44

Chapter 5 Density Functional Studies of the Fuel Cell Oxygen Reduction Reaction on Co and Ni Surfaces 51

Abstract 51

Introduction 51

Methodology 52

Results and Discussion 53

Conclusion 61

Tables and Figures 62

Chapter 6 Density Functional Studies on Oxygen Reduction Reaction on Cu, Ag, and Au Surfaces 65

Abstract 65

Introduction 65

Methodology 66

Results and Discussion 67

Conclusion 74

Tables and Figures 75

Chapter 7 Density Functional Studies on Oxygen Reduction Reaction on Pd, Rh, and Ru Surfaces 78

Abstract 78

Introduction 78

Methodology 79

Results and Discussion 80

Conclusion 86

Tables and Figures 87

Chapter 8 Density Functional Studies of the Fuel Cell Oxygen Reduction Reaction on Os and Ir Surfaces 90

Abstract 90

Introduction 90

Methodology 91

Results and Discussion 92

Conclusion 97

Tables and Figures 99

Chapter 9 Mechanism for the Oxygen Reduction Reaction on Pt_3Ni Alloy Fuel Cell Cathodes 102

Abstract 102

Introduction 102

Methodology 103

Results and Discussion 104

Conclusion 114

Tables and Figures 115

Chapter 10 Predictions of the Oxygen Reduction Reaction on Copper-Palladium Alloys 123

Abstract 123

Introduction 123

Methodology 124

Results and Discussion 125

Conclusion 132

Tables and Figures 134

References 143

List of Tables

Table 2-1. Binding energies without solvent (E_{bind}), slab charge (Q_{slab}), solvation energy (E_{solv}), and binding energy with solvation (E_{bind}^{solv}) for all intermediates. E_{bind} is calculated as $E_{Slab\text{-}adsorbate}$-$E_{Slab}$-$E_{adsorbate}$. Q_{slab}(e) is the net charge of the slab. E_{solv}(eV) is the solvation energy calculated using the continuum model. E_{bind}^{solv} (eV) is the sum of E_{bind} and E_{bind}^{solv} (eV). Both OOH configurations are atop sites. The only difference is the orientation of OOH. 15

Table 2-2. Reaction barriers without solvent (E_a) and in water-solvated phase (E_a^{solv}) for five steps involved in the O_2-dissociation and OOH-association pathways. 15

Table 3-1. Enthalpies and barriers (eV) for steps possibly important for ORR on Pt 28

Table 3-2. Enthalpies and barriers (eV) for steps possibly important for ORR on Pd 29

Table 5-1. Binding energies (eV) of various ORR species on Pt, Co, and Ni 63

Table 5-2. Reaction barriers for various steps involved in ORR 63

Table 5-3. Overall barriers for each step 64

Table 6-1. Binding energy for Ir and Os as compared with Pt, both with and without solvent. 76

Table 6-2. Reaction barriers for various steps involved in ORR. 76

Table 6-3. Overall barriers for each step. 77

Table 7-1. Binding energy for Ir and Os as compared with Pt, both with and without solvent 88

Table 7-2. Reaction barriers for various steps involved in ORR 88

Table 7-3. Overall barriers for each step 89

Table 8-1. Binding energy for Ir and Os as compared with Pt, both with and without solvent effect 100

Table 8-2. Reaction barriers for various steps involved in ORR 100

Table 8-3. Overall barriers for each step 101

Table 9-1. Binding energies of various species on various sites on Pt_3Ni and Pt without solvation 116

Table 9-2. Binding energies of various species on various sites on Pt_3Ni and Pt with solvation 117

Table 9-3. Reaction barriers for Pt_3Ni in gas phase 117

Table 9-4. Reaction barriers on Pt_3Ni with solvation 118

Table 10-1. Calculated lattice parameter as compared to experimental value 134

Table 10-2. Six most table surfaces of B2 PdCu 135

Table 10-3. Binding energies for the intermediates involved in ORR on Pt, Pd, Cu, and PdCu alloys 137

Table 10-4. Binding energies for intermediates involved in ORR on Pt, Pd, Cu, and PdCu alloys with solvent effect 138

Table 10-5. Barriers for the reaction steps involved in ORR without solvation..... 138

Table 10-6. Barriers for the reaction steps involved in ORR with solvation..... 139

List of Figures

Figure 2-1. The super slab used to calculate the solvent effect. Only the center cell has adsorbate attached. All cells surrounding the center cell contain neutral platinum atoms. Three additional layers of platinum are added to the bulk side to eliminate extraneous solvent effects. 16

Figure 2-2. Important binding sites on the closest packed Pt (111) surface 16

Figure 2-3. Potential energy surface of the O_2-dissociation mechanism without and with water solvent 17

Figure 2-4. Potential energy surface of the OOH-association mechanism without and with water solvent 17

Figure 3-1. Illustration of the sulfonic acid lined hydrophilic water channels and hydrophobic (Teflon-like) regions in Nafion (from references 64-65) showing the likely locations of the O_{2g} ➔ $2O_{ad}$, $O_{ad} + H_2O_{ad}$ ➔ $2OH_{ad}$, and $OH_{ad} + H_{ad}$ ➔ H_2O_{ad} steps in the hydrophobic channels, but H^+ ➔ H_{ad} at the boundary with the water phase. For the gas phase process we assume that the proton is chemisorbed on the surface, H_{ad}. For Pt in water at pH = 1 (typical for a fuel cell), this occurs at a potential of -0.06 eV (relative to the Standard Hydrogen Electrode [SHE]) 30

Figure 3-2. Potential energy surface (eV) for the O_{ad} hydration step of ORR. 30

Figure 4-1. Reaction path for $O_{ad} + H^+ + e$ ➔ OH_{ad} in which the electrode potential is kept fixed. The bright green line shows the optimal path. 44

Figure 4-2. Contour plot for the energy surface for the reaction $O_{ad} + H^+ + e \rightarrow OH_{ad}$ in which charge and OH formation are considered as two independent coordinates. The green curve gives an optimal reaction path at +1.0 electrode potential. 45

Figure 4-3. The optimal reaction PES at electrode potential of +1.0V versus NHE where at each point the charge is indicated 45

Figure 4-4. Optimal PES of $H^+ + O_{ad} \rightarrow OH_{ad}$ for various electrode potentials. Each line in this plot represents the "green" line selected from Figure 4-1, Figure 4-2, and Figure 4-3. In the NHE line, the reaction starts with H_{ad} because that is below the reversible potential of $H^+ \Leftrightarrow$Had and hence H_{ad} is the preferred form (see the corresponding section for details). For simplicity, here we show only the three typical cases and an imaginary line supposing reaction from H^+. 46

Figure 4-5. Potential dependent barrier for $H^+ + O_{ad} \rightarrow OH_{ad}$. Each point in the barrier line represents the TS point (highest energy point in Figure 4-4), while each point in the enthalpy curve represents the difference between the starting and ending point in Figure 4-4. 47

Figure 4-6. Barriers of reaction (1)–(4), the four steps involved in the ORR. In general, all barriers increase as electrode potential increases. OH formation dominates the ORR reaction. 48

Figure 4-7. Potential dependent PES for $H^+ \rightarrow H_{ad}$ 48

Figure 4-8. Potential dependent barriers for $H^+ \rightarrow H_{ad}$ 49

Figure 4-9. Potential dependent PES for H_2O formation 49

Figure 4-10. Potential dependent barrier for H_2O formation 50

Figure 4-11. The power output as a function of the electrode potential. Here we also consider the impact of small changes in the energetics. 50

Figure 5-1. Binding sites on FCC closed packing surface (111 surface)..... 64

Figure 6-1. Steps involved in ORR..... 77

Figure 7-1. Steps involved in ORR..... 89

Figure 8-1. Steps involved in ORR..... 101

Figure 9-1. Binding sites on Pt_3Ni surface. The blue and orange stripes indicate the partitioning of the Pt surface into two regions induced by the sublayer Ni. The O_2, O, H, OH, and OOH species prefer to move only within the blue stripes..... 119

Figure 9-2. Illustration of various binding sites on Pt_3Ni surface. For top sites t_1 and t_2, the triangle indicates the sublayer atoms. t_1 has one Ni atom beneath it, while t_2 has two. For bridge sites, the bridge itself is shown as the thick black line while the two termini of the black line connect the two surface atoms forming the bridge site. The trapezoid beneath are sublayer atoms. b_0-b_3 has 0-3 Ni atoms in this sublayer. An fcc site is in the center of a surface triangle (shown as solid triangle). f_1 and f_2 differ in the sublayer triangle beneath the surface triangle. f_1 has one Ni beneath it while f_2 has two. hcp sites are also in the center of a surface triangle. hcp sites have one sublayer atom beneath it. For h_1 it is Ni, while for h_2 it is Pt..... 120

Figure 9-3. Potential energy surface, including barriers, for the OOH-form-hydr mechanism preferred for both Pt and Pt_3Ni in gas phase..... 121

Figure 9-4. Potential energy surface, including barriers, for the O_2-diss-hydr mechanism preferred by both Pt_3Ni and Pt in solution. The purple line shows the alternative mechanism at higher coverage..... 122

Figure 10-1. Phase diagram of PdCu system. Three unique phases exists in the diagram. A bcc type phase at around 45% atomic ratio, an FCC type Cu_3Pd ($AuCu_3$ structure), and a FCC-type solid solution phase. (From ASM[115]) 140

Figure 10-2. Four type of bulk structures considered in this research. (Images taken from http://en.wikipedia.org/)..... 141

Figure 10-3. Mass activity of Pt, Pd, and Pd-Cu alloy catalysts. This shows that the 1:1 PdCu catalyst has a performance about half as good as Pt, and over twice as good as Pd. Based on the results of Deborah J. Myers, etc.[107] 142

Abbreviations

BE. Binding energies

DFT. Density functional theory

FCC. Face center cubic

GGA. Generalized gradient approximation

HCP. Hexagonal centered cubic

HER. Hydrogen evolution reaction

HOR. Hydrogen oxidation reaction

ORR. Oxygen reduction reaction, $O_2 + 4H^+ \rightarrow 2H_2O$; the cathode process in a hydrogen fuel cell

PBE. Density functional developed by Perdew, Becke, and Ernzerhof

PEMFC. Proton exchange membrane fuel cell; fuel cell that uses proton exchange membrane as separator

RDS. Rate determining step

Chapter 1 Overview

Oxygen reduction reaction (ORR) is one of the key steps in proton exchange membrane fuel cells (PEMFC). The slow kinetics and the expensive Pt-based catalysts have become a major obstacle towards more extensive usage of PEMFC for households and automobiles. Great efforts have been made to develop new materials as ORR catalysts, but few materials have reached the requirement of high economical feasibility, high discharging efficiency, and long life. Compared with the enormous experimental research, theoretical modeling for the ORR is rather limited in both range and extent. Here in this study, we examined the mechanisms of ORR on various surfaces using first principle calculations.

We systematically demonstrated way to study ORR using density-functional-theory (DFT)-based methods. We developed an implicit solvation model based on the Poisson-Boltzmann equation to correctly access the solvent effect essential for the understanding of ORR at fuel cell condition, and showed that the aqueous environment changed dramatically the energetics and the preferred mechanisms. See Chapter 2 for details of the methods and disquisitions about the importance of solvation.

In addition to the traditional mechanisms of ORR for Pt surface, we found three alternative mechanisms that could play an important role at different conditions. These three mechanisms, along with the two well-known ones, form a generic reaction network for ORR on all kinds of metal surfaces. See Chapter 3 for the discussions about the implications of the alternative reaction pathways.

H^+ may be directly involved in the ORR as a direct reactant on metal surfaces; hence we developed a reliable way to model the electron transfer between the metal surface and the anions in solution. With this approach we were able to calculate for the first time the electrode-potential-dependent barrier on a semi-infinite surface. We showed that H+ played a minor role in ORR on Pt surface. See Chapter 4 for details.

We then applied the same methods to various 8–11 column metal surfaces and studied the optimal ORR pathway. We showed the factor that limits each metal from becoming a good ORR catalyst and pointed out possible ways of improving the performance. See Chapter 5, Chapter 6, Chapter 7, and Chapter 8 for details.

Pt_3Ni and Pt_3Co alloys have shown better performance than pure Pt. Research so far attributes the improved activity to a change in band structure. We, however, examined the influence of a second metal at the atomic level. The result showed that the second metal in sublayer could bring inhomogeneity to the surface and make the reaction coverage dependent. Chapter 9 discusses Pt_3Ni as an example.

In Chapter 10, we discuss in general how to handle an unknown alloy. Taking PdCu alloy as an example, we showed how one can predict the preferred phase, surface, and ORR activity using DFT calculations.

Chapter 2 Theoretical Study of Solvent Effects on the Platinum Catalyzed Oxygen Reduction Reaction

Abstract

We report here density functional theory (DFT) studies (PBE) of the reaction intermediates and barriers involved in the oxygen reduction reaction (ORR) on a platinum fuel cell catalyst. Solvent effects were taken into account by applying continuum Poisson-Boltzmann theory to the bound adsorbates and to the transition states of the various reactions on the platinum (111) surface. Our calculations show that the solvent effects change the reaction barriers significantly compared with those in the gas phase environment (without solvation). The O_2 dissociation barrier decreases from 0.58 eV to 0.27 eV, whereas the H + O ➔ OH formation barrier increases from 0.73 eV to 1.09 eV. In the water-solvated phase, OH formation becomes the rate-determining step for both ORR mechanisms, O_2-dissociation, and OOH-association, proposed earlier for the gas phase environment. Both mechanisms become significantly less favorable for the platinum catalytic surface in water solvent, suggesting that alternative mechanisms must be considered to describe properly the ORR on the platinum surface.

Introduction

Polymer electrolyte membrane fuel cells (PEMFCs) have tremendous potential for addressing the world's energy needs but are limited by the efficiency of the cathode catalyst for the oxygen reduction reaction (ORR)[1–4]. Currently, the best catalyst is

platinum but it is too expensive and not sufficiently efficient. Many efforts are underway to find replacements or improvements by using different supports, platinum alloys, or non-platinum catalysts[5–9]. Despite these efforts there remain uncertainties concerning the fundamental reaction mechanism underlying ORR.

Numerous experimental and theoretical studies have been carried out to study the kinetics of ORR mechanisms[10–17]. Most published theoretical studies simplify the ORR as a reaction in a gas phase environment, leading to good agreement with the high vacuum surface experiments on hydrogen oxidation reactions. However, fuel cell operation involves also a solvent environment, and there is not yet a validated efficient method to estimate the contributions of water solvent to the key steps in the reaction mechanisms.

One approach to estimating the solvent effect is to add explicit water molecules[11,18] (~ 4 per unit cell) or even an entire water bilayer[16–17,19]. These explicit solvent model approaches lead to plausible results, but the optimum structure for a few waters or a bilayer may not resemble that of the fully solvated system[20], leading to questions of how to describe the relaxation around the adsorbed species. Moreover this leads to the possible direct participation of water in the reactions[21–22]. In addition, the periodicity in the solvent structure imposed by the periodic boundary conditions may introduce artificial ordering. Also, without well-justified initial and final configurations, it is difficult to identify the correct solvent structures for transition states to obtain the barriers that determine the reaction rates.

Here, we propose an alternative approach of using the fast but accurate Poisson-Boltzmann implicit continuum model to estimate solvent effects[23–25]. This approach has been applied widely in cluster studies where it has led to quite accurate results for many

systems[26–28]. The contributions of solvent and ions are considered through their electrostatic interactions with the solutes. The use of a continuum solvent environment leads to a consistent model for estimating the contribution of the solvent all along the reaction surface. Details of our approach are given below.

Methodology

The active Pt (111) surface was modeled using a metal slab that is infinitely periodic along two dimensions but finite along the third one. We used a 2 × 2 hexagonal unit cell with four metal atoms per layer and six layers in total to model the catalyst. The slab calculations were performed with the Seqquest DFT code[29] using the Perdew-Becke-Ernzerhof (PBE)[30] exchange-correlation functional of the generalized gradient approximation (GGA) [31–32]. Seqquest uses local Gaussian-type basis functions (double zeta plus polarization quality, optimized for bulk systems) rather than periodic plane waves. In Seqquest the Kohn-Sham equations[33] are solved self-consistently using two-dimensional periodic conditions. The 62 core electrons (Kr[$5s^2 4d^{10} 4f^{14}$]) of platinum are replaced with an angular momentum projected[34–35], norm-conserving[36–37], effective core potential (ECP) so that only 16 electrons are considered explicitly. The real space grid density is 7 points/Å.

All calculations were performed with the optimized cell parameter of 3.98 Å found in the bulk calculation using the PBE DFT. We allowed the atoms in the top two layers to relax to their lowest energy configuration, while fixing the atoms of the bottom four layers to their bulk positions. All binding configurations and transition states were determined using PBE DFT calculations without solvation. Then we carried out single

point calculations to include the solvent effect. The total energy was represented as the sum of gas-phase and solvation energies:

$$E_{total} = E_{gas} + E_{solv} . \quad (1)$$

We evaluated the solvent effect using the Poisson-Boltzmann implicit solvent method as implemented in the APBS[38–40] which is incorporated in the Computational Materials Design Facility[41] (CMDF) developed in the Materials and Process Simulation Center (MSC) at Caltech. Here the boundary of the continuum is taken as the solvent-accessible surface for a solvent with spherical radius of 1.4 Å and a dielectric constant of 78. Structures and charges were taken from PBE for all intermediates and transition states. To test whether more than 6 layers might be needed, we carried out calculations for 3 to 10 layers and found negligible energy changes (~ 0.02 eV) between 6 and 10 layers.

However, we were concerned that calculations of solvent effect might require larger slabs, since the electrostatic interaction between solvent and solute may converge slowly. Thus, we used an alternative approach to evaluate the solvent effect. Here, instead of solving the Poisson-Boltzmann equation for a periodic system, we cut a super cell out of the infinite pure platinum slab. The center cell was substituted by the adsorbing system of interest, while all remaining cells were similar to those in the original platinum slab. Thus, a center cell with adsorbate is surrounded by bare, and hence neutral, ones. To avoid solvent stabilization due to interaction between solvent and the back side of the slab (the bulk side), we added three additional layers of neutral platinum atoms to the bulk side. A sketch of the model is shown in Figure 2-1.

Results and Discussion

We studied systematically the adsorption preference of six adsorbed intermediates: H (atomic hydrogen), O (atomic oxygen), O_2 (molecular oxygen), OH, OOH, and H_2O on the Pt (111) surface (Table 2-1), by density function theory (DFT).

All adsorbates prefer one of four binding sites available on the (111) surface (Figure 2-2), which are denoted as μ_1 (top), μ_2 (bridge), μ_3-fcc (fcc hollow), and μ_3-hcp (hcp hollow), according to the number of surface atoms to which the adsorbate binds.

Without solvation we find that atomic oxygen (O) prefers the μ_3-fcc site, with a binding energy of BE = 3.68 eV, followed by the μ_3-hcp site with BE = 3.30 eV. This agrees with the experimental adsorption energy of 3.68 eV at the μ_3-fcc adsorption site[42]. Previous theoretical studies on 3 layer slabs using generalized gradient approximation (GGA) of Perdew and Wang (PW91) DFT led to BE = 4.03eV for the μ_3-fcc site[10]. B3LYP DFT calculations on a 35 atom Pt cluster[14] (Pt_{35}) led to BE = 3.37eV for fcc and 3.03 eV for hcp sites.

Without solvation we find that O_2 prefers the μ_3-fcc site with BE = 0.48 eV and R_{OO} = 1.41 Å, followed by the μ_2-bridge site with BE =0.41 eV and R_{OO} = 1.34 Å. This agrees well with low temperature adsorption experiments[43] that find that O_2 can absorb into both a peroxide-like (O_2^{2-}) with a vibrational frequency of 690 cm^{-1} and a weaker bound superoxo-like (O_2^{-}) with a vibrational frequency of 870 cm^{-1}. Our bond lengths agree with experimental estimates of 1.43 Å for peroxo-like and the 1.37 Å for superoxo-like species[44]. Our calculated BE is consistent with the experimental estimate of 0.38 eV for the superoxo-like configuration[45]. Earlier theoretical studies[12,46] led to 0.65 to 0.72 eV for

peroxo-like and 0.53 to 0.68 eV for superoxo-like. This difference is mainly due to the smaller number of layers included in these earlier studies. Thus we find that using only three-layer slabs as in the previous studies leads to 0.62 and 0.75 eV, respectively. B3LYP DFT calculations on a 35-atom Pt cluster[14] found the bridge site to be preferred with BE = 0.49 eV, while calculations on a 5-atom cluster[47] led to BE = 0.53 eV for the bridge site.

We find that OH prefers the μ_2 (bridge) site with BE = 2.26 eV while the μ_1 site is close with BE = 2.24 eV. This agrees with the calculations on a 3-layer slab using GGA PW91 DFT by Hu[48], who found BE = 2.22 eV for the μ_2 (bridge) site and 2.27 eV for the μ_1 site. B3LYP calculations for the Pt_{35} cluster[14] obtained BE = 2.06 eV. It is important to note that this OH structure would not be stable for a monolayer, which would reconstruct into an overlayer having a network of hydrogen bonds[48]. Here, we use this structure just to estimate the solvation energy (without considering stabilization from adjacent OH).

We find that OOH is stable only on the μ_1 (top) site, leading to an optimum configuration in which the OO bond is parallel to the surface pointing towards an adjacent Pt atom, leading to BE = 1.06 eV. An alternative configuration for OOH has the O−O bond pointing toward an adjacent fcc site with BE of 0.96 eV. This implies a 0.08 eV agostic stabilization from the adjacent surface atom. Similar results were obtained for the Pt_{35} cluster[14] with BE = 1.03 eV.

We find that H_2O is stable only on the top site, with a binding energy of 0.22 eV without solvent. This agrees with 0.29 eV for the top site in 3-layer calculations using PBE studies[49]. Calculations for the Pt_{35} cluster led to a much stronger BE = 0.61 eV. Direct comparison with experiment is difficult since H_2O tends to form a bilayer[19,49].

Our PBE calculations find that the μ_1 (BE=2.79 eV) and μ_3-fcc (BE=2.73 eV) sites are most stable for atomic hydrogen (Table 2-1). This result agrees with the high resolution electron energy loss spectroscopy (HREELS) experiment[50], which finds H in the threefold coordinated site, and with vibrational neutron spectroscopy studies[51], where hydrogen was observed in the on-top site. Our calculations for the 6-layer slab find that atomic hydrogen slightly prefers the on-top site over the threefold coordinated site, by 0.06 eV (0.02 eV after zero point energy correction). This is consistent with the small experimental hydrogen diffusion barrier of ~ 0.07 eV[52]. For such small differences, one must consider the biases in the particular form of DFT; indeed Olsen et al[53]. showed that various exchange-correlation functionals can change binding energies by up to 0.1 eV, setting a bound on the accuracy to be expected from such studies.

Two reaction pathways were proposed previously[14] for the ORR on the Pt (111) metal surface in the gas phase environment, the O_2-dissociation mechanism:

$$O_2 \xrightarrow[\text{i}]{} 2O \xrightarrow[\text{ii}]{2H} 2OH \xrightarrow[\text{iii}]{2H} 2H_2O \qquad (2)$$

and the OOH-association mechanism:

$$O_2 \xrightarrow[\text{iv}]{H} OOH \xrightarrow[\text{v}]{} O+OH \xrightarrow[\text{ii}]{H} 2OH \xrightarrow[\text{iii}]{2H} 2H_2O \qquad (3)$$

where all reactants are surface adsorbates describing the hydrogen oxidation reaction after dissociative adsorption of H_2. Both of these mechanisms are supported by subsequent calculations[11,54].

We computed transition states and barriers using nudged elastic band theory (NEB) [55–56] for all five reaction steps (i–v) involved in pathways (2) and (3). The results are shown in Table 2-2, Figure 2-3, and Figure 2-4.

The three barriers in the O_2-dissociation mechanism (2) in the gas phase environment were calculated to be 0.58 eV for O_2 dissociation, 0.73 eV for OH formation, and 0.21 eV for H_2O formation (using six-layer slabs). This can be compared with 0.52, 0.91, and 0.14 eV in DFT studies by Li et al[12]. using four layers and with 0.94 and 0.21 eV obtained by Hu[10] for OH and H_2O formation using three-layer slabs. To validate that these differences are due to slab thickness effect, we carried out similar calculations with just a three-layer slab, leading to a result of 0.52, 0.83, and 0.25 eV, which agrees well with previous results. For the Pt_{35} cluster, [14] the barriers were 0.63, 1.13 and 0.09 eV.

For the OOH-association mechanism (3), we found the barriers of 0.31 eV for OOH formation, 0.17 eV for OOH dissociation, 0.73 eV for OH formation, and 0.21 eV for H_2O formation, all with 6-layer slabs. Using only 3 layers we find the OOH to be 0.37 eV, which agrees with the 0.42 eV calculated by Li[12] for 3 layers. Again, we find OH formation to be the rate-determining step (RDS) in the OOH-association mechanism.

Summarizing, our calculations predict that the ORR on the Pt(111) surface in the gas phase environment would have a total energy barrier of 0.73 eV with the OH formation as the RDS for both the O_2-dissociation and OOH association mechanisms.

The solvent effect on all adsorbed species, ORR intermediates, and transition states were evaluated using the Adaptive Poisson Boltzmann Solver (APBS) method[38–40] at single points using the structures optimized in the gas phase. Energies and potential energy surfaces, including the solvent effects as described in equation (1), are shown in Table 2-1, Table 2-2, Figure 2-3, and Figure 2-4.

Table 2-1 shows that the solvation energy for adsorbed OH (top) is 0.54 eV, which agrees with the first-layer solvation energy of 0.54 eV estimated for an adsorbed OH/H_2O

overlayer.[57] This becomes an overall solvation of 0.59 eV after including the second layer solvation energy of 0.05 eV due to wetting of the OH/H_2O overlayer.[58]

We find that solvation stabilizes the water molecule by 0.36 eV, giving a total binding energy of 0.58 eV. This agrees with 0.62 eV from extensive calculations of water adsorption by Meng et al.[59] using up to six bilayers of explicit water.

The solvation energy for adsorbed hydrogen is only 0.07 (μ_1) or 0.12 (μ_3) eV for 6 layers, reflecting the similar electronegativity of H and Pt. This agrees with the range of 0.04 to 0.17 eV from studies of surface hydrogen using an explicit solvation method[20].

We find that the solvent strongly stabilizes adsorbed oxygen, by 0.63–0.70 eV, whereas adsorbed O_2 is stabilized by 0.41 eV and OOH is stabilized by 0.47 eV. Our calculated solvation of adsorbed O does not agree with the estimate of -0.03 eV by Norskov[60] using the water bilayer, which assumed that the O would not change the structure of the water bilayer (no details were provided).

Summarizing, we find that solvent effects significantly modify the reaction energies and ORR barriers for both mechanisms.

For the direct O_2-dissociation mechanism, the barriers for the three steps, O_2 dissociation, OH formation, and H_2O formation, are estimated to change by -0.31, 0.36, and 0.12 eV in the presence of water.

For the OOH-association mechanism, solvation changes the barriers for the four steps, OOH formation, OOH dissociation, OH formation, and H_2O formation, by -0.03, -0.17, 0.36, and 0.12 eV, respectively.

With solvation the RDS for both mechanisms becomes the OH formation step with a barrier of 1.09 eV in water solvent. Such a high barrier would seem to provide rates at the

operating temperature of a PEMFC (below 90°C) that are too low. This makes it questionable whether either of the two reaction mechanisms considered above can be responsible for the rates in water solvent. Thus:

- the chemistry must occur through surface structures different than (111) on Pt (perhaps steps)
- the OH formation and H_2O formation steps in ORR must be assumed to occur mainly through a hydronium-induced mechanism[16–17]. As discussed above, we assume that the hydrogen involved in various reaction steps is already on the surface. This assumption is based on the observation that hydrogen is easily adsorbed on the surface with a small energy barrier of 0.15 eV in the presence of the water bilayer[61]. In PEMFCs, H_3O^+ stabilized by the sulfonates of the Nafion could serve as a source of hydrogen[11] for formation of OH from O_{ad} (and possibly for forming OOH and H_2O), but consideration of H_3O^+ is beyond the scope of this publication.
- some other mechanism might exist for the ORR on the platinum surface.

Conclusion

Summarizing, we report the structures, binding energies, and reaction barriers from PBE DFT studies of the reaction intermediates involved in ORR on platinum slabs containing 6 layers of Pt. These calculations use the Poisson-Boltzmann method to include the effects of solvation. We considered two previously proposed mechanisms (O_2-dissociation and OOH-association) and find that the energetics of the ORR on the Pt surface change significantly in the presence of water solvent. In particular, the OH

formation was found to be the RDS for both mechanisms, leading to an overall energy barrier increase to 1.09 eV in solvent, compared to 0.73 eV without solvation. With such a high barrier in solvent, these two gas-phase ORR mechanisms become unfavorable and we conclude that

- the chemistry must occur through surface structures different than (111) (e.g., steps), or
- the ORR must be assumed to involve a hydronium induced mechanism, or
- another mechanism must exist for the ORR on the platinum surface.

Tables and Figures

Adsorbate	Binding sites	E_{bind} (eV)	Q_{slab}(eV)	E_{solv}(eV)	E^{solv}_{bind} (eV)	$E^{solv}_{explicit}$ (eV)
H	μ_1	-2.79	-0.11	-0.07	-2.86	-0.04 to 0.17[20]
	μ_2	-2.70	-0.21	-0.12	-2.82	
	μ_3-fcc	-2.73	-0.23	-0.12	-2.85	
	μ_3-hcp	-2.70	-0.22	-0.12	-2.82	
O	μ_1	-2.30	0.55	-0.75	-3.05	
	μ_2	-3.11	0.61	-0.63	-3.74	
	μ_3-fcc	-3.68	0.70	-0.70	-4.38	
	μ_3-hcp	-3.30	0.66	-0.63	-3.93	
OH	μ_1	-2.24	0.33	-0.54	-2.78	-0.59[57–58,60]
	μ_2	-2.26	0.25	-0.38	-2.64	
	μ_3-fcc	-1.67	0.34	-0.32	-1.99	
	μ_3-hcp	-1.55	0.34	-0.34	-1.89	
O_2	bridge	-0.41	0.40	-0.32	-0.73	
	fcc	-0.48	0.51	-0.41	-0.89	
	hcp	-0.36	0.47	-0.36	-0.72	
OOH	μ_1-bridge	-1.06	0.26	-0.47	-1.53	
	μ_1-fcc	-0.96	0.27	-0.47	-1.43	
H_2O	μ_1	-0.22	-0.10	-0.36	-0.58	-0.62[59]

Table 2-1. Binding energies without solvent (E_{bind}), slab charge (Q_{slab}), solvation energy (E_{solv}), and binding energy with solvation (E_{bind}^{solv}) for all intermediates. E_{bind} is calculated as $E_{Slab\text{-}adsorbate}$-$E_{Slab}$-$E_{adsorbate}$. Q_{slab}(e) is the net charge of the slab. E_{solv}(eV) is the solvation energy calculated using the continuum model. E_{bind}^{solv} (eV) is the sum of E_{bind} and E_{bind}^{solv} (eV). Both OOH configurations are atop sites. The only difference is the orientation of OOH.

Barriers	Reaction steps	E_a (eV)	E_a^{solv} (eV)
Barriers for steps	O_2 dissociation	0.58	0.27
	OH formation	0.73	1.09
	H_2O formation	0.21	0.33
	OOH formation	0.31	0.28
	OOH dissociation	0.17	0.00
Barriers for the overall reaction	O_2 dissociation	0.73	1.09
	OOH dissociation	0.73	1.09

Table 2-2. Reaction barriers without solvent (E_a) and in water-solvated phase (E_a^{solv}) for five steps involved in the O_2-dissociation and OOH-association pathways.

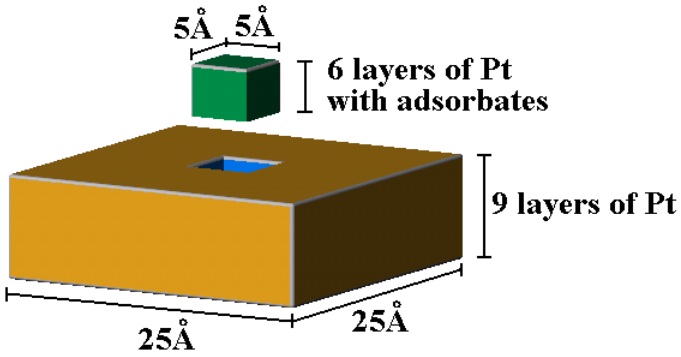

Figure 2-1. The super slab used to calculate the solvent effect. Only the center cell has adsorbate attached. All cells surrounding the center cell contain neutral platinum atoms. Three additional layers of platinum are added to the bulk side to eliminate extraneous solvent effects.

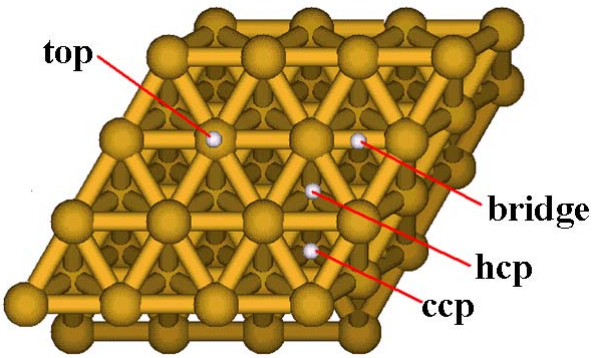

Figure 2-2. Important binding sites on the closest packed Pt (111) surface

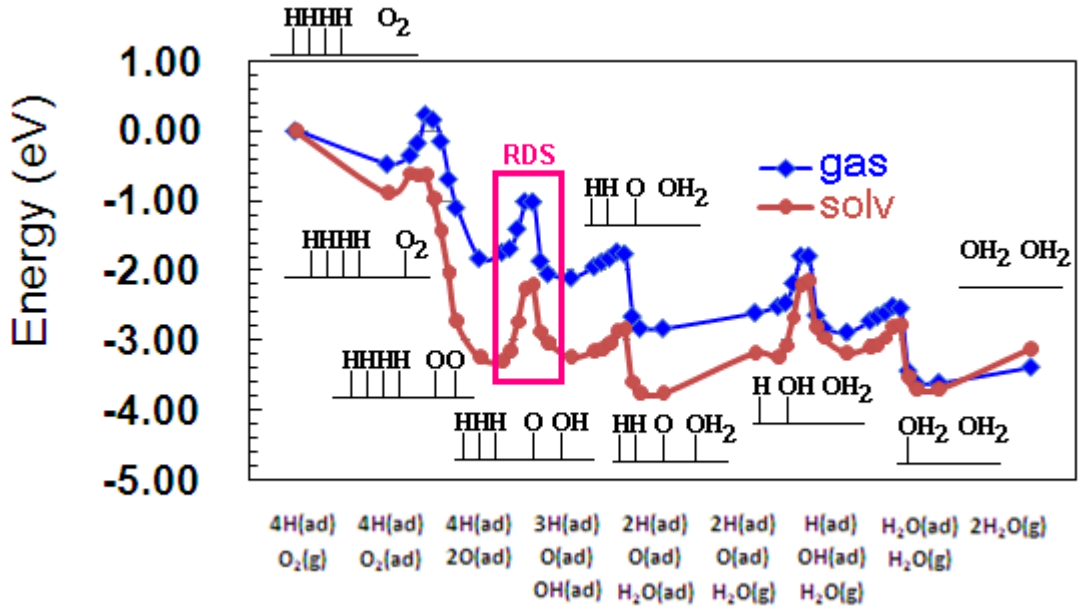

Figure 2-3. Potential energy surface of the O_2-dissociation mechanism without and with water solvent

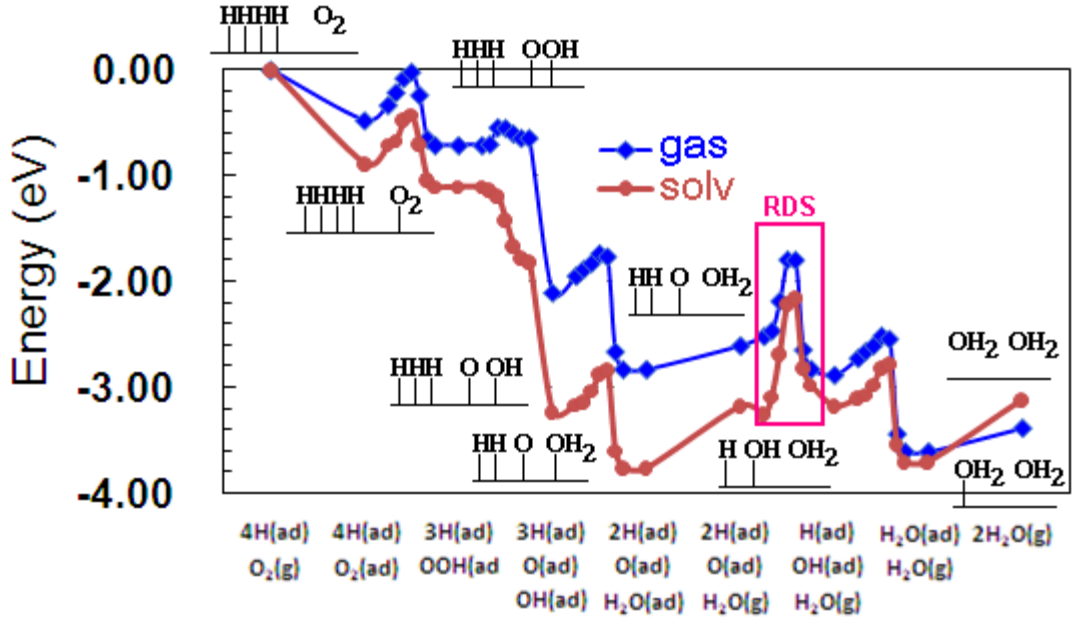

Figure 2-4. Potential energy surface of the OOH-association mechanism without and with water solvent

Chapter 3 The Oxygen Hydration Mechanism for the Oxygen Reduction Reaction at Pt and Pd Fuel Cell Catalysts

Abstract

We report the reaction pathways and barriers for the oxygen reduction reaction (ORR) on platinum, both for gas phase and in solution, based on quantum mechanics calculations (PBE-DFT) on semi-infinite slabs. We find a new mechanism in solution:

O_2 ➔ $2O_{ad}$ (E_{act} = 0.00eV),

$O_{ad} + H_2O_{ad}$ ➔ $2OH_{ad}$ (E_{act} = 0.50eV),

$OH_{ad} + H_{ad}$ ➔ H_2O_{ad} (E_{act} = 0.24eV),

in which OH_{ad} is formed by hydration of surface O_{ad}.

For the gas phase (hydrophilic phase of Nafion), we find that the favored step for activation of the O_2 is

$H_{ad} + O_{2ad}$ ➔ OOH_{ad} (E_{act} = 0.30eV ➔ $OH_{ad} + O_{ad}$ (Eact=0.12eV)

followed by

$O_{ad} + H_2O_{ad}$ ➔ $2OH_{ad}$ (E_{act} = 0.23eV), $OH_{ad} + H_{ad}$ ➔ H_2O_{ad} (E_{act} = 0.14eV).

This suggests that to improve the efficiency of ORR catalysts, we should focus on decreasing the barrier for O_{ad} hydration while providing hydrophobic conditions for the OH and H_2O formation steps

Introduction

Critical to the performance of Polymer Electrolyte Membrane Fuel Cells (PEMFC) is the efficiency of the reaction in which protons (passed through the electrolyte) from the anode reduce O_2 at the cathode to form H_2O, the oxygen reduction reaction (ORR) [1–4]. Currently the best cathode catalysts are Pt or alloys of Pt with Co or Ni[62–63], but the efficiency remains unacceptably low while the costs are too high. In order to improve the performance of current PEMFCs, it is important to understand the chemical mechanism, that is, the sequence of fundamental reaction steps taking protons delivered to the cathode and O_2 to form H_2O.

We consider here the Nafion PEMFC, in which we have shown[64–65] that for standard humidity conditions (H_2O/SO_3 ratio ~ 15) the Nafion has percolating water channels (~ 4 nm wide) with ionized sulfonic acid groups ($R\text{-}SO_3^-$) lining the surface intermixed with percolating hydrophobic (Teflon-like) regions (Figure 3-1). We assume here that O_2 accesses the catalyst surface via the hydrophobic regions (modeled as gas phase) while the protons migrate through the water channels (the solution phase).

As shown in Chapter 2, considering solvent effect, the two known mechanisms, namely the O_2-diss mechanism and the OOH-form mechanism, all have to go through an unfavorable OH formation with a barrier of 1.09eV, contrary to the fact that Pt is an effective catalyst for ORR. Here we report two alternative mechanisms which bypass the difficult OH formation.

Methodology

In this study, the Pt catalyst particle was modeled as a slab infinite in two directions (a and b) and finite in the third direction (c). We consider a 3×3 supercell of the (111) surface (9 atoms) that is six layers thick (54 atoms). The top two layers are allowed to relax, representing the active surface while the bottom four layers are fixed, representing the bulk side of the surface. The same model was applied in previous studies.[66]

All calculations employed the kinetic and exchange-correlation functional developed by Perdew, Burke and Ernzerhof (PBE) [30]. We used the Seqquest[29] implementation with an optimized double-zeta plus polarization Gaussian-type basis set contracted from calculations on the most stable unit cell of the pure elements. Angular-momentum-projected norm-conserving nonlocal effective core potentials[34–37] (pseudopotentials) were used to replace the core electrons. Thus, the Pt atom was described with 16 explicit electrons (six 5p, one 6s, and nine 5d in the ground state). The real-space grid density was 5 points per Angstrom, while the reciprocal space grid was 5×5×0 for slab calculations. All calculations allowed the up-spin orbitals to be optimized independently of the down spin orbitals (spin unrestricted DFT).

The solvation of the water phase employed a continuum model based on the Poisson-Boltzmann approximation[23–25,38]. All reaction pathways were determined using the Nudged Elastic Band[55–56] method and solvent effects were included for each point along the path.

Results and Discussion

The most common mechanism, denoted as O_2-diss-gas[14] is

1a. O_{2g} ➔ O_{2ad} (no barrier)

1b. O_{2ad} ➔ 2 O_{ad} [E_{act} = 0.57 eV (Pt), 0.72(Pd)]

1c. O_{ad} + H_{ad} ➔ OH_{ad} [E_{act} = 0.74 eV (Pt), 0.30 (Pd)]

1d. OH_{ad} + H_{ad} ➔ H_2O_{ad} [E_{act} = 0.14 eV (Pt), 0.58 (Pd)].

Many studies have focused only on the O_2 dissociation step (1b) [16–18,67], however, we find step 1c to be the rate determining step (RDS). Enthalpies and barriers for steps possibly important for ORR on Pt and Pd are presented in Table 3-1 and Table 3-2. Recently Mavrikakis, etc.[68], published gas phase barriers for the first five reactions in table 1a for Pt and Pd, but without allowing the metal surface slab to relax. As a result their barriers are 0.00–0.25eV too high for Pt and 0.00–0.65eV too high for Pd.

A second possible pathway[14], OOH-form-gas, for ORR involves activation of O_{2ad} with H_{ad} prior to dissociation:

2a. O_{2g} ➔ O_{2ad} (no barrier)

2b. H_{ad} + O_{2ad} ➔ OOH_{ad} [E_{act} = 0.30 eV (Pt), 0.55 (Pd)]

2c. OOH_{ad} ➔ OH_{ad} + Oad [E_{act} = 0.12 eV (Pt), 0.26 (Pd)]

2d. O_{ad} + H_{ad} ➔ OH_{ad} [E_{act} = 0.74 eV (Pt), 030 (Pd)]

2e. OH_{ad} + H_{ad} ➔ H_2O_{ad} [E_{act} = 0.14 eV (Pt), 0.58 (Pd)].

In this mechanism H_{ad} activates O_2 to form OOH (E_{act} = 0.30 eV) and then OOH_{ad} dissociates to form O_{ad} and OH_{ad} (E_{act} = 0.12 eV). This leads to a barrier of 0.30 eV,

making the OOH pathway preferred over the direct O_2 dissociation pathway (0.57 eV) in gas phase. However, the RDS remains step 2d (same as 1c).

In the above mechanisms, H_{ad} is assumed to be available as reactant on the surface. At normal operating potentials, H^+ is the stable form; thus the mechanisms involving H_{ad} require an additional step of the H_{ad} formation from H^+:

$H^+ + e \rightarrow H_{ad}$ (step 0).

Assuming an electrode potential of 0.80 V versus SHE leads to $\Delta E = 0.25$ eV for Pt and 0.11 eV for Pd (see Chapter 4 for more details). According to Norskov, etc.[17], the enthalpy of step 0 is related to that of

$H^+ + e \rightarrow 1/2H_2 \rightarrow H_{ad}$

which is barrierless for SHE[69]. Thus the reaction barrier at an electrode potential of 0.80 V relative to the SHE will likely be close to the reaction enthalpy. Our estimated barrier, 0.25 eV, is consistent with 0.33 eV calculated by Anderson, etc.[69], for Pt. The barriers, 0.25 eV for Pt and 0.11 eV for Pd, are smaller than the RDS barriers for all mechanisms considered in our paper and do not affect our discussions.

We report here a new mechanism, OOH-form-hydr-gas, for ORR that avoids the high barrier of 1c or 2d for OH_{ad} formation. This involves hydrolysis of O_{ad} by H_2O_{ad}, step 3d, as an alternative mechanism for forming OH_{ad} from O_{ad}:

3a. $O_{2g} \rightarrow O_{2ad}$ (no barrier)

3b. $H_{ad} + O_{2ad} \rightarrow OOH_{ad}$ [E_{act} = 0.30 eV (Pt), 0.55 (Pd)]

3c. $OOH_{ad} \rightarrow OH_{ad} + O_{ad}$ [E_{act} = 0.12 eV (Pt), 0.26 (Pd)]

3d. $O_{ad} + H_2O_{ad} \rightarrow 2OH_{ad}$ [E_{act} = 0.23 eV (Pt), 0.30 (Pd)]

3e. $OH_{ad} + H_{ad} \rightarrow H_2O_{ad}$ [E_{act} = 0.14 eV (Pt), 0.58 (Pd)].

Here OOH-form-hydr-gas involves OOH formation (E_{act} = 0.30 eV) and then OOH_{ad} dissociation to form O_{ad} and OH_{ad} (E_{act} = 0.12 eV) as in OOH-form-gas. But this is now followed by step 3d, hydration of adsorbed oxygen (E_{act} = 0.23 eV) (Figure 3-2), and then step 3e (E_{act} = 0.14 eV). Thus step 3b with E_{act} = 0.30 eV is the RDS for Pt versus 0.55 eV for Pd, indicating Pt to be much better.

Indeed, this O_{ad} hydration step has been observed in experiments by Ertl, et al.[70–71], and plays an essential role in the catalytic formation of H_2O at low temperature under UHV conditions. Our calculated barriers are consistent with the Ertl experimental result that H_2O formation ($E_{a,calc}$ = 0.14eV, $E_{a,exp}$ = 0.27eV) is much faster than OH formation ($E_{a,calc}$ = 0.23eV, $E_{a,exp}$ = 0.44eV). Under UHV conditions, the hydration of O_{ad} becomes impossible at temperature above 180 K because of the low adsorption energy of water on Pt (calculated 0.21 eV). But under ORR conditions, there is an abundant supply of water on the surface so that hydration becomes an essential step for ORR. Michaelides and Hu[10,48] using DFT methods (GGA PW91), found results similar to ours: 0.33 eV for step 3d, 0.21 eV for step 3e, 0.96 eV for step 2d—all 0.1 to 0.2 eV higher than our results, probably because they used smaller 2×2 unit cells and only three- and four-layer slabs instead of a 3×3 unit cell and a six-layer slab as in our calculations.

Next we consider how solvation affects the mechanism of ORR using our recently[66] developed approach for estimating the effect of the water phase on these barriers. The contribution of solvation is calculated implicitly using the Poisson-Boltzmann continuum model[23–24]. Including solvation we find O_2-diss-solv mechanism:

4a. O_{2g} ➔ O_{2ad} (no barrier)

4b. O_{2ad} ➔ $2O_{ad}$ [E_{act} = 0.00 eV (Pt), 0.27 (Pd)]

4c. $O_{ad} + H_{ad} \rightarrow OH_{ad}$ [E_{act} = 0.97 eV (Pt), 0.47 (Pd)]

4d. $OH_{ad} + H_{ad} \rightarrow H_2O_{ad}$ [E_{act} = 0.24 eV (Pt), 0.78 (Pd)]

Thus solvation effects dramatically influence the barriers. The O_2 dissociation barrier drops to zero for Pt (0.27 eV for Pd), because of the large solvent stabilization of O_{ad}, increasing the exothermicity from -1.23 eV in gas phase to -2.18 eV in solution for Pt (from -1.02 eV to -1.91 eV for Pd). However, the barrier for OH_{ad} formation (step 4c) increases dramatically from 0.74 eV to 0.97 eV, making this mechanism unlikely. Reaction of OH_{ad} with H_{ad} to form H_2O is quite favorable with a barrier of 0.24 eV.

In solvent the OOH_{ad}-form-gas mechanism, involving formation and dissociation of OOH, becomes OOH-form-solv:

5a. $H_{ad} + O_{2ad} \rightarrow OOH_{ad}$ [E_{act} = 0.22 eV (Pt), 0.74 (Pd)]

5b. $OOH_{ad} \rightarrow OH_{ad} + O_{ad}$ [E_{act} = 0.00 eV (Pt), 0.10 (Pd)]

5c. $O_{ad} + H_{ad} \rightarrow OH_{ad}$ [E_{act} = 0.97 eV (Pt), 0.47 (Pd)]

5d. $OH_{ad} + H_{ad} \rightarrow H_2O_{ad}$ [E_{act} = 0.24 eV (Pt), 0.78 (Pd)].

Again the RDS becomes OH formation for Pt with a barrier of 0.97 eV and H_2O formation for Pd with a barrier of 0.78 eV. The OOH_{ad} formation barrier is higher than the direct dissociation of O_{2ad}, making it less favorable than the direct O_2 dissociation, step 4b. Thus, we will ignore this mechanism.

In solvent the barrier for OH formation from step 4c or 5c is 0.97 eV, clearly too high to play an important role at PEMFC operating temperatures. Therefore neither O_2-diss-solv nor OOH-form-solv is appropriate for Pt in an aqueous environment. Instead we find that O_2-diss-hydr-solv is most favorable for solution:

6a. $O_{2g} \rightarrow O_{2ad}$ (no barrier)

6b. O_{2ad} ➔ $2O_{ad}$ [E_{act} = 0.00 eV (Pt), 0.27 (Pd)]

6c. $O_{ad}+H_2O_{ad}$ ➔ $2OH_{ad}$ [E_{act} = 0.50 eV (Pt), 0.49 (Pd)]

6d. $OH_{ad} + H_{ad}$ ➔ H_2O_{ad} [E_{act} = 0.24 eV (Pt), 0.78 (Pd)].

Here O hydration (step 6c) is the RDS with a barrier of 0.50 eV for Pt. For Pd the RDS is H_2O formation (step 6d) with a barrier of 0.78 eV, consistent with the decreased performance of Pd. This new mechanism suggests that a strategy for improving efficiency of ORR catalysts is to focus on decreasing the E_{act} for O_{ad} hydration. We have examined this hydration step for 11 metals in columns 8, 9, 10, and 11 of the periodic table and find that the lowest barriers are for Ni (0.20 eV) and Co (0.04 eV), which are already known to increase the efficiency of platinum catalysts[62–63]. (Of course the improved performance might arise from other effects, for example, easier OH removal[63] and lower coverage benefiting O_2 dissociation.) We also find low hydration barriers for Os (0.54 eV), Ru (0.69 eV), and Ir (0.69 eV), suggesting that alloying with these elements might also improve the efficiency of Pt cathodes.

The above solvation calculations considered reactions involving H_{ad} formed from H^+ in solution. There might be a direct pathway for H_3O^+ to transfer the H^+ directly to OH_{ad} with a lower barrier than the 0.24eV we calculate for H_{ad}, but since this is not the RDS we did not consider it. Similarly a direct process for O_{ad} ➔ OH_{ad} involving H_3O^+ could lower the barrier below the 0.94eV we find for H_{ad}, but we suspect that the hydration of O_{ad} is still the favorable step.

The above discussion considered separately the gas phase and solution phase reactions, but the PEMFC allows the O_2 to access the catalyst through the hydrophobic regions of the Nafion membrane while the protons to form H_2O arrive through the

sulfonic acid lined water channels (illustrated in Figure 3-1). In this case, the O_{2g} would dissociate to form $O_{ad\ in}$ the hydrophobic region, which would stay fixed since the barrier for O_{ad} migration is 0.42 eV (Pt). Thus we expect that some H_2O will migrate into this region to form OH_{ad} via the O_{ad} hydrolysis mechanism. However we do not want a full monolayer of H_2O in this hydrophobic region since it would impede O_2 dissociation.

Next we must account for H_2O formation. We assume that the OH_{ad} is formed initially in the hydrophobic region, but since the OH_{ad} migration barrier is < 0.1 eV, it can migrate to the part of the Pt in contact with the water channels to react directly with H_3O^+ at the interface. Alternatively it could remain in the hydrophobic region to react with H_{ad} moving along the surface (barrier only 0.09 eV) from the part of the catalyst in contact with the water channel. A third alternative is that OH in the middle of a monolayer of H_2O in the hydrophobic region could exchange hydrogen ($OH_{ad} + H_2O_{ad} \rightarrow H_2O_{ad} + OH_{ad}$, E_{act} = 0.03 eV) to effectively migrate the OH_{ad} to the water channel for reaction with H_3O^+.

Probably the best design would have the O_2 dissociate on the Pt at the interface between hydrophobic and water phases of Nafion so that the O_{ad} could contact H_2O_{ad} to form OH_{ad} on the hydrophobic side but next to the water phase, allowing extraction of the proton from H_3O^+ to form H_2O_{ad}. Thus the optimum membrane for Pt might have the aqueous and hydrophobic phases alternate to maximize the contact length between these phases on the catalyst's surface.

Conclusion

In this study we studied systematically the ORR mechanisms on the Pt (111) surface. In addition to the two known mechanisms, namely O_2 dissociation and OOH formation, we proposed two novel mechanisms involving the O hydration reaction $O_{ad} + H_2O_{ad} \rightarrow 2OH_{ad}$. Without solvent effect, the preferred mechanism becomes OOH-form-hydr-gas mechanism involving OOH formation, OOH dissociation, O hydration, and H_2O formation with an overall barrier of 0.30eV for Pt, as compared to 0.55eV for Pd. This agrees with the fact that Pt is a better catalyst for hydrogen oxidation, as compared to Pd. With solvent effect, the preferred mechanism is O_2-diss-hydr-solv with an overall barrier of 0.50eV for Pt, as compared with the 0.78eV for Pd. It also agrees with the experimental result that Pt is a good catalyst for ORR in aqueous condition. The RDS for Pt with solvation is the O hydration step. Hence it suggests that to improve the efficiency of ORR catalysts, we should focus on decreasing the barrier for O_{ad} hydration while providing hydrophobic conditions for the OH and H_2O formation steps

Tables and Figures

Reaction Step Barriers Pt	E(gas)	E_{act}(gas)	E(solv)	E_{act}(solv)	E(gas,exp)
O_2 Dissociation	-1.23	0.44*	-2.18	0.00	0.30[45]
OH Formation	-0.32	0.74	-0.07	0.97	
H_2O Formation	-0.78	0.14	-0.56	0.24	0.27[71]
OOH Formation	-0.24	0.30	-0.19	0.22	
OOH Dissociation	-1.30	0.12	-2.07	0.00	
H-OOH dissociation	-1.62	0.14	-2.14	0.00	
O hydration	0.46	0.23	0.49	0.50	0.44[71]

Table 3-1. Enthalpies and barriers (eV) for steps possibly important for ORR on Pt

*We find coverage dependence for O_2 dissociation. The barrier is 0.51eV for c(2x2), 0.45eV for c(3x3), and 0.44eV for (4x4) for a three layer slab. The experimental value is for the limit of zero coverage.

Reaction Step Barriers Pd	E(gas)	E_{act}(gas)	E(solv)	E_{act}(solv)
O_2 Dissociation	-1.02	0.72	-1.91	0.27
OH Formation	-0.35	0.30	-0.03	0.47
H_2O Formation	-0.59	0.58	-0.39	0.78
OOH Formation**	0.12	0.55	0.05	0.74
OOH Dissociation**	-1.49	0.26	-1.99	0.10
H-OOH dissociation*	-1.85	0.12	-2.01	0.12
O hydration	0.24	0.30	0.36	0.49

* Under conditions with high H_{ad}, another mechanism producing OH is possible, but this is unlikely under ordinary operating fuel cell conditions. See footnote 1.

** The H-associated OOH_{ad} dissociation mechanism is not preferred because of the O_2 dissociation step.

Table 3-2. Enthalpies and barriers (eV) for steps possibly important for ORR on Pd

[1] When hydrogen is present, it can react with surface OOH_{ad} to form two OH_{ad}, leading to a barrier of 0.14 eV in gas phase. Combining this step with formation of OOH leads to the **HighH-gas** mechanism:

7a. O_{2g} → O_{2ad} (no barrier)

7b. $H_{ad} + O_{2ad}$ → OOH_{ad} [E_{act} = 0.30 eV (Pt), 0.55 (Pd)]

7c. $H_{ad} + OOH_{ad}$ → $2HO_{ad}$ [E_{act} = 0.14 eV (Pt), 0.12 (Pd)]

7e. $OH_{ad} + H_{ad}$ → H_2O_{ad} [E_{act} = 0.14 eV (Pt), 0.58 (Pd)].

Here the RDS is OOH formation for both gas phase and solvent with E_a = 0.30 eV. This mechanism might be favorable only under extremely high coverage of H_{ad}, since the barrier for 7c ($H_{ad} + OOH_{ad}$) is higher than for 3c (OOH_{ad} dissociation). In operating fuel cells, such a high H_{ad} coverage is not likely.

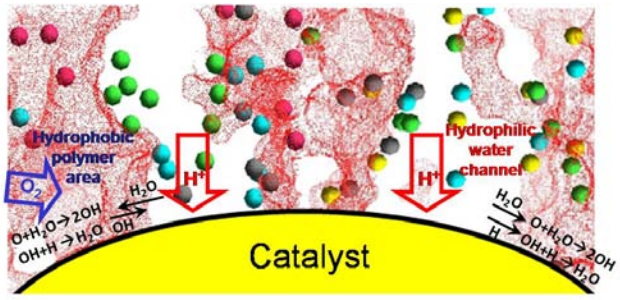

Figure 3-1. Illustration of the sulfonic acid lined hydrophilic water channels and hydrophobic (Teflon-like) regions in Nafion (from references 64-65) showing the likely locations of the O_{2g} ➔ $2O_{ad}$, $O_{ad} + H_2O_{ad}$ ➔ $2OH_{ad}$, and $OH_{ad} + H_{ad}$ ➔ H_2O_{ad} steps in the hydrophobic channels, but H^+ ➔ H_{ad} at the boundary with the water phase. For the gas phase process we assume that the proton is chemisorbed on the surface, H_{ad}. For Pt in water at pH = 1 (typical for a fuel cell), this occurs at a potential of -0.06 eV (relative to the Standard Hydrogen Electrode [SHE]).

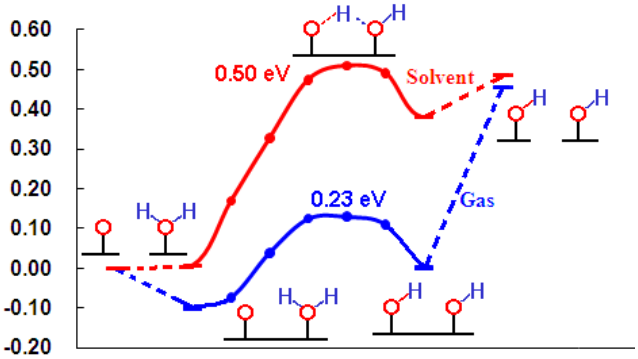

Figure 3-2. Potential energy surface (eV) for the O_{ad} hydration step of ORR.

Chapter 4 Prediction of Optimum Operating Voltage for the Fuel Cell Oxygen Reduction Reaction from DFT Calculations

Abstract

In order to use density functional theory (DFT) to seek improved catalysts for the Oxygen Reduction Reaction (ORR) in Proton Exchange Membrane Fuel Cells (PEMFC), we develop a systematic way to handle the barriers of electron transfer reactions [e.g., $H^+ + e + O_{ad} \rightarrow OH_{ad}$] within the DFT framework. We apply this new method to determining the optimum operating electrochemical potential for the Pt-catalyzed fuel cell and show how much the efficiency can be increased by changes in the reaction barriers.

Introduction

Proton exchange membrane fuel cells (PEMFC) are most promising emission-free energy systems for homes and families[1–4]. However, poor kinetics for the catalytic oxygen reduction reaction (ORR) $\frac{1}{2} O_2 + 2 H^+ + 2 e \rightarrow H_2O$ is a formidable obstacle in lowering the costs to a practical level. Density functional theory (DFT) provides a powerful method for finding new materials to improve these catalysts. Many DFT calculations relevant to ORR have been published[16,66,68,72–75] in the past decade. However, a critical issue in such studies is accounting for the dependence of the electron transfer steps on the external electrochemical potential[17,73,76].

We develop here a systematic approach for handling the electron transfer step along with the solvation effects, and including the effect of the external electrochemical potential on the electron transfer reactions involved in ORR.

We consider the following steps for ORR:

- $H^+(aq) + e \Leftrightarrow H_{ad}$ (1)
- $O_{2gas} \rightarrow O_{2ad} \rightarrow 2O_{ad}$ (2)
- $O_{ad} + (H^+ + e)/H_{ad} \rightarrow OH_{ad}$ (3)
- $OH_{ad} + (H^+ + e)/H_{ad} \rightarrow H_2O_{ad}$. (4)

For each of these reactions we carried out DFT calculations on the Pt (111) surface using the PBE functional, as described in the Method Details section below. The resulting gas phase barriers were corrected for solvation effects as described in our previous paper[66]. For reactions 1, 3, and 4 it is necessary to correct these DFT calculations for the external chemical potential. To do this for 1 we must consider the following steps:

H^+ (solv) + e $\rightarrow 1/2H_2 \rightarrow H_{ad}$.

At the normal hydrogen electrode (NHE), the free energy of H^+ in solution is equal to the energy of H_2 in solution. At an external potential of +V, the free energy of H^+ relative to H_2 becomes –V. The DFT calculations for $1/2H_2 \rightarrow H_{ad}$ on Pt is -0.44eV, thus the total enthalpy of reaction 1, is

$\Delta H_1 = -0.44eV + V$. (a)

The other steps lead to

$\Delta H_2 = -2.51eV$ (b)

$\Delta H_3 = -0.28eV + V$ (c)

ΔH_4 = -1.15 eV+ V . (d)

Methodology

In this study, we used Seqquest[29], where the Kohn-Shan equation is self-consistently solved in a periodic system. The Pt (111) surface is approximated as a semi-infinite slab with a c(2x2) unit cell and three layers of atoms. One side (the bottom layer) is fixed to approximate the bulk side while the other side (the top two layers) is relaxed to approximate the surface.

The solvent effect for such charged system can be evaluated by taking the DFT-calculated Mulliken charge as input for the Poisson-Boltzmann equation as described in our earlier paper[66]. Here, we used the Adaptive Poisson Boltzmann Solver (APBS) method[38–40] solver incorporated in the Computational Materials Design Facility[41] (CMDF).

The reaction path is optimized by nudge elastic band[55–56] (NEB) method. Every image along the path is reoptimized at different charge (+q) with atoms deciding the reaction coordinates fixed. Due to the periodic nature of the method, a partial charge is allowed. The partial electron given away by the surface is assumed to go to the Fermi surface, ending with an energy gain of qE_{fermi}.

E_{fermi} is not directly taken from the gas phase DFT calculation because of the difficulty in deciding the work function with solvation. Nor did we use the experimental value because it may not be compatible with the calculated value due to possible systematic bias. Instead, we first benchmark the calculated values using the standard cycle as follows.

H^+ (solv) ➔ H^+ (gas) ➔ H^+ (gas) + e ➔ $1/2H_2$

The first step is the solvation of H^+ which had been accurately calculated as +11.92eV[77]. The second step involves getting an electron from the Fermi level of the electrode, so the energy cost is exactly $E_{fermi, NHE}$. The third step can be calculated by DFT as -15.86eV. So the total energy cost is +11.92 + E_{fermi} + (-15.86) = E_{fermi} - 3.94eV. From the fact that H ($1/2H_2$) = H (H^+_{solv}), we have E_{fermi} - 3.94eV = 0eV. So the NHE work function consistent with our method would be 3.94eV. At ORR condition (0.8V relative to NHE), the work function is hence -4.74eV.

Our calculations showed that a change in Efermi from DFT calculation does not change the binding energy as well as the reaction barriers. The details are shown in supporting information. So in this study we use the above value (-3.94eV and -4.74eV) in equation (*) and ignore any change brought by a change in work function.

In order to determine the reaction barriers for reactions 1, 2, and 3 we have to determine the reaction barrier as a function of charge. We do this by considering the full reaction surface for fixed total charges ranging from zero to +1 in 0.1 increments as shown in Figure 4-1 (taking reaction 2 as example). This leads to the surface shown in Figure 4-2 where the two coordinates are charge and reaction progress. Based on Figure 4-2 we construct the reaction path in which q adjusts along the reaction path to find the lowest overall barrier for the overall reaction. This leads to the overall reaction path shown in Figure 4-3, where the charge changes continuously from +1 to +0.7 at the transition state and then changes from 0.7 to zero as we proceed to the products. In Figure 4-1, Figure 4-2, and Figure 4-3 we assumed the external potential to be zero.

For an external potential of +V relative to NHE, the relationship between q and the external potential is given by

$E_{+q,\ corrected,\ solv} = E(+q)_{gas,DFT} + q * E_{fermi} + E_{solvation}$ (*)

$E_{fermi} = E_{fermi}(NHE) + V$.

Using equation (*) we carried out similar calculations for V = 0.0 – 1.2 in 0.1 increments and calculated the PES at different electrode potentials, leading to results as in Figure 4-4. Figure 4-4 summarizes the net barrier as a function of external potential. Here we see that the barrier = 0.68eV and ΔH=0.40eV are independent of the external potential up to V=0.6eV, because H_{ad} is either more stable or slightly less stable than H^+. Then from V=0.6 to 1.2 the ΔH increases linearly to 0.95eV at 1.23eV while the barrier increases monotonically to 0.96eV at 1.23eV, because H^+ is increasingly more stable than H_{ad} and the reaction becomes strongly endothermic.

The barriers and ΔH for reactions (1) and (4) are shown in Figure 4-6. We see that throughout the operating range (0.0-1.23V), OH formation dominates the reaction.

Results and Discussion

Hydrogen reduction reaction (Volmer Reaction) $H^+ \rightarrow H_{ad}$

The first step, the hydrogen evolution reaction (Volmer reaction[78]) is

$H^+ (aq) + e \rightarrow 1/2H_2$.

The reaction enthalpy as a function of V is shown in Figure 4-8 and the reversible potential can be calculated by using the following cycle

$H^+ (aq) \rightarrow 1/2H_2 (gas) \rightarrow H_{ad} (solv)$.

The first step has reaction enthalpy of 0.00eV because $H(H^+(aq)) = H(1/2H_2)$ by definition. The second step is the binding energy of H_{ad} and has an enthalpy of -0.62eV, leading to an overall reaction enthalpy of -0.62eV. This implies that H_{ad} would be preferred at potential below 0.62eV versus NHE, differing from the experimental value of 0.40V[79–80]. The difference comes from the stabilization of H_3O^+ near the surface. Using equation (*) and starting from $H_3O^+_{surface}(solv)$ near the surface, the reaction has ΔH = -0.44eV. As the electrode potential goes higher, the reaction changes from endothermic to endothermic, making H_3O^+ the more stable form. The calculated reversible potential 0.44V agrees with the experimentally measured 0.40V[79–80], as well as the H_{upd} region on the cyclovoltammetry curve in acid media[63].

Using similar methods as described above, we calculated the PES of Volmer reaction at +0.0V, +0.3V, +0.7V, and +1.0V and used it to determine the barrier of the Volmer reaction at various potentials, as shown in Figure 4-8. We see that as the potential increases, the reaction changes from exothermic to endothermic and the reaction begins to have a barrier. These results show that as the potential goes above 0.44V relative to NHE, H_{ad} becomes less available. Although endothermic, the Volmer reaction can still proceed as the source of H_{ad}. As the electrode potential continues to increase, at sufficiently high electrode potential the Volmer step would become the RDS for all mechanisms involving H_{ad}.

OH formation reaction $H^+ + O_{ad} \rightarrow OH_{ad}$

Equation (**) shows the reaction enthalpy as a function of external potential for reaction (c).

$$H^+(aq) + O_{ad}(solv) \rightarrow 1/2H_2(gas) + O_{ad}(solv) \rightarrow OH_{ad}(solv) \qquad (**)$$

The reaction enthalpy is -0.47eV at 0.0V relative to NHE, leading to a reversible potential of 0.47V. For the ORR condition, the reaction enthalpy increases to 0.33eV at a potential of 0.80V versus NHE due to solvent effect.

Similar to the case of Volmer reaction, starting from a H_3O^+ near the surface, we have a slightly different reaction enthalpy. At 0.0V relative to NHE, the reaction enthalpy calculated by equation (*) is -0.27eV, smaller than the -0.47eV for free H_3O^+(solv), due to the stabilization of H_3O^+ near the surface. As a comparison, as the potential at the electrode increases, the reaction becomes endothermic. At 0.8V relative to NHE, the reaction enthalpy becomes 0.52eV. However, as discussed earlier, H_{ad} is the preferred form at 0.0V relative to NHE. In the presence of a nearby O_{ad}, this preference becomes as large as 0.67eV. So at 0.0V relative to NHE, H_3O^+ would first get adsorbed onto the surface leading to H_{ad}, which would then react with O_{ad}, either directly or indirectly (through a H_2O bridge). The preference is flipped at electrode potentials larger than 0.67V. Consequently, at low potential (0–0.67V versus NHE) the reaction proceeds as $H^+ \rightarrow H_{ad} \rightarrow OH_{ad}$, while at higher potential (> 0.67V versus NHE) the reaction proceeds as $H^+ \rightarrow OH_{ad}$. The reversible potential between H^+, O_{ad} and OH_{ad} is -0.27V relative to NHE, while the reaction $H_{ad} + O_{ad} \rightarrow OH_{ad}$ (through a H_2O bridge) is always endothermic on Pt surface.

Using similar methods, we were able to determine the PES at various electrode potentials. Figure 4-4 shows the PES for formation of OH from H_{ad} at 0.0V and from H^+ at 0.8V and 1.23V versus NHE. The hypothetical PES starting from H+ at NHE potential is also provided, although H_{ad} is the preferred form. At 0.0V versus NHE, the barrier is

0.68eV. As potential increases, barrier increases and OH formation from H^+ and H_{ad} becomes more unfavorable. At the ORR condition (0.8V), it has a barrier of 0.70eV.

As shown in our previous paper[66], the barrier for direct formation of OH_{ad} from O_{ad} and H_{ad} is 0.97eV. Since the barrier for $H^+ + e \rightarrow H_{ad}$ is always smaller than that of $H^+ + O_{ad} \rightarrow OH_{ad}$, the H^+/H_{ad} balance could be viewed as always being at equilibrium. The one-step reaction $H^+ + O_{ad} \rightarrow OH_{ad}$ is preferred, because the barrier is always smaller than 0.97eV. Thus the actual OH formation mechanism has two different regions:

- For 0.0V to 0.34V relative to NHE, it is $H^+ \rightarrow H_{ad} \rightarrow OH_{ad}$ (through a H_2O).
- For > 0.34V relative to NHE, it is $H^+ + O_{ad} \rightarrow OH_{ad}$

Water formation reaction $H_3O^+ + OH_{ad} \rightarrow H_2O_{ad}$

Similarly, the reaction enthalpy from a free H^+ in solution can be directly calculated using the cycle

$H^+(solv) + OH_{ad}(solv) \rightarrow 1/2H_2(gas) + OH_{ad}(solv) \rightarrow H_2O_{ad}(solv)$. (**)

The reaction enthalpy ΔH = -1.02eV on Pt surface. At ORR condition, however, it increases to -0.22eV at 0.8V versus NHE. Taking into the interaction between H_3O^+ and the surface OH_{ad}, the reaction enthalpy becomes -1.15eV. Again, H_{ad} is the preferred form at NHE potential by 0.69eV, lowering the reaction enthalpy to -0.46eV. As electrode potential increases to above 0.69eV, H_3O^+ directly react with OH_{ad} to form H_2O_{ad}.

Due to the exothermic nature of the reaction, it does not have a barrier in the range of 0.0–1.15V relative to NHE. The PES of the reaction at 0.0 starting from H_{ad} and at 0.8, 1.23V relative to NHE are shown in Figure 4-9. We also included a hypothetical PES

starting from H^+. The reaction enthalpies and barriers at different electrode potential are plotted in Figure 4-10.

Summary of specific reactions

These results showed that OH_{ad} formation is endothermic with a large barrier. Indeed the reverse reaction is exothermic and fast with a barrier of 0.17eV at 0.8V versus NHE. However H_2O formation from OH_{ad} and H^+ is exothermic and efficient with no barrier. These two effects should limit the amount of OH_{ad} on the surface when the H^+ concentration is high. Comparing the OH formation barrier from O_{ad} + H^+/H_{ad} and that from O + H_2O, we see that O hydration is much preferred with a barrier of 0.50eV. The OH_{ad} formed then quickly reacts with H^+ to form H_2O.

On the other hand if H^+ is limited, the surface will have OH_{ad}. Combining the OH dissociation and the H_2O formation gives the overall reaction

$2OH_{ad}$ ➔ $O_{ad} + H_2O$.

As we showed in our previous paper, O_{ad} can react with surface H_2O to form two OH_{ad} with a barrier of 0.50eV (solvated). This implies that on the Pt surface, OH_{ad}, O_{ad} and H_2O_{ad} should be in equilibrium. An H^+ approaching the surface would reacts with OH_{ad} to form H_2O irreversibly. The overall picture of the ORR on Pt is hence

O_2 ➔ O_{ad} ➔ OH_{ad} ➔ H_2O .

Summarizing, the three factors governing the overall kinetics are

(1) dissociation of O_2

(2) forming OH_{ad} from O_{ad}

(3) the formation of H_2O from OH_{ad}.

Most metals in columns 8–11 have low or no barrier for (1), except Au. For (2), only Au and Ag have a favorable reaction enthalpy perspective from O_{ad} + H^+. All other metals go through O hydration. For (3), our earlier results showed that only Au, Ir, Os, Pt, and Pd would be able to form H_2O from OH_{ad} and H^+ at above 0.8V versus NHE, which agrees with experimental studies showing only Pt and Pd are effective catalysts.

To improve ORR catalysts, we want a weaker O binding energy to make the OH formation easier. Also a weak OH binding energy is desired if the surface is not composed of Pt or Pd to make H_2O formation exothermic at above 0.8V versus NHE.

Optimal power

Figure 4-6 shows the barriers of the various ORR reaction steps (1), (3), and (4) from Figure 4-5, Figure 4-8, and Figure 4-10, as compared with the potential independent barrier for (2). We see that the RDS is reaction (c) in all cases. Writing the total current as

$$I = AExp(-E_{a,RDS}(V)/RT)$$

the total power is

$$P = IV = AVexp(-E_{a,RDS}(V)/RT)$$

which is plotted as a function of V in Figure 4-11. Here we see that the optimal potential is predicted to be V= 0.68V. Normally, the ORR fuel cell is operated at 08V relative to NHE. Our results suggest, however, that an operating potential of 0.68 would lead to a power 2.8 times larger than for 0.8V versus NHE.

This model can help assess the impact of potential improvements. For example, if we can modify the catalyst to decrease the barrier for forming OH_{ad} from H_{ad} by 0.05eV, Figure 4-11 shows that the power would improve by a factor of 2.81 and the optimal

operating potential would drop to V_{op} = 0.60. Such a change in the barrier could be also be achieved by making H_{ad} less stable by 0.10–0.40eV, perhaps by alloying. (For example, Ni binds H 0.34eV less strongly than Pt, and it is well known that Pt_3Ni leads to improved rates[63]).

Alternatively we might destabilize H^+ relative to H_{ad} by modifying the solvent (lowing the dielectric constant). Thus changing the dielectric constant from 80 to 40 would destabilize H^+ by 0.12 eV.

Comparison to previous methods

Norskov, etc.[17], tried to handle the effect of electrode potential by approximating the energy of the electron as the Fermi level calculated by $E_{fermi} = E_{fermi,\ NHE} + \Delta E$ (relative to NHE) and using the fact that $G(1/2H_2) = G(H_3O^+) = 0$. Then the energy of each intermediate can be calculated directly. The method has been used to predict the overpotential of oxygen reduction reaction from the reaction enthalpy perspective. However this method can only handle one unit of electron transfer. For transition states (TS), the charge of the system is undetermined, so this method is not applicable for barrier calculations.

In contrast, Anderson et al.[76,81] used a finite system and assumed that the electron transfer step is the transition state. Thus they scanned the potential energy surface (PES) of the diatomic association reaction Pt + H ➔ PtH and Pt + H^+ ➔ PtH^+ and assumed that a configuration serves as the TS when the Fermi level coincides with the average of ionization potential (IP) and electron affinity (EA). The method gives an approximate barrier at various potentials. But the assumption of a diatomic model and the Fermi level makes this unreliable for a real ORR system.

Furthermore, both methods ignore solvent effects, likely an essential factor for the ORR in a fuel cell[66]. Assuming a +1 charge for the system, H_3O^+ ➔ $H_2O + H_{ad}^+$ is barrierless because of the high energy from charge separation in H_3O^+. In comparison, aqueous H_3O^+ is stabilized by a huge solvation energy of 11.92eV[82–83]. The Norskov approach, bypasses this problem by using the $G(H_2)=G(H_3O^+)$, but this can only work with the starting and ending states. The Anderson approach can be used to calculate the solvent effect for the cluster, but this is likely very different than for a full electrode surface. Recently, we developed a new approach[66] for using the Poisson Boltzmann continuum model[23–24] to predict solvent stabilization. We found that the calculated implicit solvation energy agrees well with known explicit solvation[66] for ORR system on Pt. We found that including solvation leads to a substantial change in the favored mechanism for ORR on Pt[84].

Conclusion

In this study, we studied systematically the three typical reactions involving electron transfer for ORR. The results showed that H_{ad} is preferred at 0.44V or lower relative to NHE, while H^+ is preferred at higher electrode potential. At the ORR potential, OH formation from H^+ and O_{ad} is the preferred mechanism rather than direct formation from H_{ad} and O_{ad}, but it still bears a barrier of 0.70eV at ORR potential. Considering the O_{ad} hydration barrier of 0.50eV, O_{ad} hydration is the major source of OH_{ad} on the surface.

H_2O formation poses a fundamental limit for ORR on metals towards higher operating voltage. On Pt, the 1.15eV reversible potential makes it impossible to develop Pt-based materials operating at higher than 1.15eV. For the current developments for

substitutes of Pt, with this limitation, metals with stronger binding energy with OH_{ad} can be directly eliminated from the candidate list of better ORR catalysts. Only Pd-, Rh-, and Au- based materials will have fair enough H_2O formation efficiency.

Tables and Figures

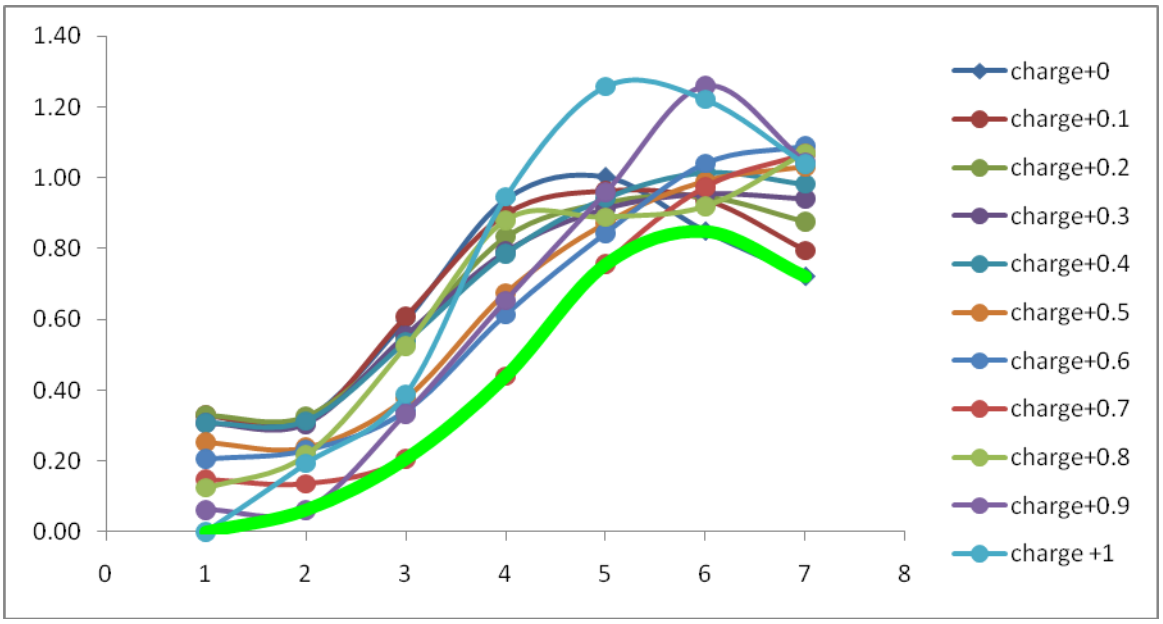

Figure 4-1. Reaction path for $O_{ad} + H^{+} + e \rightarrow OH_{ad}$ in which the electrode potential is kept fixed. The bright green line shows the optimal path.

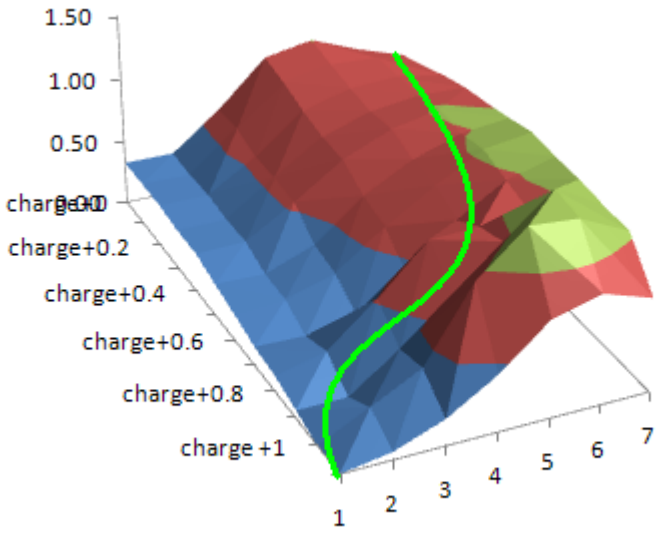

Figure 4-2. Contour plot for the energy surface for the reaction $O_{ad} + H^+ + e \rightarrow OH_{ad}$ in which charge and OH formation are considered as two independent coordinates. The green curve gives an optimal reaction path at +1.0 electrode potential.

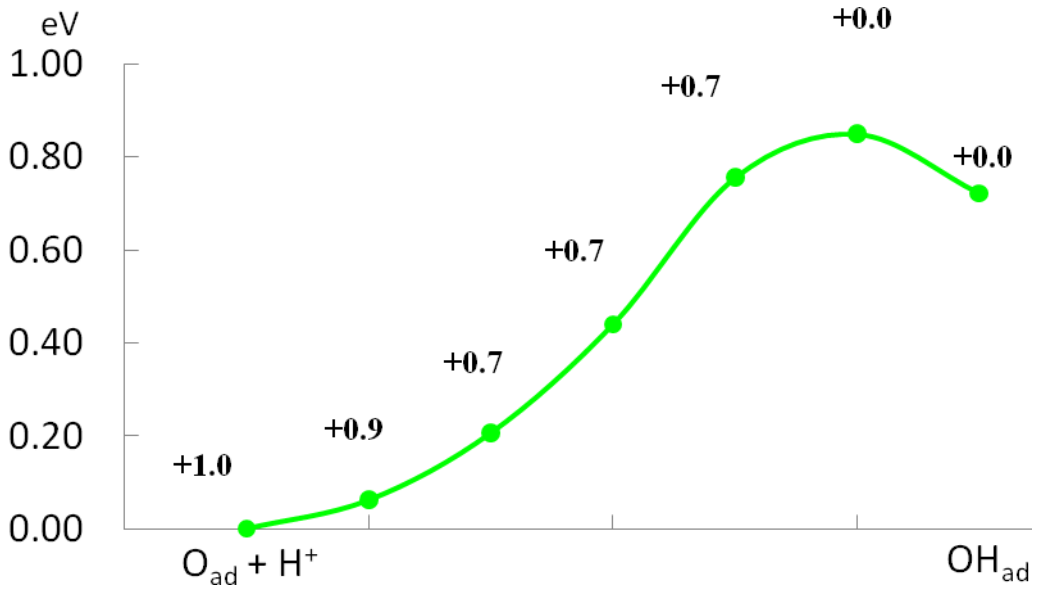

Figure 4-3. The optimal reaction PES at electrode potential of +1.0V versus NHE where at each point the charge is indicated

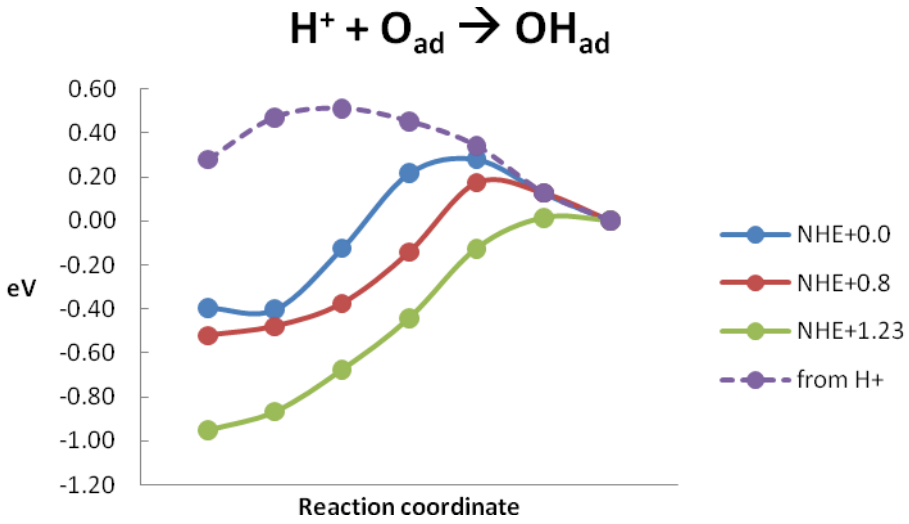

Figure 4-4. Optimal PES of $H^+ + O_{ad}$ ➔ OH_{ad} for various electrode potentials. Each line in this plot represents the "green" line selected from Figure 4-1, Figure 4-2, and Figure 4-3. In the NHE line, the reaction starts with H_{ad} because that is below the reversible potential of H^+ ⇔Had and hence H_{ad} is the preferred form (see the corresponding section for details). For simplicity, here we show only the three typical cases and an imaginary line supposing reaction from H^+.

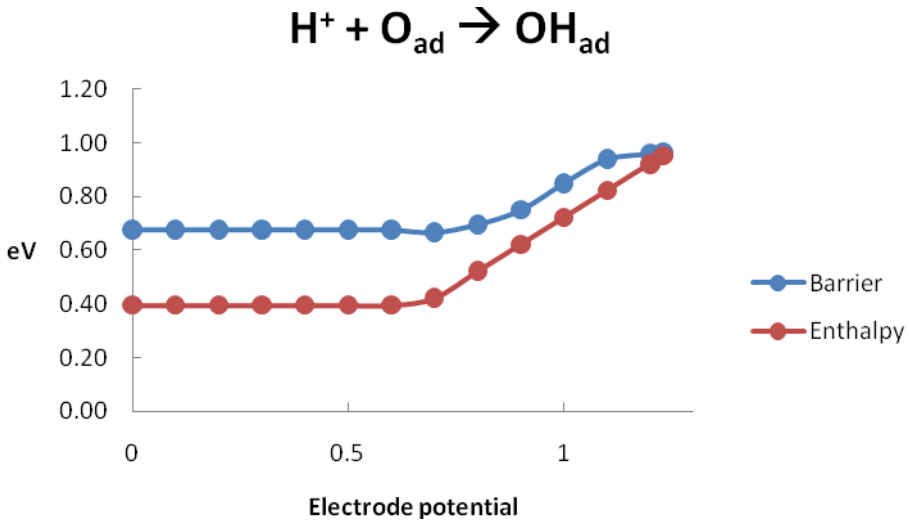

Figure 4-5. Potential dependent barrier for $H^+ + O_{ad}$ ➔ OH_{ad}. Each point in the barrier line represents the TS point (highest energy point in Figure 4-4), while each point in the enthalpy curve represents the difference between the starting and ending point in Figure 4-4.

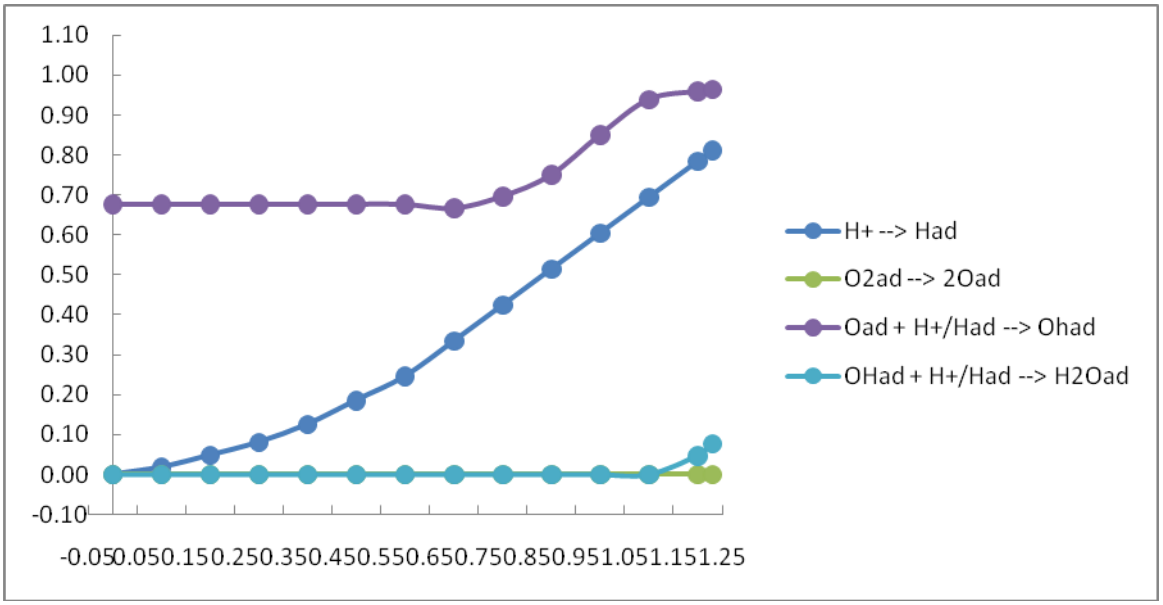

Figure 4-6. Barriers of reaction (1)–(4), the four steps involved in the ORR. In general, all barriers increase as electrode potential increases. OH formation dominates the ORR reaction.

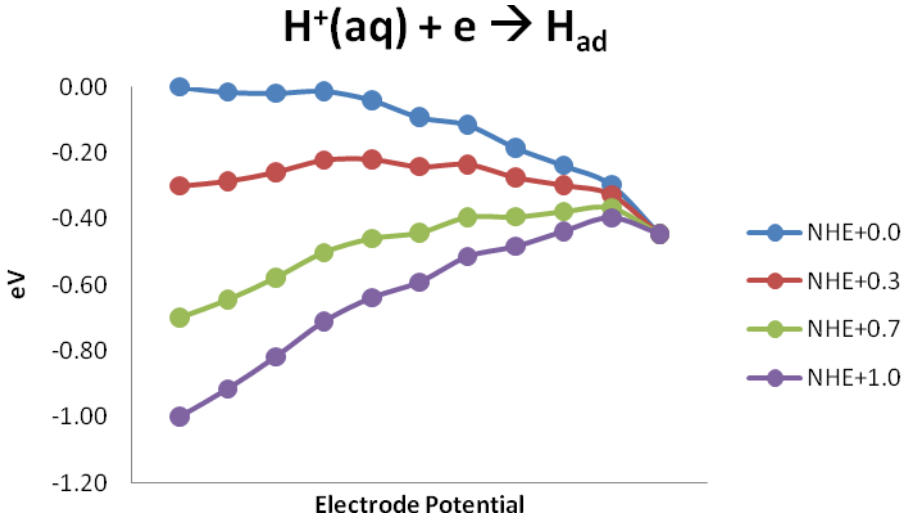

Figure 4-7. Potential dependent PES for H^+ ➔ H_{ad}

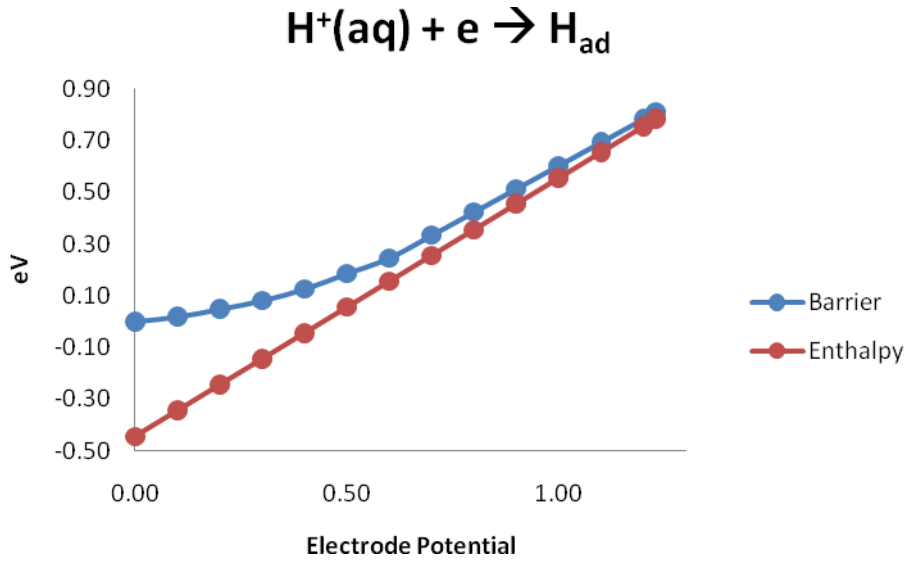

Figure 4-8. Potential dependent barriers for H^+ ➔ H_{ad}

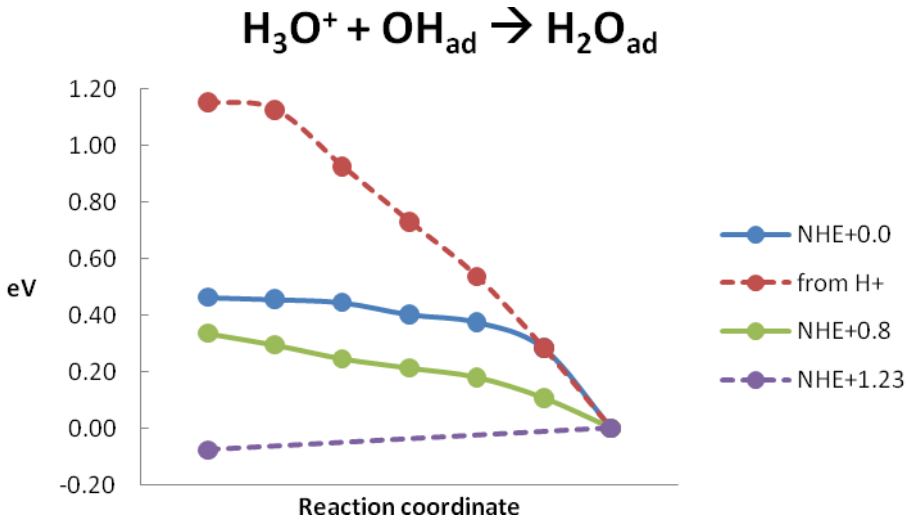

Figure 4-9. Potential dependent PES for H_2O formation

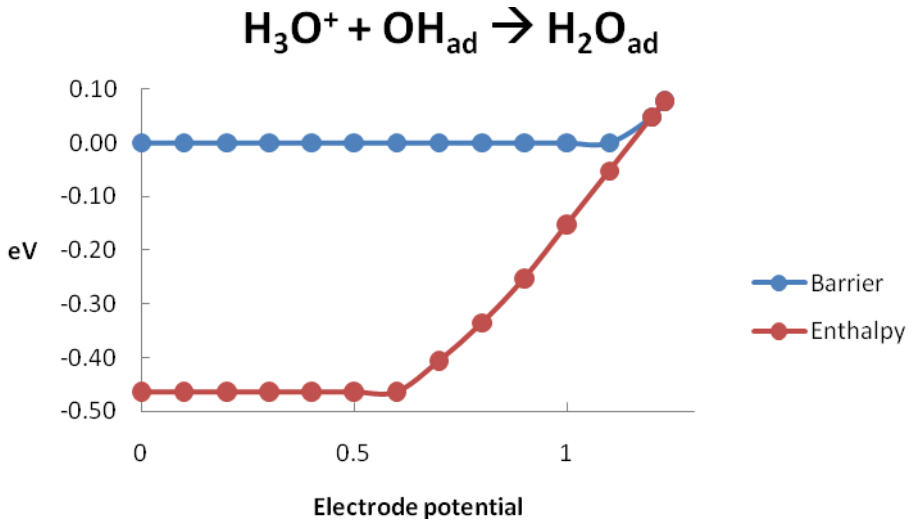

Figure 4-10. Potential dependent barrier for H_2O formation

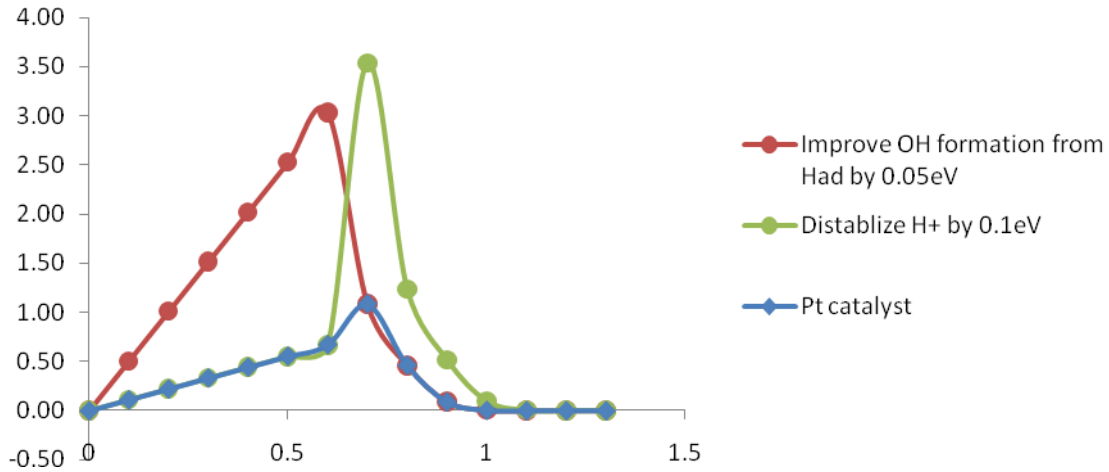

Figure 4-11. The power output as a function of the electrode potential. Here we also consider the impact of small changes in the energetics.

Chapter 5 Density Functional Studies of the Fuel Cell Oxygen Reduction Reaction on Co and Ni Surfaces

Abstract

We calculated the binding preferences of various intermediates involved in the oxygen reduction reaction (ORR) on the closest packed surfaces of Co (0001) and Ni (111). In addition we calculated the barriers for all plausible steps for all five ORR pathways that have been discussed or suggested on these surfaces. These calculations were carried out under two conditions:

- hydrophobic or gas phase, assuming the Teflon part of the Nafion electrolyte to be in contact with the catalyst surface, and
- hydrophilic for the part of the catalysts exposed to the water channel of the Nafion.

These studies were undertaken as part of a project to determine how various parts of the ORR are affected by choice of the metal or solvent. Both Ni and Co lead to huge H_2O formation barriers (1.00eV for Ni and 1.43eV for Co), mainly due to the very large binding energy of OH_{ad} to these electropositive metals. To complete the ORR, Co and Ni must be combined with a metal having a low H_2O formation barrier such as Pt or Au.

Introduction

The inefficiency of the oxygen reduction reaction (ORR) is a key impediment for commercial use of PEMFC in automobiles[1–4]. The best current catalysts are still Pt and the Pt_3Ni[63] and Pt_3Co alloys[62]. A great amount of experimental research has been carried

out searching for improved catalysts, but progress has been slow. Consequently we have embarked on a project to systemically examine the various possible ORR reactions, first on various pure transition metals and then on the various alloys. The hope is that these systematic studies may point the way to build alloys that can achieve fast kinetics and stability. Our first such systematic study[84] was on Pt and Pd where we discovered a new mechanism, involving hydration of surface oxygen, O_{ad}, as the rate determining step (RDS) for ORR on Pt, (E_a = 0.50 eV). This suggests a strategy for improving the ORR efficiency by alloying Pt with an element that could decrease the hydration barrier. Indeed we show here that of the 12 metals in columns 8-11 of the periodic table the two with the lowest hydration barriers are Ni (E_a = 0.48) and Co (E_a = 0.62). In this study, we study systematically all possible ORR mechanisms on Ni and Co to learn how they affect various mechanisms of ORR and why alloying with Pt leads to reduced barriers.

Methodology

In this study, the Ni and Co catalysts were modeled as a slab infinite in two directions (a) and (b) and finite in the third direction (c). We consider a 3×3 supercell of the (111) surface (9 atoms) that is six layers thick (54 atoms). The top two layers are allowed to relax, representing the active surface while the bottom four layers are fixed, representing the bulk side of the surface. The same model was applied in previous studies on Pt[66].

All calculations employed the kinetic and exchange-correlation DFT functional were developed by Perdew, Burke, and Ernzerhof (PBE) [30]. We used the Seqquest[29] implementation with an optimized double-zeta plus polarization Gaussian type basis set contracted from calculations on the most stable unit cell of the pure elements. We used

the small-core angular-momentum-projected norm-conserving nonlocal effective core potentials[34–37] (pseudopotentials) to replace the core electrons. Thus, the neutral Ni atom was described with 16 explicit electrons (six 3p, one 4s, and nine 3d in the ground state), while neutral Co has 15 electrons (the comparison calculations with Pt included the 5p, 5d, 6s electrons on the Pt, so neutral Pt has 16 electrons). The real space grid density was 5 points per angstrom, while the reciprocal space grid was 5×5×0 for slab calculations. All calculations allowed the up-spin orbitals to be optimized independently of the down-spin orbitals (spin-unrestricted DFT). The two periodic cell parameters are based on the optimized Co and Ni bulk structure (which are 2.6% and 1.4% smaller than the experimental value).

The implicit solvation of the water phase employed a continuum model based on the Poisson-Boltzmann approximation[23–25,38]. All reaction pathways were determined using the nudged elastic band[55–56] method and solvent effects were included for each point along the path.

Results and Discussion

Binding sites and energies

For the closed packing surfaces (111 for Ni and 0001 for Co), we find [14,66] four types of binding sites to be important:

- top site (μ^1),
- bridging site (μ^2),
- fcc hollow site (μ^{3f}), at the C site when the top 2 closest packed layers are AB,
- hcp hollow site (μ^{3h}) at the A site when the top 2 closest packed layers are AB.

Thus our first step was to determine the preferred binding sites for each intermediate species that might plausibly be involved in the ORR on Ni and Co. The binding energies for H, O, O_2, OH, OOH, H_2, and H_2O_2 are shown in Table 5-1. The binding sites are illustrated in Figure 5-1.

Generally, Ni and Co surfaces have much stronger interaction with electronegative species than Pt. Thus:

- $BE_{gas}[O_{ad}]$ = 5.28eV for Co (μ^{3h}) gas phase and $BE_{sol}[O_{ad}]$ = 5.88 eV for Co (μ^{3h}) in water solvent.
- $BE_{gas}[O_{ad}]$ = 4.84eV for Ni (μ^{3f}) gas phase and $BE_{sol}[O_{ad}]$ = 5.37 eV for Ni (μ^{3f}) in water solvent.

(For comparison, $BE_{gas}[O_{ad}]$ = 3.59eV on Pt (μ^{3f}) gas phase and $BE_{sol}[O_{ad}]$ = 4.28 eV for Pt (μ^{3f}) in water solvent.)

This makes O 1.69eV and 1.25eV more stable on Co and Ni than Pt. Solvent effect helped balance the difference, leading to a smaller, yet still huge, difference of 1.54eV and 1.04eV for Co and Ni, respectively.

Similarly, Co and Ni also bind stronger with OH as compared with Pt. Thus

- $BE_{gas}[OH_{ad}]$ = 3.56 eV for Co (μ^{3h}) gas phase and $BE_{sol}[OH_{ad}]$ = 3.83 eV for Co (μ^{3h}) in water solvent, and
- $BE_{gas}[OH_{ad}]$ = 3.13 eV for Ni (μ^{3c}) gas phase and $BE_{sol}[OH_{ad}]$ = 3.44 eV for Ni (μ^{2}) in water solvent,

as compared with BE_{gas} $[OH_{ad}]$ = 2.23 eV on Pt (μ^{2}) gas phase and BE_{sol} $[OH_{ad}]$ = 2.71 eV for Pt (μ^{1}) in water solvent.

However H_2O does not have strong binding with any of the metals.

- BE_{gas} [H_2O_{ad}] = 0.21 eV for Co (μ^1) gas phase and BE_{sol} [H_2O_{ad}] = 0.55 eV for Co (μ^1) in water solvent, and
- BE_{gas} [H_2O_{ad}] = 0.36 eV for Ni (μ^1), gas phase and BE_{sol} [H_2O_{ad}] = 0.70 eV for Ni (μ^1) in water solvent,

as compared with BE_{gas} [H_2O_{ad}] = 0.21 eV on Pt (μ^1) gas phase and BE_{sol} [H_2O_{ad}] = 0.59 eV for Pt (μ^1) in water solvent.

On the other hand, H binds more weakly to Ni than to Pt. H binds as strongly to Co as to Pt.

- BE_{gas} [H_{ad}] = 2.79 eV for Co (μ^{3c}) gas phase and BE_{sol} [H_2O_{ad}] = 2.85 eV for Co (μ^{3c}) in water solvent, and
- BE_{gas} [H_{ad}] = 2.64 eV for Ni (μ^{3c}), gas phase and BE_{sol} [H_2O_{ad}] = 2.72 eV for Ni (μ^{3c}) in water solvent,

as compared with BE_{gas} [H_2O_{ad}] = 2.78 eV on Pt (μ^1) gas phase and BE_{sol} [H_2O_{ad}] = 2.86 eV for Pt (μ^1) in water solvent.

This implies that at ORR condition, it will be harder to get form H_{ad} from H^+ in the solvent for Co. This makes H_{ad} less available for all reactions involving H_{ad}. As discussed in the supplemental mater of our previous paper[84], the energy cost can be estimated by using the method developed by Norskov, etc.[17], as

$H_3O^+ \Leftrightarrow 1/2H_2$ (gas) $\rightarrow$ H (gas) $\rightarrow H_{ad}$.

Using our PBE bond dissociation energy of 2.31eV for $1/2H_2$, the energy cost is 2.31 $-BE_{sol}$ [H_{ad}] + $\boldsymbol{\mathcal{V}}$, where $\boldsymbol{\mathcal{V}}$ is the potential of the cathode relative to normal hydrogen

electrode (NHE). Consequently, at 0.0V relative to NHE, the energy cost to get H_{ad} is exothermic by -0.54eV, -0.41eV, and 0.-51eV for Co, Ni, and Pt, respectively. Thus assuming an operating voltage of 0.80V versus NHE, the H^+ ➔ H_{ad} becomes endothermic with reaction enthalpy of 0.26eV, 0.39eV, and 0.29eV for Co, Ni, and Pt respectively. These barriers are lower than that of our calculated RDS barrier.

O_2 binds much stronger to Co and Ni, as compared with Pt. Thus:

- BE_{gas} [O_{2ad}] = 1.78 eV for Co (μ^{3c}) gas phase and BE_{sol} [O_{2ad}] = 2.43 eV for Co (μ^{3c}) in water solvent, and
- BE_{gas} [O_{2ad}] = 1.51 eV for Ni (μ^{3c}), gas phase and BE_{sol} [O_{2ad}] = 1.51 eV for Ni (μ^{3c}) in water solvent,

as compared with BE_{gas} [O_{2ad}] = 0.42 eV on Pt (μ^1) gas phase and BE_{sol} [O_{2ad}] = 0.83 eV for Pt (μ^1) in water solvent.

Since binding O_2 to the surface must compete with H_2O for space, the strong binding for O_2 suggests that for Ni and Co, H_2O flooding would not block the ORR.

OOH binds more strongly to Ni and Co than Pt. Thus:

BE_{gas} [OOH_{ad}] = 1.73 eV for Co (μ^1) gas phase and BE_{sol} [OOH_{ad}] = 2.24 eV for Co (μ^1) in water solvent, and

BE_{gas} [OOH_{ad}] = 1.68 eV for Ni (μ^1), gas phase and BE_{sol} [OOH_{ad}] = 2.14 eV for Ni (μ^1) in water solvent,

as compared with BE_{gas} [OOH_{ad}] = 1.02 eV on Pt (μ^1) gas phase and BE_{sol} [OOH_{ad}] = 1.47 eV for Pt (μ^1) in water solvent.

Taking into account the strong binding energy of O_2 and H, it is much harder to form OOH on Ni and Co surfaces. Moreover, the OOH_{ad} formed is expected be much easier to dissociate. Thus for Ni and Co, OOH formation and dissociation does not serve as the lower barrier process to dissociate O_2 that it does for Pt.

Simply by comparing the binding energies, we would expect Co and Ni to have a smaller O_2 dissociation barrier due to the strong exothermicity. For the same reason, the OH formation and H_2O formation barrier will be higher for Ni and Co. The calculated barriers for all seven steps involved in ORR84 are discussed next.

Reaction Barriers and Mechanisms

Our previous research showed that six fundamental steps are involved in the various possible mechanisms, namely,

- O_2 dissociation: $O_{2ad} \rightarrow 2O_{ad}$
- OH formation: $O_{ad} + H_{ad} \rightarrow OH_{ad}$
- H_2O formation: $OH_{ad} + H_{ad} \rightarrow H_2O_{ad}$
- OOH formation: $O_{2ad} + H_{ad} \rightarrow OOH_{ad}$
- OOH dissociation: $OOH_{ad} \rightarrow OH_{ad} + O_{ad}$
- hydration: $O_{ad} + H_2O_{ad} \rightarrow OH_{ad} + O_{ad}$.

In putting these fundamental steps into an overall mechanism we can distinguish three categories:

- OO bond activation: This includes O_2 dissociation (a) and OOH formation (d) followed by OOH dissociation (e).
- OH Formation: This includes OH formation (b) and O hydration (f).
- OH consumption: This includes H_2O formation (c).

To make a good catalyst, a metal must be able to have a step with a low barrier in each of these three categories.

Starting from the preferred sites, we calculated the barriers for all six steps on Co and Ni. The barriers and the comparison with pure Pt are shown in Table 5-2.

Gas phase processes

OO bond activation: O_2 dissociation (step a) has much lower barrier on Co and Ni (0.00eV for Co 0.15eV for Ni as compared with 0.57eV for Pt) because of the much stronger O binding energy, As suggested from the relative binding energies, OOH formation (step d) is much less favorable on Co and Ni (E_a = 0.97eV and 1.52eV as compared with 0.30eV for Pt). In addition the OOH formed would dissociate immediately (step e). Thus OOH formation is the dominant mechanism on Pt but is not competitive with the direct O_2 dissociation for Co and Ni.

OH formation: OH formation (step b) on Co (E_a = 0.55eV) and Ni (E_a = 0.59eV) are much easier than on Pt (E_a = 0.74eV). So we expect the OH formation rate for step b on Ni and Co to be much faster than Pt on Co and Ni. O hydration on Ni and Co have larger barriers than Pt (0.48eV for Ni 0.47eV for Co compared to 0.23eV Pt). Comparing both methods, O hydration has a lower barrier for all of Co, Ni, and Pt. Hence O hydration is the preferred way.

OH consumption (step c): Due to the large stability of OH_{ad}, the formation of H_2O from OH becomes much harder on Co and Ni surfaces than on Pt. The H_2O formation barrier is 1.30eV on Co and 0.81eV on Ni as compared to the 0.14eV on Pt.

Putting all these steps together, for Co and Ni we have direct O_2 dissociation as the preferred way of breaking O_2, and O hydration as the main way of forming OH, followed by the H_2O formation. Hence the preferred mechanism is O_2-dis-hydr

- O_{2ad} ➔ $2O_{ad}$ [E_a = 0.00eV (Co), 0.15eV(Ni)]
- $O_{ad}+H_2O_{ad}$ ➔ $2OH_{ad}$ [E_{act} = 0.48 eV (Co), 0.47eV (Ni)]
- $OH_{ad} + H_{ad}$ ➔ H_2O_{ad} [E_{act} = 1.30 eV (Co), 0.81eV (Ni)]

So the RDS is H_2O formation with a barrier of 1.30eV on Co and 0.81eV on Ni. As comparison, the preferred mechanism on Pt is OOH-form-hydr mechanism.

- $O_{2ad} + H_{ad}$ ➔ OOH_{ad} [E_a = 0.30eV on Pt]
- OOH_{ad} ➔ $O_{ad} + OH_{ad}$ [E_a = 0.12eV on Pt]
- $O_{ad} + H_2O_{ad}$ ➔ $2OH_{ad}$ [E_a = 0.23eV on Pt]
- $OH_{ad} + H_{ad}$ ➔ H_2O_{ad} [E_a = 0.14eV on Pt]

The RDS for Pt is hence OOH formation with a barrier of 0.30eV.

Solution phase processes

O_2 dissociation: As discussed in our previous paper, O_2 dissociation benefits dramatically from solvent effects. In solvent the O_2 dissociation barriers become negligible for all three metals (0.00eV for Pt and Co, 0.04eV for Ni). For Ni and Co, the more stable O_{2ad} and H_{ad} lead to stronger solvent stabilization. Hence the solvent effect increases the barrier for OOH formation. The barrier is 1.24eV on Co and 0.62eV on Ni as compared to the 0.22eV on Pt. So, similar to the gas phase case, OOH formation is more difficult on Co and Ni than on Pt. With solvent, O_2 dissociation becomes the dominant way of activating O_2 on all three metals.

OH formation: Due to stronger solvent effect for O than for OH, solvation increases the barrier for direct OH formation. The barrier increases to 0.84eV for Co and 0.74eV for Ni as compared with the 0.97eV for Pt. O hydration is also more difficult with a barrier of 0.62eV on Co and 0.54eV on Ni as compared to the 0.23eV on Pt. Hence, O hydration dominates the direct OH as the main way of forming OH_{ad}.

OH consumption: OH_{ad} in general has stronger solvent effect then H_2O_{ad}. Consequently, H_2O formation has higher barrier when considering solvation. The barrier is 1.43eV on Co, 1.00eV on Ni, and 0.24eV on Pt.

Putting all these together, we have direct O_2 dissociation as the preferred way of dissociating the O=O bond, and O hydration as the preferred way of forming OH. The overall mechanism is hence:

- O_{2ad} ➔ $2O_{ad}$ [E_{act} = 0.00eV (Co), 0.04eV (Ni) and 0.00eV (Pt)]
- $O_{ad}+H_2O_{ad}$ ➔ $2OH_{ad}$ [E_{act} = 0.62eV(Co), 0.54eV (Ni) and 0.50 eV (Pt)]
- $OH_{ad} + H_{ad}$ ➔ H_2O_{ad} [E_{act} = 1.43eV(Co), 1.00eV (Ni) and 0.24 eV (Pt)]

H_2O formation is the RDS on Co and Ni, while O hydration is the RDS for Pt. The overall barriers for Ni and Co are 1.00eV and 1.43eV, respectively, as compared to the 0.50eV on Pt. Comparing with Pt we can see that Co and Ni are inferior as ORR catalysts because they can successfully reduce O_2 to OH but fail to remove the OH from the surface.

For Co and Ni, the high binding energy to O and OH makes Ni and Co good materials for reducing O_2 to OH. But this comes with the price that OH_{ad} is extremely stable and almost reluctant to have any further reaction, including forming H_2O. By comparison, Pt has reasonably strong binding with O but weaker binding with OH, making it easy for

OH to form H_2O and harder to form OH through O hydration. So the proper way of improving the ORR activity of Pt would be alloying with other metals to lower the O_{ad} binding energy and increase OH_{ad} binding energy to lower the O hydration barrier. Alloying with Co and Ni could be the reason for this improvement.

Discussion

Given that reactions involving O_2 might occur in the hydrophobic regions, while those involving H^+ might occur in hydrophilic regions, the best process for Co or Ni would be to dissociate O_2 in the hydrophobic region, forming OH with H_2O nearby, then migrate to the hydrophilic region and form H_2O. Of course it is well known that alloys of Co and Ni with Pt have excellent performance.

Conclusion

We studied the binding site preferences, reaction step barriers, and ORR mechanisms on Ni and Co surfaces using DFT calculations. The prefered mechanism for Ni and Co in gas phase is O_2-diss-hydr with an overall barrier of 1.30eV for Co and 0.81eV for Ni. H_2O formaton is the RDS for both metals. With solvation, the situation is worse, with an overall barrier of 1.43eV for Co and 1.00eV for Ni. Hence to have a good Co- or Ni-based catalyst, one needs to find a way to lower the H_2O formation barrier. Os could be a promising candidate with a stronger binder with Os and lower H_2O formation barrier.

Tables and Figures

Binding Energy (eV)		Gas			Solv		
Species	Binding Site	Pt	Ni	Co	Pt	Ni	Co
M-H	μ_1	-2.78	-2.32	-2.28	-2.86	-2.41	-2.37
	μ_{2*}	-2.69	-2.47	-2.64	-2.81	-2.54	-2.69
	μ_3-ccp	-2.70	-2.64	-2.79	-2.82	-2.72	-2.85
	μ_3-hcp	-2.66	-2.60	-2.76	-2.77	-2.67	-2.82
M-O	μ_1	-2.57	-3.32	-4.06	-3.19	-3.81	-4.67
	μ_2	-3.17	-4.37	-4.96	-3.84	-4.91	-5.56
	μ_3-ccp	-3.59	-4.84	-5.25	-4.28	-5.37	-5.86
	μ_3-hcp	-3.30	-4.69	-5.28	-3.93	-5.24	-5.88
$M-H_2$		0.22	0.28	0.22	0.17	0.25	0.18
M-OH	μ_1	-2.22	-2.68	-2.82	-2.75	-3.13	-3.27
	μ_2	-2.23	-3.09	-3.33	-2.61	-3.45	-3.68
	μ_3-ccp	-2.22	-3.13	-3.49	-2.57	-3.44	-3.81
	μ_3-hcp	-2.20	-3.11	-3.56	-2.54	-3.43	-3.83
$M-O_2$	bridge	-0.43	-1.40	-1.47	-0.75	-1.72	-1.98
	ccp	-0.42	-1.51	-1.78	-0.83	-1.97	-2.43
	hcp	-0.36	-1.47	-1.78	-0.74	-1.94	-2.39
M-OOH	μ_{1b}	-1.02	-1.68	-1.73	-1.47	-2.14	-2.24
	μ_{ic}	-0.92	-1.53	-1.65	-1.39	-2.01	-2.18

M-H_2O_2	bridge	-0.33	-0.55	-0.42	-0.69	-0.86	-0.73
M-H_2O	μ_1	-0.21	-0.36	-0.21	-0.59	-0.70	-0.55

Table 5-1. Binding energies (eV) of various ORR species on Pt, Co, and Ni

* μ_2 is not a stable site for H on Ni and Co.

	Barriers-gas			Barriers-solv		
Reaction Barriers	Pt	Ni	Co	Pt	Ni	Co
H_2 Dissociation	0.00	0.11	0.03	0.00	0.08	0.00
O_2 Dissociation	0.57	0.15	0.00	0.00	0.04	0.00
OH Formation	0.74	0.59	0.55	0.97	0.74	0.84
H_2O Formation	0.14	0.81	1.30	0.24	1.00	1.43
OOH Formation	0.30	0.52	0.97	0.22	0.62	1.24
OOH Dissociation	0.12	0.00	0.00	0.00	0.00	0.00
H-OOH dissociation	0.14	0.00	0.00	0.00	0.00	0.00
O hydration	0.23	0.47	0.48	0.50	0.54	0.62

Table 5-2. Reaction barriers for various steps involved in ORR

	Barriers-gas			Barriers-solv		
Reaction Barriers	Pt	Ni	Co	Pt	Ni	Co
O_2-diss	0.74	0.81	1.30	0.97	1.00	1.43
OOH-form	0.74	0.81	1.30	0.97	1.00	1.43
O_2-diss-hydr	0.57	0.81	1.30	0.50	1.00	1.43
OOH-form-hydr	0.30	0.81	1.30	0.50	1.00	1.43
H-OOH Dissociation	0.30	0.81	1.30	0.24	1.00	1.43
Overall	0.57	0.81	1.30	0.50	1.00	1.43

Table 5-3. Overall barriers for each step

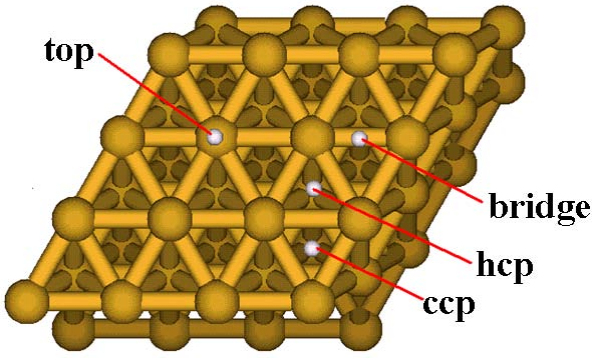

Figure 5-1. Binding sites on FCC closed packing surface (111 surface)

Chapter 6 Density Functional Studies on Oxygen Reduction Reaction on Cu, Ag, and Au Surfaces

Abstract

We study theoretically the binding preferences of various intermediates involved in oxygen reduction reaction (ORR) on the (111) surface of Cu, Ag, and Au. Barriers for all necessary steps for all five possible pathways known on Pt are calculated. Au shows a high O_2 dissociation barrier of 1.40eV (aq) which prevents the ORR. We find that Ag and Cu have low O_2 dissociation barriers (0.00eV and 0.12eV) and O hydration barriers (0.12eV and 0.35eV), but that they suffer from a huge H_2O formation barrier (0.98eV and 1.08eV) as compared with Pt (0.30eV). This suggests that phase-separated Ag/Pt alloy or Cu/Pt alloy might be promising candidates, since O_2 can first dissociate and form OH on Ag/Cu, and then the OH can migrate to the Pt area and finish the H_2O formation (which is much easier on Pt).

Introduction

The oxygen reduction reaction (ORR) has been studied extensively in the past few decades because it is among the key problems in creating an economically efficient hydrogen fuel cell[1–4]. Great efforts have been made to synthesize different metal catalysts to accelerate the slack kinetics of ORR [62–63].

Despite the fruitful experimental studies on many metals and alloys, most theoretical studies have only focused on Pt and Pt-related materials[16–17,85–86]. We consider it

important to understand why all other metals have inferior performance in catalyzing ORR and have embarked on a series of theoretical studies to elucidate the mechanisms and kinetics of other systems.

Previously, we successfully modeled the ORR on a Pt surface with solvent effect and electrode potential consideration[66,87]. We found five mechanisms for Pt (111) surface[84]. We also compared the kinetics of ORR on Pt with that on Ni and Co, where we attribute the great performance of Pt to the less-stable OH_{ad} and the corresponding lower H_2O formation barrier[88]. Herein, we studied systematically the ORR on Ag, Au, and Cu surfaces to explore why these three metals cannot serve as ORR catalysts.

Methodology

The closed packing surface (111) is modeled as a c(3x3) slab with six layers of atoms, big enough to eliminate the interaction between images of the adsorbents. The four bottom layers are fixed to mimic the bulk/support side of the catalyst while the top two layers are relaxed to cover the interaction between the surface and the adsorbates. All calculations are carried out by using Seqquest DFT code[29], where the Kohn-Shan equation is self-consistently solved under periodic boundary conditions. We used norm-conserving pseudo potentials[34–37] for the core electrons and Gaussian type orbitals for the valence electrons. The solvent effect of the system is estimated by using the implicit solvent method we developed earlier, which is based on the Poisson-Boltzmann continuum model[23–25,38,66]. Mulliken charge from Seqquest is taken as input for the APBS solver.

Results and Discussion

Binding site preference and binding energies

Similar to the case of Pt, all the three metals involved in this research have FCC structure. On the (111) surface, there are in general four unique binding sites, μ_1, μ_2, μ_3-ccp, and μ_3-hcp. μ_1, μ_2, and μ_3 indicate how many surface metal atoms the adsorbate is bonded to at the same time. The binding energies for different species on Ag, Au, and Cu as compared with Pt are shown in Table 6-1.

H prefers to bind to μ_3-ccp sites with a binding energy of 2.08eV, 2.12eV, and 2.44 eV in gas phase on Ag, Au, and Cu, respectively. The binding energy is smaller than the 2.72eV of Pt. The small binding energy will make the reaction $H^+ \rightarrow H_{ad}$ unfavorable under ORR conditions, making it a great challenge for ORR on Ag, Au, and Cu. The gas phase H binding energy on Au agreed with the 2.11eV of Barton, etc.[89].

O prefers μ_3-ccp sites on Ag, Au, and Cu with a binding energy of 3.06eV, 2.41eV, and 4.23eV in gas phase, respectively. Comparing with the 3.66eV on Pt, the binding is stronger for Ag and Cu but dramatically weaker for Au. This agrees with the fact that Au is noble because of the weak binding with O. Dissociative adsorption of O_2 on Au is simply endothermic. The gas phase binding energy of 2.41eV on Au agrees with earlier theoretical work of 2.53eV by Mavrikakis, etc. [90].

OH prefers μ_2 and μ_3 sites on Ag, Au, and Cu with similar binding energies. μ_1 sites are less stable by 0.46eV, 0.14eV, and 0.38eV than the optimum binding sites. This property is unique on the three metals because on Pt, all sites have similar binding energy. OH binding energy of Au agreed with the 1.90eV calculated by Barton, etc.[89].

O_2 prefers hcp sites on Cu with a binding energy of 0.57eV, stronger than the 0.46eV on Pt. Au does not have an effective binding with O_2, which agrees with earlier experiments[91–92] and calculations[90,93]. Ag can only weakly adsorb O_2 on the μ_3 with a binding energy of 0.13eV.

Our calculations showed that OOH and H_2O can only bind with top sites, which agrees with previous research[94–95]. For OOH, the binding energy is 0.65eV on Ag, 0.35eV on Au, and 1.18eV on Cu, weaker than the 1.06eV on Pt. For H_2O the binding energy is 0.50eV on Ag, 0.48eV on Au, and 0.54eV on Cu with solvent effect as compared with the 0.58eV on Pt. It agreed with the 0.45–0.58eV Michaelides, etc.[94], got from a more accurate simulation using explicit water. The corresponding binding energies without solvent also agrees well with their result[94] and the 0.19eV, 0.12eV, and 0.26eV reported recently by Wang, etc. [95].

In summary, binding with OH, O_2, and OOH is stronger on Cu than on Pt but is weaker on Au and Ag. It agrees with the fact that Cu is not noble. H binds more weakly on all of Ag, Au, and Cu as compared with Pt.

Barriers for reaction steps and the pathways

There are seven possible steps involved in the ORR reaction, as shown in Figure 6-1. O_2 can directly dissociate into $2O_{ad}$ or it may react with H_{ad} to form OOH_{ad}, which dissociates into O_{ad} and OH_{ad}. O_{ad} then can either react with H_{ad} directly or go through hydration to form OH_{ad}. The final step of ORR is the formation of H_2O from OH_{ad} and H. So the six steps involved in the ORR are O_2 dissociation, OOH formation, OOH dissociation, OH formation, O hydration, and H_2O formation. The barriers are shown in Table 6-2.

We can see that O_2 dissociation is difficult on Au, with a barrier of 2.12eV in the gas phase. Solvation helps lower the barrier to 1.40eV but it is still a barrier that is impossible to overcome at the operating temperature. For Ag, the barrier is 0.93eV in gas phase, implying that the dissociation of O_2 on Ag surface will not happen in gas phase. Solvation helps to stabilize the formed O_{ad} and lowers the barrier to 0.05eV. On Cu, the O_2 dissociation barrier is 0.15eV in gas phase and 0.02eV in solution. So O_2 dissociation would be fast on Ag and Cu, similar to the case of Pt.

OOH formation has a barrier of 0.24eV, 0.00eV, and 0.42eV on Ag, Au, and Cu, respectively, similar to the 0.19eV on Pt. The corresponding dissociation for OOH, however, is more difficult, with a barrier of 0.39eV on Ag and Cu and 0.58eV on Au. Comparing with the competing direct O_2 dissociation, we can see that, the preferred way of reducing O_2 on Au is OOH formation/dissociation, while the direct O_2 dissociation is preferred on Ag and Cu. The small barrier agreed with the previous belief that OOH formation is easy on Au clusters[93].

Formation of OH is much easier on Ag, Au, and Cu than on Pt, with barriers of 0.00eV, 0.16eV, and 0.00eV as compared to the 0.72eV in gas phase, respectively. With solvation the barrier increases to 0.00eV on Ag, 0.32eV on Au, and 0.08eV on Cu, mainly due to the strong solvation of O_{ad}. Comparing with the high barrier of 1.09eV on Pt surface, we can see that OH formation should not be a problem for all three of the metals.

O hydration is the alternative way of forming OH. O_{ad} reacts with H_2O to form $2OH_{ad}$ directly. On Pt, this is the rate-determining step (RDS), with a barrier of 0.50eV. On Ag,

Au, and Cu, the barriers are 1.29eV, 0.87eV, and 0.83eV, much higher than on Pt. We can see that direct OH formation is not preferred.

The formation of H_2O is more difficult on Ag, Au and Cu with a barrier of 0.86eV, 0.37eV and 0.87eV, much higher than the 0.17eV on Pt.

Mechanisms and overall barriers without solvation

Combining all the barriers, we can get the RDS barrier for the same five possible mechanisms as in our previous study[84]. The overall barriers are shown in Table 6-3.

On Ag and Au surfaces, OOH formation has a much lower barrier (0.21eV and 0.00eV on Ag and Au) than O_2 dissociation (0.78eV on Ag and 1.82eV on Au), hence mechanisms involving O_2 dissociation are as not likely to happen on both surfaces. The consequent OOH dissociation has a high barrier of 0.87eV on Ag and 0.88eV on Au. The following OH formation is barrierless on Ag and has only a small barrier of 0.10eV on Au. Consequently, O hydration is the dominant way of consuming O_{ad}, similar to the case of Pt. H_2O formation has a high barrier of 0.72eV on Ag and a low barrier of 0.29eV on Au. These lead to the OOH-form-hydr mechanism consists of OOH formation, OOH dissociation, formation hydration, and H_2O formation, as shown in equation 1a–1d. This is also the preferred mechanism of ORR on Pt in gas phase.

(1a) $O_2 + H_{ad} \rightarrow OOH_{ad}$ [E_a (Ag) = 0.21eV, Ea (Au) = 0.00eV, E_a (Pt) = 0.33eV]

(1b) $OOH_{ad} \rightarrow O_{ad} + OH_{ad}$ [E_a (Ag) = 0.87eV, E_a (Au) = 0.88eV, E_a (Pt) = 0.04eV]

(1c) $O_{ad} + H_2O_{ad} \rightarrow 2OH_{ad}$ [E_a (Ag) = 0.00eV, E_a (Au) = 0.10eV, E_a (Pt) = 0.22eV]

(1d) $OH_{ad} + H_{ad} \rightarrow H_2O_{ad}$ [E_a (Ag) = 0.72eV, E_a (Au) = 0.29eV, E_a (Pt) = 0.12eV]

The overall RDS is OOH dissociation with a barrier of 0.87eV on Ag and 0.88eV on Au, as compared to the 0.33eV on Pt.

On Cu, as comparison, O_2 dissociation (E_a = 0.11eV) is much easier than OOH formation (E_a = 0.29eV). Hence the predominant way of consuming O_2 is through direct O_2 dissociation. Similar to the case of Pt, Cu has lower barrier of O hydration (E_a = 0.24eV) than OH formation (E_a = 0.44eV), so the former is preferred. Combining the essential H_2O formation with a barrier of 0.98eV gives the O_2-dis-hydr mechanism.

(2a) O_2 ➔ $2O_{ad}$ [E_a (Cu) = 0.11eV]

(2b) $O_{ad} + H_2O_{ad}$ ➔ $2OH_{ad}$ [E_a (Cu) = 0.24eV]

(2d) $OH_{ad} + H_{ad}$ ➔ H_2O_{ad} [E_a (Cu) = 0.98eV]

The overall RDS is H_2O formation with a barrier of 0.98eV in the gas phase.

Mechanisms and overall barriers with solvation

As discussed in our previous studies[66,84], solvation dramatically changed the reaction barriers and the consequent preferred mechanism. So it's very important to see how solvation could change ORR activity on Ag, Au, and Cu.

On Ag surface O_2 dissociation becomes barrierless with solvation due to the strong solvent stabilization of O_{ad}. Cu also has a low barrier of 0.12eV. This is much lower than the 0.25eV and 0.31eV OOH formation barrier on Ag and Cu, hence direct O_2 dissociation is the dominant way of consuming O_2. For the same reason, OH formation from O_{ad} and H_{ad} becomes more difficult with solvation, with a barrier of 0.39eV and 0.59eV on Ag and Au, respectively. As comparison, O hydration has a lower barrier (0.12eV on Ag and 0.35eV on Au) and is hence the preferred way of consuming O_{ad}.

Combining with the last step, H_2O formation with a barrier of 0.98eV on Ag and 1.08eV on Cu, leads to O_2-dis-hydr-solv:

(step zero) H^+ ➔ H_{ad} [E (Ag) = 0.31eV, E (Cu) = -0.14eV, E (Pt) = -0.68eV]

(3a) O_2 ➔ $2O_{ad}$ [E_a (Ag) = 0.00eV, E_a (Cu) = 0.12eV, E_a (Pt) = 0.00eV]

(3b) $O_{ad} + H_2O_{ad}$ ➔ $2OH_{ad}$ [E_a (Ag) = 0.12eV E_a (Cu) = 0.35eV, E_a (Pt) = 0.49eV]

(3d) $OH_{ad} + H_{ad}$ ➔ H_2O_{ad} [E_a (Ag) = 0.98eV E_a (Cu) = 1.08eV, E_a (Pt) = 0.30eV].

The overall RDS is hence H_2O formation for both Ag and Cu with a barrier of 0.98eV and 1.08eV, making ORR impossible on both metals. As comparison, the RDS for Pt is O hydration which leads to an overall barrier of 0.49eV with solvation.

The case of Au is more complicated. Solvation still lowered the barrier of O_2 dissociation from 1.82eV in gas phase to 0.96eV with solvation, but the barrier is still higher than the barrierless OOH formation. The formed OOH then directly dissociates into O_{ad} and OH_{ad} with a barrier of 0.57eV, 0.31eV lower than the case without solvation. O hydration barrier on Au is 0.28eV with solvation, slightly higher than the 0.10eV without solvation. Similarly, H_2O formation has a barrier of 0.38eV, higher than the gas phase barrier of 0.29eV. This gives an overall mechanism of OOH-form-hydr:

(step zero) H^+ ➔ H_{ad} [E (Au) = 0.29eV at 0.0V versus NHE, E (Au) = 1.09eV, at 0.80V versus NHE]

(4a) $O_2 + H_{ad}$ ➔ OOH_{ad} [E_a (Au) = 0.00eV]

(4b) OOH_{ad} ➔ $O_{ad} + OH_{ad}$ [E_a (Au) = 0.57eV]

(4c) $O_{ad} + H_2O_{ad}$ ➔ $2OH_{ad}$ [E_a (Au) = 0.28eV]

(4d) $OH_{ad} + H_{ad}$ ➔ H_2O_{ad} [E_a (Au) = 0.38eV].

The overall RDS is hence OOH dissociation with a barrier of 0.57eV.

Another factor that needs to be taken into account is the availability of H_{ad}, especially at higher potential. The H reduction reaction is H^+ ➔ H_{ad}. This step is potentially dependent and can be estimated using Norskov's[17] and our approach[87] as follows:

$H^+(solv) \Leftrightarrow 1/2H_2$ ➔ H_{ad} .

The corresponding reaction enthalpy for Ag, Au, Cu, and Pt are 0.31eV, 0.29eV, -0.14eV, and -0.65eV at 0.0V versus normal hydrogen electrode (NHE). At fuel cell condition (0.8V versus NHE), the reaction enthalpy becomes 1.11eV, 1.09eV, 0.66eV, and 0.15eV for Ag, Au, Cu, and Pt. Comparing with the RDS barrier mentioned above, we can see that H reduction becomes the RDS for Ag and Au, with a barrier of 1.11eV and 1.09eV.

Summarizing all of the above discussions, with solvation, Ag and Cu prefer the O_2-diss-hydr-solv mechanism while Au prefers the OOH-form-hydr-solv mechanism. The RDS for Au and Ag is H reduction with a barrier of 1.11eV and 1.09eV. For Cu the RDS is H_2O formation with an overall barrier of 1.08eV. So none of Ag, Au, or Cu are effective ORR catalysts.

Hence for Au and Ag, the availability of H_{ad} becomes the fundamental limit toward a better catalyst. Co, Ir, Os, Pd, Pt, Rh, and Ru all have large binding energy with H_{ad} and could be good candidates. They need to be combined with a second metal with good affinity with H_{ad}. For Cu, the most important improvement to look for is the H_2O formation. Among the 8–11th column metals, Au and Pt both have a low barrier for forming H_2O and are hence promising choices.

Conclusion

We systematically studied the ORR on Ag, Au, and Cu surfaces and compared with Pt. The preferred mechanisms for Ag and Cu are both O_2-diss-hydr with an overall barrier of 0.98eV and 1.08eV. On Au the preferred mechanism is OOH-form-hydr-solv with an overall barrier of 0.57eV, but Au suffers from the availability of H_{ad}. In contrast, the overall barrier for Pt is 0.49eV. The two main problems for these three metals is the formation of H_2O due to the high stability of OH_{ad} and the reduction of H^+ due to small binding energy with H_{ad}.

Tables and Figures

Binding Energy (eV)	OH species	Gas				Solv			
		Ag	Au	Cu	Pt	Ag	Au	Cu	Pt
M		0.00	0.00	0.00	0.00	0.00	0.00	0.00	0.00
M-H	μ_1	-1.54	-1.93	-1.99	-2.89	-1.63	-1.94	-2.02	-2.97
	μ_2	-1.87	-1.97	-2.32	-2.77	-1.89	-2.00	-2.35	-2.89
	μ_3-ccp	-1.99	-2.00	-2.37	-2.74	-2.00	-2.03	-2.41	-2.86
	μ_3-hcp	-1.98	-1.99	-2.42	-2.72	-2.00	-2.03	-2.45	-2.83
M-O	μ_1	-1.87	-1.47	-2.80	-2.54	-2.93	-2.07	-3.54	-3.31
	μ_2	-2.85	-2.19	-4.00	-3.30	-3.80	-2.87	-4.51	-3.96
	μ_3-ccp	-3.13	-2.50	-4.35	-3.75	-4.06	-3.21	-4.92	-4.44
	μ_3-hcp	-3.06	-2.36	-4.25	-3.36	-4.04	-3.07	-4.81	-4.02
M-H_2		0.21	0.18	0.36	0.18	0.20	0.17	0.33	0.12
M-OH	μ_1	-2.02	-1.74	-2.54	-2.35	-2.75	-2.28	-3.01	-2.86
	μ_2	-2.42	-1.84	-2.90	-2.35	-2.98	-2.28	-3.22	-2.73
	μ_3-ccp	-2.45	-1.82	-2.96	-2.32	-2.93	-2.21	-3.22	-2.67
	μ_3-hcp	-2.42	-1.80	-2.92	-2.35	-2.93	-2.20	-3.18	-2.70
M-OO	Bridge	-0.13	0.11	-0.54	-0.54	-0.45	0.01	-0.92	-0.87
	μ_3-ccp	-0.13	0.08	-0.78	-0.56	-0.38	0.03	-1.32	-0.96

	μ_3-hcp	-0.10	0.10	-0.77	-0.51	-0.42	0.05	-1.28	-0.88
M-OOH	μ_1-b	-0.66	-0.45	-1.14	-1.13	-1.33	-0.91	-1.62	-1.57
	μ_1-c	-0.68	-0.32	-1.08	-1.02	-1.36	-0.81	-1.59	-1.48
M-H_2O_2	Bridge	-0.18	-0.17	-0.23	-0.33	-0.50	-0.50	-0.54	-0.69
M-H_2O	μ_1	-0.11	-0.10	-0.17	-0.24	-0.48	-0.47	-0.50	-0.64

Table 6-1. Binding energy for Ir and Os as compared with Pt, both with and without solvent.

	Gas				Solv			
Reaction Barriers	Ag	Au	Cu	Pt	Ag	Au	Cu	Pt
H_2 Dissociation	1.26	0.99	0.22	0.00	1.24	0.97	0.05	0.00
O_2 Dissociation	0.78	1.82	0.11	0.45	0.00	0.96	0.12	0.00
OH Formation	0.06	0.28	0.44	0.79	0.39	0.40	0.59	1.02
H_2O Formation	0.72	0.29	0.98	0.12	0.98	0.38	1.08	0.30
OOH Formation	0.21	0.00	0.29	0.33	0.25	0.00	0.31	0.23
OOH Dissociation	0.87	0.88	0.21	0.04	0.27	0.57	0.00	0.00
H-OOH dissociation	0.02	0.00	0.77	0.06	0.13	0.04	0.78	0.00
O hydration	0.00	0.10	0.24	0.22	0.12	0.28	0.35	0.49

Table 6-2. Reaction barriers for various steps involved in ORR.

	Gas				Solv			
Reaction Barriers	Ag	Au	Cu	Pt	Ag	Au	Cu	Pt
O_2-diss	0.78	1.82	0.98	0.79	0.98	0.96	1.08	1.02
OOH-form	0.87	0.88	0.98	0.79	0.98	0.57	1.08	1.02
O_2-diss-hydr	0.78	1.82	0.98	0.45	0.98	0.96	1.08	0.49
OOH-form-hydr	0.87	0.88	0.98	0.33	0.98	0.57	1.08	0.49
High-H*	0.72	0.29	0.98	0.33	0.98	0.38	1.08	0.30
Overall*	0.72	0.29	0.98	0.33	0.98	0.38	1.08	0.49*

Table 6-3. Overall barriers for each step.

*The High-H mechanism consistes of OOH formation, H associated OOH dissociation, O hydration and H_2O formation is less likely to happen with limited H_{ad} supply.

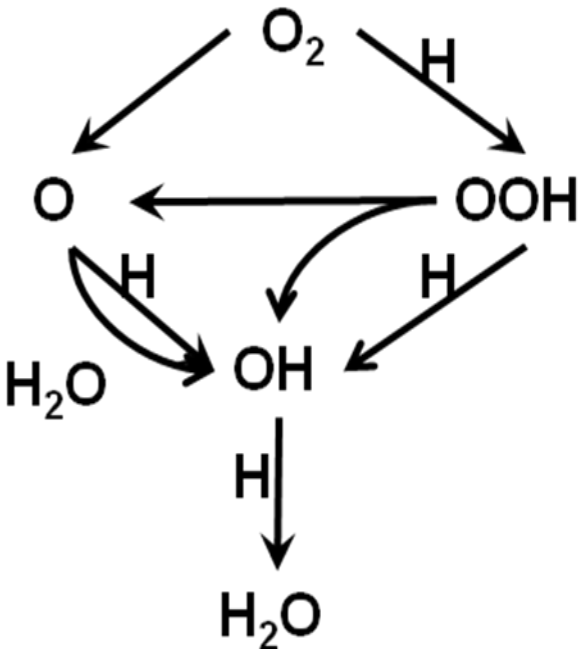

Figure 6-1. Steps involved in ORR.

Chapter 7 Density Functional Studies on Oxygen Reduction Reaction on Pd, Rh, and Ru Surfaces

Abstract

In this study, we studied theoretically the binding preferences of various intermediates involved in oxygen reduction reaction (ORR) on the (111) surface of Pd, Rh, and Ru, calculating barriers (with and without solvation) for all necessary steps for all five possible pathways known on Pt. All metals within this group have large H_2O formation barriers. Without solvation Rh and Ru showed behavior quite different than Pt. Rh and Ru prefer the O_2-diss-hydr mechanism involving O_2 dissociation, O hydration and H_2O formation with an overall barrier of 0.89eV and 1.09eV. In contrast, Pd and Pt prefer the OOH-form-hydr mechanism with overall barriers of 0.58eV and 0.33eV. Including solvation, all four metals prefer O_2-diss-hydr mechanism with barriers of 0.89eV, 1.28eV 0.79eV and 0.49eV for Rh, Ru, Pd and Pt, respectively. The major problem with all Pd group metals is the high H_2O formation barrier due to strong OH_{ad} binding. Alloys should at least contain one other metal to decrease the OH_{ad} binding energy and the consequent H_2O formation barrier. Pt Ir, Au, Ag, and Cu could be good choices.

Introduction

Developing efficient catalyst for the slow oxygen reduction reaction process on the cathode of PEMFC is one of the key problems for more economically feasible usage in automobiles[1–4]. Pt and Pt alloys are so far the best catalysts[62–63]. There had been

numerous studies focusing on synthesizing new materials as substitutes[5–9]. Compared to the fruitful experimental studies, there had been limited theoretical understanding of the ORR mechanism and how one could go about improving the kinetics. Most theoretical studies focused on the gas phase reaction for lack of a proper way of handling the solvent effect[10,14,17–18,47,70]. In our previous study, we developed a practical way of estimating the solvation effect by using the implicit solvation model based on Poisson-Boltzmann equation[66]. We showed that the solvation dramatically changes the kinetics and leads to the superior performance of Pt in catalyzing ORR. . We had systematically studied the ORR mechanism on Pt, Pd, Ni, Co, Ag, Au and Cu. In this study, we focus on the binding preference, reactions steps and ORR mechanisms on Rh and Ru, the two Pd group metals, and explore the possibility of developing Rh and Ru based alloys as the next generation ORR catalyst. .

Methodology

The calculations were carried out by using Seqquest DFT code[29] where Kohn-sham equation is solved with periodic boundary condition in a self-consistent way. Norm-conserving potential[34–37] and Gaussian type orbitals are used to represent the metal atoms. A c(3x3) unit cell with six layers of atoms is used to represent surface. The system is hence periodic in to reactions (x and y) and finite in the third (z) direction, making it a slab. Four bottom layers are fixed as the optimal bulk structure to mimic the bulk side while the other two layers are relaxed to represent the surface. Implicit solvation based on Poisson-Boltzmann equation[23–25,38,66] is calculated using Mulliken charge calculated from gas phase calculation, details of which were shown in our previous paper[66,84].

Results and Discussion

Binding sites and Binding energies

As discussed in previous papers, there are in general four types of binding sites on the closed packing surface, namely,

- top site (μ^1),
- bridging site(μ^2),
- fcc hollow site (μ^{3f}), at the C site when the top 2 closest packed layers are AB
- hcp hollow site (μ^{3h}) at the A site when the top 2 closest packed layers are AB

We calculated the binding preferences of H, O, OH, O2, OOH, H2O and H2O, all the intermediates involved in the reaction.

H prefers to bind to bind to (μ^{3f}) site on Rh and Ru without solvation with a binding energy of 2.72eV and 2.87eV, similar to the case of Pd (BE=2.85eV). With solvation, the binding energies increase to 2.87eV and 3.06eV for Rh and Ru, as compared to the 2.99eV on Pd. (μ^1) is less stable by 0.23eV and 0.52eV without solvation and 0.25 and 0.40 eV with solvation on Rh and Ru. As compared to the relatively flat PES for Pt, H has stronger preference over high coordination on Pd, Rh and Ru surface.

O prefers to bind to bind to (μ^{3f}) site on Rh with a binding energy of 4.46eV without solvation and 4.98eV with solvation. Ru showed strong preference towards (μ^{3h}) site with a large binding energy of 5.37eV without solvation and 5.94eV with solvation. (μ^2) is not stable on both metals, similar to Pt and Pd and serve as the transition state for the diffusion of O on the surface, giving a barrier of 0.45eV and 0.41eV without solvation and 0.48 and 0.31eV with solvation.

OH prefers to bind to (μ^2) site on Rh and Ru with binding energy of 2.88eV and 3.22eV without solvation and 3.21eV and 3.53eV with solvation, as compared to the 2.32eV and 2.67eV for Pt. Similar to the case of Pd and Pt, the binding energies on (μ^{3f}) (μ^{3c}) and (μ^2) for OH are close, implying that OH can easily migrates along the surface.

O_2 prefers to bind to (μ^{3f}) site on both Rh and Ru with a binding energy of 1.35eV for Rh and 1.82eV for Ru without solvation. With solvation, the binding energy becomes 1.72eV and 2.38eV. Comparing with the 0.56eV binding energy without solvation and the 0.96eV with solvation, we can see that Rh and Ru binds much stronger to the surface, leading to a weakened O=O bond. Hence we expect easier O_2 dissociation.

OOH binds to (μ^1) site with binding energy of 1.51eV and1.80eV without solvation for Rh and Ru, respectively. Taking solvation into account, the binding energies increase to 1.92 and 2.30eV. The binding energies are much stronger than that of Pt (1.13eV without solvation and 1.57eV with solvation). H_2O also binds to (μ^1) site with a binding energy of 0.32eV and 0.42eV on Rh and Ru without solvation and 0.70eV and 0.78eV with solvation, also stronger than that of Pt (0.24 and 0.64eV)

Summarizing the binding energies, we can see that Ru and Rh binds stronger to O, OH, OOH and H_2O and are hence less noble than Pt. This would lead to easier O_2 dissociation and more difficult H_2O formation.

Barriers and Preferred Mechanism

In general, there are six possible reactions on metal surfaces, including

(1) O_2 dissociation, $O_{2ad} \rightarrow 2O_{ad}$

(2) OH formation: $O_{ad} + H_{ad} \rightarrow OH_{ad}$

(3) H_2O formation: $OH_{ad} + H_{ad} \rightarrow H_2O_{ad}$

(4) OOH formation: $O_{2ad} + H_{ad} \rightarrow OOH_{ad}$

(5) OOH dissociation: $OOH_{ad} \rightarrow O_{ad} + OH_{ad}$

(6) O hydration: $O_{ad} + H_2O_{ad} \rightarrow 2OH_{ad}$

The barriers are shown in Table 7-2. As in previous studies, the ORR process can be roughly divided into three steps.

Dissociation of O=O bond: O_2 can directly dissociate into two O. Or alternatively, it can react with H to form OOH which consequently dissociates into O and OH, hence breaks the O=O bond.

O_2 dissociation has low barriers of 0.17eV on Rh and 0.03eV on Ru and is hence much easier than on Pt without solvation. Solvation is known to help with the O_2 dissociation by stabilizing the resulting O_{ad}. When solvent effect is taken into account, O_2 dissociation on both Ru and Rh become barrierless, similar to the case of Pt.

OOH formation has barrier of 0.42 and 0.62eV on Rh and Ru without solvation. Solvent effect has little influence for the OOH formation barrier. The barrier only slightly increases to 0.64eV and 0.69eV with solvation. The consequent OOH dissociation is barrierless on both Rh and Ru, regardless of whether solvent effect is included.

Comparing the barrier of the competing OOH formation and O_2 dissociation, we can see that O_2 dissociation is the dominant way of dissociating O=O bond, resulting with O_{ad} on the surface.

Formation of OH. O can either react with an H to form an OH or get's hydrated by reacting with an H_2O, forming two OH at the same time.

OH formation is easier on Rh than on Pt with a barrier of 0.61eV without solvation and 091eV without solvation. On Ru surface, the direct OH formation becomes difficult with a high barrier of 0.93eV without solvent and 1.45eV with solvation. Similar to the case of Pt (E_a = 0.79 without solvation and E_a = 1.02 with solvation), OH formation is simply too slow to happen at ambient temperature.

O hydration on Rh and Ru have barrier of 0.27eV and 0.34eV on Rh and Ru in gas phase, respectively. The solution phase barriers are 0.44 and 0.36eV. The gas phase barriers are slightly higher than the Pt while the solution phase barriers are lower than the case of Pt.

Comparing with the direct OH formation from O and H, O hydration has a much lower barrier and hence is the dominant way of forming OH on both Ru and Rh, similar to the case of Pt.

Formation of H_2O. Formation of H_2O has barrier of 0.78eV and 1.09eV on Rh and Ru without solvation. With solvation, the barriers increase to 0.89 and 1.28eV. It is larger than the e barriers are larger than Pt, leading to more difficult OH removal.

Overall mechanism

Gas phase, As discussed earlier, on Rh and Ru, O_2 dissociation (E_a = 0.17eV and 0.00eV) dominates OOH (E_a = 0.42eV and 0.62eV) and act as the major way of breaking O_2. This if followed by the hydration of O_{ad} with barriers of 0.27eV on Rh and 0.34eV on Ru. Direct OH formation from O_{ad} and H_{ad} is less likely to happen higher barriers of 0.61eV and 0.93eV. Combining with the H_2O formation with a barrier of 0.78eV on Rh and 1.09eV on Ru, this leads to the O_2-diss-hydr mechanism as shown in 1a-1c.

(1a) O_{2ad} ➔ $2O_{ad}$ [E_a (Rh) = 0.17eV, E_a (Ru) = 0.00eV]

(1b) $O_{ad} + H_2O_{ad} \rightarrow 2OH_{ad}$ [E_a (Rh) = 0.27eV, E_a (Ru) = 0.34eV]

(1c) $OH_{ad} + H_{ad} \rightarrow H_2O_{ad}$ [E_a (Rh) = 0.78eV, E_a (Ru) = 1.09eV]

The overall rate determining step (RDS) is hence H_2O formation with an overall barrier of 0.89eV for Rh and 1.09eV for Ru. This is different from the preferred OOH-form-hydr mechanism of Pd and Pt without solvation as shown in equation 2a-d. The RDS for Pd is H_2O formation with a barrier of 0.58eV while the RDS for Pt is OOH formation with a barrier of 0.33eV.

(2a) $O_2 + H_{ad} \rightarrow OOH_{ad}$ [E_a (Pd) = 0.56eV, E_a (Pt) = 0.33eV]

(2b) $OOH_{ad} \rightarrow O_{ad} + OH_{ad}$ [E_a (Pd) = 0.24, E_a (Pt) = 0.04eV]

(2c) $O_{ad} + H_2O_{ad} \rightarrow 2OH_{ad}$ [E_a (Pd) = 0.27eV, E_a (Pt) = 0.22eV]

(2d) $OH_{ad} + H_{ad} \rightarrow H_2O_{ad}$ [E_a (Pd) = 0.58eV, E_a (Pt) = 0.12eV]

So without solvation none of Rh, Ru and Pd could be comparable to Pt as ORR catalyst.

With solvation. Similar to the case of Pt and Pd, solvation dramatically changes the barriers and the consequent preferred mechanism. For the four metals involved in this study, solvation stabilizes O_{ad}, and OH_{ad}, especially O_{ad}. It leads to lower barrier for O_2 dissociation and higher barriers for OH formation and H_2O formation.

O_2 dissociation becomes barrierless for Rh and Ru, similar to the case of Pt. The corresponding barrier for Pd is also greatly lowered by 0.40eV to 0.26eV. This makes O_2 dissociation the dominate way of breaking O_2 for all the four metals discussed. Higher OH formation barrier makes it impossible to directly form OH_{ad} from H_{ad} and O_{ad}. O hydration becomes the only possible way with a barrier of 0.44eV, 0.35eV, 0.46eV and

0.49eV for Rh, Ru, Pd and Pt, respectively. Combining with the essential H_2O formation step leads to O_2-diss-hydr-solv mechanism, as shown in 3a-3c.

(3a) O_{2ad} ➔ $2O_{ad}$ [E_a (Rh) = 0.00eV, E_a (Ru) = 0.00eV, E_a (Pd) = 0.26eV, E_a (Pt) = 0.00eV]

(3b) $O_{ad} + H_2O_{ad}$ ➔ $2OH_{ad}$ [E_a (Rh) = 0.44eV, E_a (Ru) = 0.35eV, E_a (Pd) = 0.46eV, E_a (Pt) = 0.49eV]

(3c) $OH_{ad} + H_{ad}$ ➔ H_2O_{ad} [E_a (Rh) = 0.89eV, E_a (Ru) = 1.28eV, E_a (Pd) = 0.79eV, E_a (Pt) = 0.30eV]

Hence H_2O formation (3a) is the RDS for all of Rh, Ru and Pd with a high barrier of 0.89eV 1.28eV and 0.79eV. As comparison, RDS for Pt is O hydration with a barrier of 0.49eV, much lower than the overall barrier for Rh, Ru and Pd, making Pt a better catalyst.

We can see that the biggest problem with Pd group metals are the high H_2O formation barrier which origins from the stronger binding with OH as shown in Table 7-1. So materials based on Rh, Ru and Pd will need to resolve this issue. Pd group based alloys will need a weaker OH_{ad} binding, Pt, Ir, Cu, Au and Ag would be good candidates for this purpose.

To make a good ORR catalyst, a material has to has low barriers for all of O=O bond splitting, OH bond formation and H_2O formation. With the help of solvation, O_2 dissociation is not a problem for almost all the metals in group 8-11 due to the solvent stabilization of O_{ad}. So an ideal catalyst should have a weak binding for O_{ad} and a relatively strong OH binding energy. This guarantees a low barrier for both O hydration/OH formation and H_2O. Pt has a weak binding of OH which leads to an ideal

H_2O formation barrier of 0.30eV, but the 0.49eV hydration barrier is still a little bit high. Hence alloying of Pt should aim at a weaker binding of O. Pd has about the same binding with O_{ad} as Pt and could be a promising candidate. Another approach would be alloying Pt with another metal to make OH_{ad} binding stronger. All of Rh, Ru and Pd could be good candidates.

Conclusion

In this study we studied systematically the ORR on Ru and Rh surface and compared it with OOR of Pd and Pt, calculating the binding site preference and the corresponding binding energies and barriers for all possible steps involved. The preferred mechanism for both Ru and Rh is O_2-dis-hydr mechanism, independent of solvent. H_2O formation is the RDS with a barrier of 0.78eV (Rh) and 1.09eV (Ru) without solvation and 0.89eV (Rh) and 1.28eV (Ru) with solvation. To improve activity for Rh and Ru based materials, we suggest combining it with another material having weaker OH_{ad} binding (leading to lower H_2O formation barrier). Promising candidates include Ag, Au, Cu, Ir and Pt.

Tables and Figures

		Gas				Solv			
Binding Energy (eV)	OH species	Pd	Pt	Rh	Ru	Pd	Pt	Rh	Ru
M		0.00	0.00	0.00	0.00	0.00	0.00	0.00	0.00
M-H	μ_1	-2.45	-2.89	-2.49	-2.35	-2.56	-2.97	-2.62	-2.66
	μ_2	-2.72	-2.77	-2.63	-2.75	-2.87	-2.89	-2.78	-2.90
	μ_3-ccp	-2.85	-2.74	-2.72	-2.87	-2.99	-2.86	-2.87	-3.06
	μ_3-hcp	-2.80	-2.72	-2.67	-2.85	-2.94	-2.83	-2.81	-2.90
M-O	μ_1	-2.77	-2.54	-3.19	-3.98	-3.46	-3.31	-3.88	-4.59
	μ_2	-3.51	-3.30	-4.01	-4.69	-4.07	-3.96	-4.50	-5.32
	μ_3-ccp	-3.91	-3.75	-4.46	-5.10	-4.47	-4.44	-4.98	-5.63
	μ_3-hcp	-3.67	-3.36	-4.32	-5.37	-4.20	-4.02	-4.81	-5.94
$M-H_2$		-0.03	0.18	0.18	0.20	-0.06	0.12	0.14	0.08
M-OH	μ_1	-2.43	-2.35	-2.65	-2.79	-2.93	-2.86	-3.12	-3.29
	μ_2	-2.65	-2.35	-2.88	-3.21	-3.02	-2.73	-3.19	-3.49
	μ_3-ccp	-2.64	-2.32	-2.88	-3.22	-2.95	-2.67	-3.21	-3.53
	μ_3-hcp	-2.61	-2.35	-2.84	-3.27	-2.95	-2.70	-3.11	-3.51
$M-O_2$	bridge	-1.09	-0.54	-1.31	-1.67	-1.27	-0.87	-1.64	-2.05
	ccp	-1.02	-0.56	-1.35	-1.82	-1.30	-0.96	-1.72	-2.28
	hcp	-0.99	-0.51	-1.35	-1.73	-1.25	-0.88	-1.72	-2.31

M-OOH	μ_{1b}	-1.41	-1.13	-1.51	-1.80	-1.86	-1.57	-1.92	-2.30
	μ_{1c}	-1.36	-1.02	-1.41	-1.61	-1.80	-1.48	-1.90	-2.14
M-H_2O_2	bridge	-0.61	-0.33	-0.50	-0.28	-0.93	-0.69	-0.82	-0.82
M-H_2O	μ_1	-0.42	-0.24	-0.32	-0.42	-0.76	-0.64	-0.70	-0.78

Table 7-1. Binding energy for Ir and Os as compared with Pt, both with and without solvent

	Gas				Solv			
Reaction Barriers	Pd	Pt	Rh	Ru	Pd	Pt	Rh	Ru
H_2 Dissociation	0.00	0.00	0.00	0.00	0.00	0.00	0.00	0.02
O_2 Dissociation	0.66	0.45	0.17	0.00	0.26	0.00	0.00	0.00
OH Formation	0.35	0.79	0.61	0.93	0.52	1.02	0.91	1.45
H_2O Formation	0.58	0.12	0.78	1.09	0.79	0.30	0.89	1.28
OOH Formation	0.56	0.33	0.42	0.62	0.82	0.23	0.54	0.69
OOH Dissociation	0.24	0.04	0.00	0.00	0.08	0.00	0.00	0.00
H-OOH dissociation	0.18	0.06	3.55	0.00	0.22	0.00	3.94	0.00
O hydration	0.27	0.22	0.27	0.34	0.46	0.49	0.44	0.35

Table 7-2. Reaction barriers for various steps involved in ORR

	Gas				Solv			
Reaction Barriers	Pd	Pt	Rh	Ru	Pd	Pt	Rh	Ru
O_2-diss	0.66	0.79	0.78	1.09	0.79	1.02	0.91	1.45
OOH-form	0.58	0.79	0.78	1.09	0.82	1.02	0.91	1.45
O_2-diss-hydr	0.66	0.45	0.78	1.09	0.79	0.49	0.89	1.28
OOH-form-hydr	0.58	0.33	0.78	1.09	0.82	0.49	0.89	1.28
High-H**	0.58	0.33	3.55	1.09	0.82	0.30	3.94	1.28
Overall*	0.58	0.33	0.78	1.09	0.79	0.30	0.89	1.28

Table 7-3. Overall barriers for each step

*The High-H mechanism consisting of OOH formation, H associated OOH dissociation, O hydration, and H_2O formation is less likely to happen with limited H_{ad} supply.

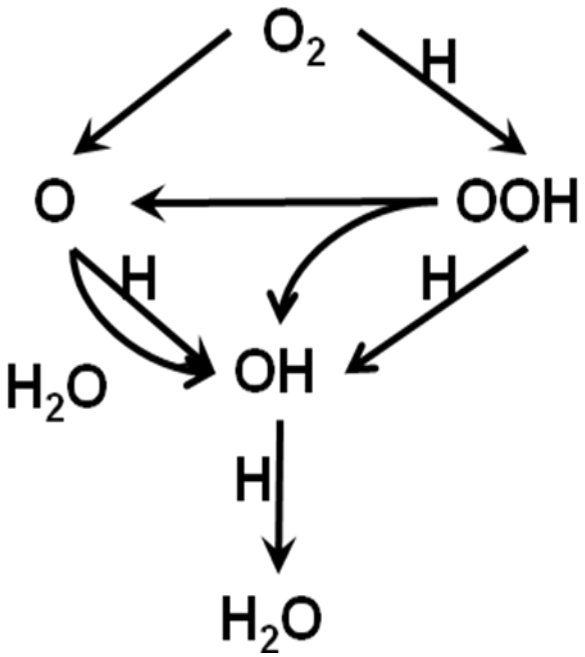

Figure 7-1. Steps involved in ORR

Chapter 8 Density Functional Studies of the Fuel Cell Oxygen Reduction Reaction on Os and Ir Surfaces

Abstract

We studied theoretically the binding preferences of various intermediates involved in the oxygen reduction reaction (ORR) on the (111) surface of Os and Ir, where in all cases the quantum mechanical reaction surfaces are corrected for aqueous solvation. Barriers for all necessary steps for all five possible pathways known on Pt are calculated. Ir and Os show similar behavior with Pt for almost all pathways. The OH formation barrier is 1.08eV for Ir and 1.66eV for Os, much higher than for Pt (1.02eV). So the only viable pathway for Ir and Os is the O_2-dis-hyd mechanism. The hydration barriers for Ir and Os (0.35eV and 0.56eV) are lower than the H_2O formation barrier (0.61eV and 0.67eV, making H_2O formation the rate determining step [RDS]. To get improved ORR activity, it is necessary to lower the H_2O formation barrier. Alloying with a second metal with a better H_2O formation barrier could be a promising approach. Ag, Au, Cu, Pd, Pt, and Rh are good candidates.

Introduction

The PEM fuel cell is one of the most promising environment-friendly ways of converting chemical energies into electricity to power automobiles[1–4]. The lack of a powerful catalyst for the slack oxygen reduction reaction on a cathode is among the biggest obstacles towards wider commercial usage of such systems. Pt and Pt alloys are

so far the best catalysts, but they still suffer a huge potential loss (operating at 0.80eV as compared to the theoretical limit of 1.23V) and slow kinetics.

Lots of research has been done in the past decade to find better alternatives, as well as to better understand the mechanism[5–9]. Most theoretical studies[10,14,17–18,47,70] about the ORR on metal surfaces focused on the hydrogen oxidation reaction (HOR) in gas phase, assuming that a good HOR catalyst may also be a good ORR catalyst. This approach was the most expedient without a correct way of handling the solvent effect. Recently[66], we developed a systematical way to calculate solvation energy and showed that ORR kinetics differs a lot from those of HOR. O_2 dissociation becomes barrierless with the help of solvent, making the formation of OH_{ad} and H_2O_{ad} the more important steps in ORR. Here, we study the ORR mechanism on Os and Ir using density functional theory (DFT) calculations, and suggest possible ways of developing improved Os/Ir-based material as catalysts for ORR.

Methodology

The calculations were carried out by using Seqquest DFT code[29] where the Kohn-sham equation is solved with a periodic boundary condition in a self-consistent way. Norm-conserving potential[34–37] and Gaussian type orbitals are used to represent the metal atoms. A c(3x3) unit cell with six layers of atoms is used to represent surface. The system is periodic in two directions (x and y) and finite in the third (z) direction, making it a slab. Four bottom layers are fixed as the optimal bulk structure to mimic the bulk side, while the other two layers are relaxed to represent the surface. Implicit solvation based on the

Poisson-Boltzmann equation[23–25,38,66] is calculated using Mulliken charge calculated from gas phase calculation, details of which were shown in our previous paper[66].

Results and Discussion

Binding sites and binding energies

In general, as mentioned in previous papers, there are four possible sites for adsorbates on the closed packing surface (111 surface of Ir and 100 surfaces of Os).

- top site (μ^1),
- bridging site(μ^2),
- fcc hollow site (μ^{3f}), at the C site when the top 2 closest packed layers are AB,
- hcp hollow site (μ^{3h}) at the A site when the top 2 closest packed layers are AB.

Thus the first step is to decide the preferred binding sites for all the intermediates involved. The binding energies of H, O, O_2, OH, OOH, H_2O, and H_2O_2 are summarized in Table 8-1.

H prefers to bind to top site (μ^1) for both Ir and Os with a binding energy of 2.79eV and 2.70eV without solvent, as compared to the 2.89eV of Pt. When solvent is present the binding energies changes to 2.90eV for Ir and 2.77eV for Os. This agrees with the experimentally observed result that Ir binds to top sites [96–97]. Similar to the case of Pt, the PES for H on the surface is relatively flat. Binding energies on different sites differ by less than 0.21eV for all of Ir, Os, and Pt.

O prefers to bind to (μ^{3f}) on Ir with a binding energy of 4.36eV without solvation and 4.89eV with solvation, similar to the case of Pt. For Os, O prefers (μ^{3h}) with a binding

energy of 3.94eV without solvation and 5.67eV with solvation. The bridging site is unstable for both Ir and Os and serves as the transition state for the diffusion of O between the adjacent (μ^{3f}) and (μ^{3h}) site. The corresponding barrier is hence 0.44eV and 0.47eV for Ir and Os in gas phase, and 0.43eV and 0.38eV with solvation. The barrier makes it difficult for oxygen to migrate on the surface once formed.

OH prefers to bind to (μ^{2}) on Ir with a binding energy of 2.73eV and to a (μ^{1}) site without solvation. The PES of OH is flat on Ir surface without solvation, given that the binding energies differ by less than 0.06eV, similar to the case of Pt. However, with solvation (μ^{1}) becomes the most stable form with a binding energy of 3.28eV. For Os, (μ^{3f}) are the preferred binding sites with binding energies of 3.08eV. In solvent (μ^{3h}) becomes the preferred site for OH with a binding energy of 3.47eV. The binding of OH is stronger on both Ir and Os than on Pt.

O_2 prefers to bind with a (μ^{2}) site on Ir with a binding energy of 1.34eV without solvation and 1.89eV with solvation, as compared to the 0.56eV and 0.96eV on Pt, implying a strong interaction and great weakening of the O=O bond. Similarly, on Os, the (μ^{3h}) is preferred without solvation with a binding energy of 1.55eV and the (μ^{3c}) site is preferred with solvation with a binding energy of 2.34eV, even stronger than in the case of Ir.

OOH prefers to bind to a (μ^{1}) site for both Ir and Os, similar to the case of Pt. Again, the binding energy of 1.61eV and 1.74eV without solvation and 2.19eV and 2.26eV with solvation are all stronger for both than the 1.13eV and 1.57eV on Pt.

H_2O prefers to bind to (μ^1), similar to Pt. The binding energies are 0.38eV and 0.40eV without solvation and 0.79eV and 0.91eV with solvation for Ir and Os, respectively. They are only slightly stronger than the 0.24eV and 0.64eV of Pt.

Barriers for possible reaction steps

In general, there are six reactions involved in the ORR:

- O_{2ad} ➔ $2O_{ad}$
- O_{ad} + Had ➔ OH_{ad}
- OH_{ad} + Had ➔ H_2O_{ad}
- O_{2ad} + Had ➔ OOH_{ad}
- OOH_{ad} ➔ O_{ad} + OH_{ad}
- O_{ad} + H_2O_{ad} ➔ 2OH .

The barriers for all the six steps on Os and Ir are calculated and shown in Table 8-2. As discussed in previous studies[66,84,88,98–99], it's convenient to divide the reactions into three categories: (1) splitting the O=O bond, (2) forming the OH bond, and (3) forming H_2O.

Splitting the O=O bond. There are two possible ways of splitting O_2 for ORR on metal. One way is direct O2 dissociation where an adsorbed O_2 dissociates into two adjacent threefold sites. The other is through formation and dissociation of OOH.

O_2 dissociation (O_{2ad} ➔ $2O_{ad}$): On the Ir and Os surface, the O_2 can both directly dissociate into two O_{ad} with a barrier of 0.03eV without solvation, much lower than the 0.45eV of Pt. The low barrier is mainly due to the strong bonding of O with the surface, as shown by the large binding energy of both O_{2ad} and O_{ad}. With solvation, the barriers are lowered to 0.00eV.

OOH association and dissociation (O_{2ad} + H_{ad} ➔ OOH_{ad} ➔ O_{ad} + OH_{ad}): OOH formation has a barrier of 0.51eV and 0.52eV on Ir and Os without solvation, respectively, higher than the 0.33eV on Pt. Solvation does not change the 0.51eV OOH formation barrier on Ir. For Os, solvation lowers the barrier by 0.12eV to 0.40eV with solvation. OOH dissociation is much easier than its formation, with a low barrier of 0.14eV on Ir, as compared to the 0.04eV for Pt. For Os, the reaction is barrierless and hence (μ^1)-OOH is only metastable on Os. With solvation, dissociation of OOH is barrierless for all of Ir, Os, and Pt.

Comparing the direct dissociation of O_2 and association of OOH_{ad}, we can see that the barrierless O_2 dissociation dominates and serves as the major way of dissociating the O=O bond.

Formation of OH. There are two possible ways of forming OH_{ad}, either through direct OH formation or through hydration of O_{ad}.

OH formation (O_{ad} + H_{ad} ➔ OH_{ad}): OH formation is difficult for all of Ir, Os, and Pt. The barrier without solvation is 0.86eV and 1.26eV for Ir and Os, as compared with the 0.79eV of Pt. The situation is worse when solvent effect is taken into account. Solvation in general stabilizes O_{ad} more than OH_{ad} (as indicated by Table 8-1), leading to a higher barrier for OH formation. The barriers increase to 1.08eV on Ir and 1.66eV on Os, as compared to 1.02eV for Pt. As discussed our previous studies[66,84], these high barriers actually make the direct OH formation impossible.

O hydration (O_{ad} + H_2O_{ad} ➔ $2OH_{ad}$): O_{ad} can also react with another H_2O to form two OH_{ad}. The barriers are 0.22eV for Ir and 0.33eV for Os without solvation. Similar to the case of OH formation, solvation makes O_{ad} more stable and increases the barriers to

0.35 and 0.56eV on Ir and Os when solvation is taken into account. The barriers are higher than that of Pt (0.22 without solvation and 0.49 with solvation), implying that hydration on both metals would be more difficult than on Pt.

Comparing the two possible ways of forming OH and consuming the O_{ad} produced by the previous steps (O_2 dissociation or OOH dissociation), we can see that O hydration is the preferred one for Ir and Os, similar to Pt.

Formation of H_2O. H_2O formation reaction ($OH_{ad} + H_{ad}$ ➔ H_2O_{ad}) has barrier of 0.51eV on both Ir and Os without considering solvent effect, as compared to the low barrier of 0.12eV on Pt. When the solvation is taken into account, the barriers increase to 0.61eV and 0.67eV, much higher than the 0.30eV on Pt.

Summarizing the preferred reaction in the three categorizes, we can see that for Os and Ir, the preferred mechanism is O_2-diss-hydr:

(1a) O_{2ad} ➔ $2O_{ad}$ [E_a (Ir) = 0.03eV, E_a (Os) = 0.03eV]

(1b) $O_{ad} + H_2O_{ad}$ ➔ 2OH [E_a (Ir) = 0.22eV, E_a (Os) = 0.33eV]

(1c) $OH_{ad} + H_{ad}$ ➔ H_2O [E_a (Ir) = 0.51eV, E_a (Os) = 0.51eV] .

The rate determining step (RDS) is hence H_2O formation with a barrier of 0.51eV for both Ir and Os. As comparison, the preferred mechanism for Pt is OOH-form-hydr[84]:

(2a) $O_{2ad} + H_{ad}$ ➔ OOH_{ad} [E_a (Pt) = 0.33eV]

(2b) OOH_{ad} ➔ $O_{ad} + OH_{ad}$ [E_a (Pt) = 0.04eV]

(2c) $O_{ad} + H_2O_{ad}$ ➔ 2OH [E_a (Pt) = 0.22eV]

(2d) $OH_{ad} + H_{ad}$ ➔ H_2O [E_a (Pt) = 0.12eV] .

The RDS is hence OOH formation with a barrier of 0.33eV.

Comparing Os and Ir with Pt, we can see that without solvation, Pt has better performance than Os and Ir. It agrees with the fact that Pt is the best catalyst of hydrogen oxidation reaction.

Solvation greatly changes the barriers and the preferred mechanism for Pt. With solvation, all of Ir, Os, and Pt have O_2-diss-hydr mechanism as the preferred mechanism:

(3a) O_{2ad} ➔ $2O_{ad}$ [E_a (Ir) = 0.00eV, E_a (Os) = 0.00eV, Ea (Pt) = 0.00eV]

(3b) $O_{ad} + H_2O_{ad}$ ➔ 2OH [E_a (Ir) = 0.35eV, E_a (Os) = 0.56eV, Ea (Pt) = 0.49eV]

(3c) $OH_{ad} + H_{ad}$ ➔ H_2O [E_a (Ir) = 0.61eV, E_a (Os) = 0.67eV, Ea (Pt) = 0.30eV]

Hence the H_2O formation step is the RDS for ORR on Ir and Os, leading to overall barriers of 0.61eV and 0.67eV. As discussed in our previous studies[84], the RDS for Pt is O hydration with a barrier of 0.49eV.

The results showed that Ir and Os are better in reducing O_2 to O_{ad} and reducing O_{ad} to OH_{ad}. But they are not efficient in converting OH_{ad} formed on the surface. The hydrophilic OH_{ad} formed hence aggregates on the surface and generates unfavorable kinetics. To get improved activity for Ir- and Os-related catalysts, it is essential to improve the H_2O formation. For this reason, materials with weaker binding with OH than Ir and Os (3.28eV and 3.47eV with solvation) are preferred as the second alloying metal. Good candidates include Ag (2.98eV), Au (2.28eV), Cu (3.22eV), Pd (3.02eV), Pt (2.86eV), and Rh (3.21eV).

Conclusion

We examined the mechanism of ORR on Ir and Os surfaces, calculating the binding site preference of all the intermediates involved in this reaction. We showed that the

preferred mechanism on both Os and Ir is the O_2-diss-hydr mechanism which involves (1) O_2ad ➔ 2Oad (2) $O_{ad} + H_2O_{ad}$ ➔ $2OH_{ad}$ (3) $OH_{ad} + H_{ad}$ ➔ H_2O. The overall RDS is the H_2O formation step (step three), giving an overall barrier of 0.61eV and 0.67eV for Ir and Os, respectively. The barriers are higher than the 0.49eV overall barrier of Pt (O hydration being RDS). To obtain improved performance for Ir- and Os-based materials, the H_2O formation barrier needs to be decreased. Alloying with metals with weaker binding with OH is a promising approach, suggesting Ag, Au, Cu, Pd, Pt, and Rh as good candidate alloying elements.

Tables and Figures

		Gas			Solv		
Binding Energy (eV)	OH species	Ir	Os	Pt	Ir	Os	Pt
M		0.00	0.00	0.00	0.00	0.00	0.00
M-H	μ_1	-2.79	-2.70	-2.89	-2.90	-2.77	-2.97
	μ_2	-2.60	-2.59	-2.77	-2.81	-3.00	-2.89
	μ_3-ccp	-2.61	-2.64	-2.74	-2.80	-3.31	-2.86
	μ_3-hcp	-2.58	-2.53	-2.72	-2.72	-2.81	-2.83
M-O	μ_1	-3.45	-3.91	-2.54	-4.26	-4.60	-3.31
	μ_2	-3.92	-4.34	-3.30	-4.46	-5.05	-3.96
	μ_3-ccp	-4.36	-4.81	-3.75	-4.89	-5.43	-4.44
	μ_3-hcp	-4.11	-4.94	-3.36	-4.60	-5.67	-4.02
$M-H_2$		0.37	0.43	0.18	0.30	0.31	0.12
M-OH	μ_1	-2.73	-2.84	-2.35	-3.28	-3.33	-2.86
	μ_2	-2.75	-2.98	-2.35	-3.02	-3.16	-2.73
	μ_3-ccp	-2.69	-3.06	-2.32	-3.02	-3.47	-2.67
	μ_3-hcp	-2.74	-3.08	-2.35	-3.00	-3.33	-2.70
$M-O_2$	bridge	-1.34	-1.44	-0.54	-1.89	-2.11	-0.87
	ccp	-1.19	-1.43	-0.56	-1.61	-2.34	-0.96
	hcp	-1.21	-1.55	-0.51	-1.61	-2.25	-0.88

M-OOH	μ_1b	-1.61	-1.74	-1.13	-2.19	-2.26	-1.57
	μ_2c	-1.32	-1.53	-1.02	-1.88	-2.04	-1.48
M-H_2O_2	bridge	-0.43	-0.51	-0.33	-0.77	-0.84	-0.69
M-H_2O	μ_1	-0.38	-0.40	-0.24	-0.79	-0.91	-0.64

Table 8-1. Binding energy for Ir and Os as compared with Pt, both with and without solvent effect

	Gas			Solv		
Reaction Barriers	Ir	Os	Pt	Ir	Os	Pt
H_2 Dissociation	0.00	0.00	0.00	0.00	0.00	0.00
O_2 Dissociation	0.03	0.03	0.45	0.00	0.00	0.00
OH Formation	0.86	1.26	0.79	1.08	1.66	1.02
H_2O Formation	0.51	0.51	0.12	0.61	0.67	0.30
OOH Formation	0.51	0.52	0.33	0.51	0.40	0.23
OOH Dissociation	0.14	0.00	0.04	0.00	0.00	0.00
H-OOH dissociation	0.58	0.00	0.06	0.85	0.00	0.00
O hydration	0.22	0.33	0.22	0.35	0.56	0.49

Table 8-2. Reaction barriers for various steps involved in ORR

	Gas			Solv		
Reaction Barriers	Ir	Os	Pt	Ir	Os	Pt
O_2-diss	0.86	1.26	0.79	1.08	1.66	1.02
OOH-form	0.86	1.26	0.79	1.08	1.66	1.02
O_2-diss-hydr	0.51	0.51	0.45	0.61	0.67	0.49
OOH-form-hydr	0.51	0.52	0.33	0.61	0.67	0.49
High-H*	0.58	0.52	0.33	0.85	0.67	0.30
Overall*	0.51	0.51	0.33	0.61	0.67	0.30

Table 8-3. Overall barriers for each step

*The High-H mechanism consists of OOH formation, H associated OOH dissociation, O hydration and H_2O formation is less likely to happen with limited H_{ad} supply.

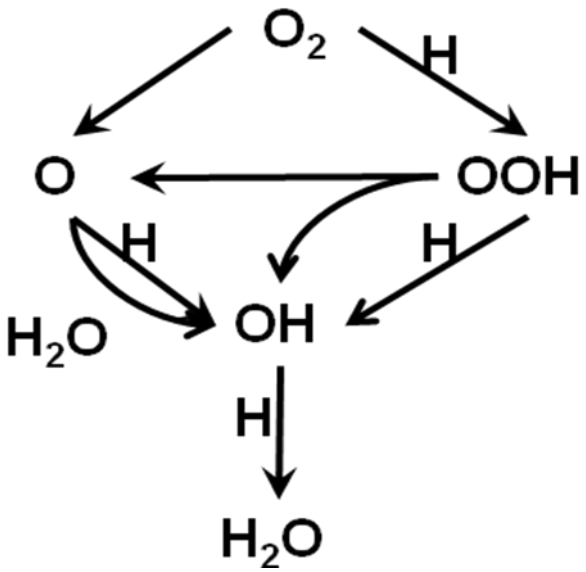

Figure 8-1. Steps involved in ORR

Chapter 9 Mechanism for the Oxygen Reduction Reaction on Pt_3Ni Alloy Fuel Cell Cathodes

Abstract

We use quantum mechanics (QM) (density functional theory (DFT) at the PBE level) to predict the binding-site preferences and reaction barriers for all intermediates involved in the oxygen reduction reaction (ORR) on the low-energy surface of Pt_3Ni alloy. Here we calculate that the surface layer is Ni depleted (100% Pt) while the second layer is Ni enriched (50% Pt) as shown by experiment. Even though the top layer is pure Pt, we find that the sublayer Ni imposes strong preferences in binding sites for most intermediates, which in turn strongly influences the reaction barriers. This strong preference leads to a strong site dependence for the barriers. Considering water as the solvent, we predict that at low coverage (of O and OH), the barrier of the rate determining step (RDS) is 0.81eV, whereas at high coverage, this barrier decreases to 0.38eV. This can be compared to a barrier of 0.50 for pure Pt, explaining the improved rate for the alloy. We report the results both for gas phase and for aqueous phase environments.

Introduction

The efficiency of the oxygen reduction reaction (ORR) ($4H^+ + 4e- + O_2 \rightarrow 2\ H_2O$) at the cathode of proton electrolyte membrane fuel cells (PEMFC) is a critical issue for commercial application of PEMFC in automobiles[1–4]. The best current catalysts are Pt and Pt-based binary alloys, including[63] Pt_3Ni and[100] Pt_3Co. Several different hypotheses

have been put forward for the improved ORR activity of these alloys, including the shift in the d-band[101] or a decrease in the surface lattice parameter to values optimal for ORR[102]. Also it has been argued that that the alloy makes OH removal favorable, increasing the surface area available for O_2 binding[63].

A relatively rare property of Pt_3Ni and Pt_3Co is the surface segregation observed experimentally[103] in 1985 from quantitative analysis of LEED experiments[104]. Our quantum mechanics (QM) (density functional theory [DFT] at the PBE level) calculations using finite slabs find the same segregation of the Pt_3Ni alloy into a structure with 100% percent Pt on the surface layer, 50% on the second layer, and 75% for deeper layers. We consider that this strong segregation to form a pure Pt surface layer (analogous to a core-shell system) may be important in ensuring a long lifetime for these catalysts.

Starting with this segregated surface of Pt_3Ni alloy, we use QM to predict the binding-site preferences and reaction barriers for all intermediates involved in the oxygen reduction reaction (ORR). This leads to a new detailed atomistic-level chemical mechanism explaining the increased reactivity on Pt_3Ni alloys. In particular, we find that subsurface Ni influences the ORR kinetics on the surface even though the surface is 100% Pt.

Methodology

We model the Pt_3Ni alloy as a two-dimensionally infinite periodic slab with four atoms per cell and six layers of atoms. We consider the atomic Pt composition as 100-50-75-75-75-75, as observed experimentally[103] and calculated theoretically[105]. All calculations use the Perdew-Becke-Ernzerhof (PBE) functional of DFT. We use small-

core, norm-conserving, angular momentum projected pseudopotentials[34–37] in which the 3p, 3d, and 4s electrons of Ni and the 5p, 5d, 6s electrons on the Pt are treated explicitly with 16 electrons for neutral Ni and Pt. We use optimized double zeta plus polarization-quality Gaussian-type orbitals on the Pt and Ni with the Seqquest software[29]. To represent the effects of solvent polarization, we use the implicit model developed earlier. [66] The periodic cell parameters of the slab are based on the optimized Pt_3Ni bulk structure (which is 0.08% smaller than the experimental value[106]).

Results and Discussion

Binding site preferences

First, we studied the preference of H, O, OH, H_2O, O_2, and OOH on the various binding sites shown in Figure 9-1. Generally a closest packed (111) surface of FCC metals has four types of sites:

- On top, bonded to one Pt (μ_1), denoted as t,
- Bridging between two Pt (μ_2), denoted as b,
- Bridging between three Pt (μ_3) but in the fcc position (not above atoms of the top or second layer), denoted as f,
- Bridging between three Pt (μ_3) but in the hcp position (above atoms of the second layer), denoted as h.

However for the Pt_3Ni surface, we need to take into account that the second layer is 50% Ni and 50% Pt, while the third layer 25% Ni. We find that the binding energies to the pure Pt layer depend strongly on the nature of the second layer atoms. The various cases are tabulated in Table 9-1. See Figure 9-2 for details.

Considering only the first and second layers, we have two types of top sites: t_1 with one Ni neighbor in the second layer and t_2 with two. Considering also the third layer, we can distinguish t_{1a} with no Ni in the third layer directly beneath the surface and t_{1b} with one. All t_2 sites are the same, even considering the third-layer Ni, as shown in Figure 9-2.

Considering just the top two layers there are four μ_2 bridge sites, depending on the number of Ni atoms underneath it: b_0, b_1, b_2, and b_3, with 0, 1, 2 and 3 Ni atoms in the second layer. Considering also the third layer, there are two subtypes for b_1, b_2, and b_3 depending on the distance to the Ni in the third layer. We denote the subtypes closer to the third layer Ni as b_{1a}, b_{2a}, b_{3a}, and the others as b_{1b}, b_{2b}, b_{3b}, respectively. The b_0, b_{1a}, b_{1b}, b_{2a}, b_{2b}, b_{3a}, and b_{3b} sites are shown in Figure 9-2.

Considering just the top two layers there are two FCC sites: f_1 and f_2 with one and two Ni atoms in the sublayer triangle, but considering the third layer, f_1 splits into f_{1a} and f_{1b}, with f_{1a} on top of the third-layer Ni and the f_{1b} on top of the third-layer Pt.

Similarly, for just the top two layers there are two hcp sites: h_1 and h_2. Here h_1 is on top of the sublayer Ni while h_0 is on top of the sublayer Pt. Considering the third-layer the h_1 splits into h_{1a} and h_{1b}, in which one and zero Ni atoms are in the projected triangle of third-layer atoms as shown in Figure 9-2.

Binding of H. As shown in Table 9-2, the preferred binding sites for H on the Pt_3Ni surface are t_{1a} with a binding energy of 2.70eV, followed by t_{1b} and b_0 with binding energy of 2.60eV without solvation. On the other hand, the b_{3a}, b_{3b}, and t_2 sites in the purple region have binding energy of 2.39–2.44eV without solvation, making them higher than the preferred binding site by 0.28eV without solvation.

With solvation the preferred sites become t_{1a}, b_2, and f_{1b}, with binding energies ranging from 2.78–2.83eV, followed by t_{1b}, b_0, b_{1a}, f_2, h_2, h_{1a}, h_{1b}, and h_2, with binding energy ranging from 2.68–2.74eV,. This favorable region of H is colored orange in Figure 9-1. The barrier for migration of H within the orange region is small. The b_{3a}, b_{3b}, and t_2 sites in the purple region have binding energies of 2.48–2.54eV with solvation, making them higher than the preferred binding site by 0.35eV.

Consequently the blue region serves as a barrier region preventing hydrogen from diffusing between different orange stripes. For the pure Pt surface, the binding energies of H are 2.70–2.80eV without solvation and 2.81–2.81eV with solvation, with no such forbidden region, allowing H to migrate easily in all directions to react with other species.

Binding of O atom. On pure Pt, O_{ad} binds strongly to the FCC site, with a net bonding energy of 3.66eV without solvation and 4.36eV with solvation. For Pt_3Ni, the binding energy for O_{ad} depends dramatically on the site. f_2 is preferred, with a binding energy of 3.47eV, followed by $f_{1a,}$ with 3.06–3.17eV gas phase. With solvent, f_2 and f_{1b} become the two dominant binding sites, with binding energy of 4.49eV and 4.28eV. All other binding sites are at least 0.60eV less stable than f_2. This strong stabilization of f_2 arises because the two electropositive Ni in the second layer enhance the charge transfer to the surface O, stabilizing it, as illustrated by the surface total charge of 0.079 on f_1 and 0.114 on f_{2a} and f_{2b}.

The next-best sites in gas phase are b_0, f_{1b}, and h_2, which are weaker than f_2 by 0.40eV. With solvation, all other sites are weaker than f_2 by at least 0.6eV. All the other sites have small barriers to fall into the f_2 site (except at extremely high coverage).

The binding energy for the FCC site on pure Pt surface is 0.19eV stronger without solvation but 0.13 eV weaker with solvation than f_2.

The smaller Ni atoms allow the surface Pt above two Ni to contract toward the bulk by 0.29A, whereas the surface Pt above one Ni contracts by 0.19A.

These results indicate that dissociation of O_2 strongly prefers to give O_{ad} at the f_2 site, with no migration to other sites.

Binding of OH. On pure Pt, OH has almost the same binding energy on all sites, with a binding energy of 2.22–2.28eV without solvation and 2.57–2.77eV with solvation.

For Pt_3Ni the best site without solvation is b_0 with a binding energy of 2.42eV. Here the OH bond tilts toward h_{1b} (away from f_2). t_{1a}, t_{1b}, f_2, h_2, and b_{1a} are less stable than b_0 by 0.13, 0.20, 0.13, 0.10eV, and 0.17eV without solvation. With solvation, t_{1a} is the most preferred site, with binding energy of 2.83eV, followed by f_2, b_0, and t_{1b}, with binding energy of 2.73–2.75eV. As comparison, OH binds much more weakly to t_2, b_{3a}, and b_{3b}, with binding energy of 2.24–2.47eV. Hence OH selectively binds to the orange region, just as does H. OH_{ad} at other binding sites has a strong preference to migrate to this preferred region. This differs dramatically from the case of the Pt surface where the binding energies of OH range over 0.10eV without solvation and 0.06 eV with solvation, indicating that it can migrate easily.

Binding of O_2. For pure Pt, we find a binding energy of 0.46eV without solvation and 0.87eV with solvation, with a range of just 0.19 and 0.17 eV for various sites for gas phase and solution phase, respectively.

For the Pt_3Ni surface O_2 binds most strongly (0.33–0.59 eV without solvation and 0.62–0.76eV with solvation) to b_0, b_{1a}, b_{2a}, and f_2. All other sites are higher by at least

0.3eV. Thus O_2 has a small preferred binding region near f_2 on Pt_3Ni that is adjacent to the f_2 site for O_{ad} and the b_0 site for OH. This gives a favorable migration pathway for formation of OOH

Binding of OOH. For pure Pt, OOH binds to the top sites with the terminal O bonded to the Pt and the OOH plane parallel to the surface. OOH prefers to have the O=O bond heading to an adjacent Pt atom, leading to a binding energy of 1.06eV without solvation and 1.52eV with solvation.

For Pt_3Ni, we find that t_{1a} is quite favorable, with binding energies of 1.05eV in gas phase and 1.55eV with solvation. Here the preferred orientation for the O=O bond is also toward the adjacent Pt atom, similar to Pt.

All other sites cannot bind OOH, leading instead to dissociation, so once formed OOH cannot migrate on the surface.

Binding of H_2O. H_2O binds only to top sites, but it does not have strong preference between different sites, with binding energies of 0.18–0.20eV in gas phase and 0.57–0.60eV with solvation, all close to the 0.22 and 0.58eV on Pt. Comparing with the 0.40eV solvent stabilization of bulk H_2O, H_2O shows positive binding to both surfaces.

However H_2O does not bind to bridge, fcc, or hcp sites. Thus migration of H_2O from one top site to the next is through adsorption and dissociation. Hence the migration barrier is 0.20eV in gas phase and 0.20eV in solvation (0.60eV binding energy minus the 0.40eV solvation of H_2O).

Binding of H_2O_2. H_2O_2 has a binding energy on Pt_3Ni of 0.23–0.31eV without solvation and 0.58–0.67eV with solvation, close to the 0.27eV and 0.61eV on Pt.

Summary for binding preferences

We find that O_2 prefers b_0, b_{1a}, b_{1b}, and f_2, placing it close to f_2, the only site preferred by O. H prefers to move within in the orange region, allowing it to attack O at the f_2 site to form OH at the b_0, t_{1a}, or t_{1b} site. OH can also move along b_0, t_{1a}, t_{1b}, f_2, and h_2. OOH prefers top sites with second O orienting nearby Pt. H_2O prefers all top sites and H_2O_2 prefers bridge sites.

We see that there is a strong regional preference for O_2, O, H, OH, and OOH to remain in the orange stripes. Of the top sites, t_{1a} and t_{1b} are most preferred for all species. Similarly, b_0 is predominantly preferred among bridge sites. As for threefold binding sites (fcc and hcp, f_{1a}, f_{1b}, f_2, h_{1a}, h_{1b}, h_2), f_2 is strongly preferred. So when the surface is exposed to all the intermediates, at lower coverage (quarter layer), sites b_0, f_2, and t_{1a} (also t_{1b}) are preferred. Only at higher coverage will the adsorbates bind to other sites.

The big picture is that the chemistry prefers the orange region. The direct effect of this is that reaction barriers depend on whether the starting and ending sites are inside the preferred region.

Reaction barriers and possible mechanisms

Our previous studies showed that six fundamental steps are involved in the various possible mechanisms, namely,

a) O_2 dissociation: $O_{2ad} \rightarrow O_{ad} + O_{ad}$

b) OH formation: $O_{ad} + H_a \rightarrow OH_{ad}$

c) H_2O formation: $OH_{ad} + H_a \rightarrow H_2O_a$

d) OOH formation: $O_{2a} + H_a \rightarrow OOH_{ad}$

e) OOH dissociation: $OOH_{ad} \rightarrow OH_{ad} + O_{ad}$.

f) hydration: $O_{ad} + H_2O_a \rightarrow OH_{ad} + O_{ad}$

In putting these fundamental steps into an overall mechanism we distinguish three categories.

- **OO bond activation.** There are two mechanisms: O_2 dissociation (a) and OOH formation (d) followed by OOH dissociation (e).
- **OH formation**. There are two mechanisms: OH formation (b) and O hydration (f).
- **OH consumption**. There is one mechanism, H_2O formation (c).

A good catalyst must provide a low barrier in each of these three categories and for a pathway for connecting them

Starting from the preferred sites, we calculated the barriers for all six steps on Pt_3Ni. The barriers and the comparison with pure Pt are shown in Table 9-4.

Gas phase barriers at high coverage

OO bond activation: On Pt_3Ni, the mechanism of OOH formation followed by OOH dissociation leads to a barrier of 0.32eV (OOH formation barrier since OOH dissociation only has a small barrier of 0.04eV), compared to 1.02eV for the direct dissociation. This is similar to the case of Pt where OOH formation has a barrier of 0.28, compared to 0.58eV for direct dissociation.

OH formation: On Pt_3Ni, O hydration has a barrier of 0.34eV, compared with 0.57eV for the direct OH formation. This preference for O hydration is similar to the case of Pt where the O hydration barrier is 0.29eV, compared to 0.72eV for the direct OH formation.

OH consumption: On Pt_3Ni, H_2O formation has a small barrier of 0.11eV, which is the same as the 0.11eV barrier for the Pt case.

Summarizing the three steps, we have the following preferred mechanism (denoted OOH-form-hydr) for both Pt_3Ni and Pt.

- $O_{2ad} + H_{ad} \rightarrow OOH_{ad}$ (E_a = 0.32eV for Pt_3Ni and 0.28eV for Pt)
- $OOH_{ad} \rightarrow O_{ad} + OH_{ad}$ (E_a = 0.04eV for Pt_3Ni and 0.14eV for Pt)
- $O_{ad} + H_2O_{ad} \rightarrow 2OH_{ad}$ (E_a = 0.34eV for Pt_3Ni and 0.29eV for Pt)
- $OH_{ad} + H_{ad} \rightarrow H_2O_{ad}$ (E_a = 0.11eV for Pt_3Ni and 0.11eV for Pt)

The RDS for this mechanism is O hydration with a barrier of 0.34eV for Pt3Ni. For Pt, the RDS is OOH formation with a barrier of 0.29eV. Hence for the gas phase, Pt out performs Pt_3Ni.

Solution phase barriers at low coverage

OO bond activation: The best O_2 dissociation pathway starts from an f_2-bound O_2 and dissociates to form two O_{ad} at f_2 sites, with a barrier of 0.00eV (because solvent strongly favors dissociation). This is similar to that on Pt surface. On Pt_3Ni, we find that OOH formation has a barrier of 0.17eV, similar to the 0.19eV on Pt. OOH dissociation on Pt_3Ni is barrierless, similar to that on Pt. Thus OOH formation and dissociation are not the favored pathways for the solvated system.

OH formation: For the second step, Pt_3Ni has a direct OH formation barrier of 1.02eV, 0.07eV lower than the 1.09eV on Pt. The O hydration step is less favorable on Pt_3Ni, leading to a barrier of 0.81eV, compared with 0.50eV for Pt. As illustrated in our previous paper [84], O hydration is the dominant mechanism for forming OH on Pt. Hence O hydration is the preferred mechanism for both Pt_3Ni and Pt, with barriers of 0.81eV and 0.50eV. This suggests that P_3Ni would have worse performance for formation of OH_{ad}.

OH Consumption: For the consumption of OH, water formation on Pt_3Ni (0.25eV barrier) is slightly worse than for Pt (0.17eV barrier).

Summarizing these three steps, leads to the O_2-diss-hydr-low mechanism

- O_{2ad} ➔ $2O_{ad}$ (E_a = 0.00 for Pt_3Ni and Pt)
- $O_{ad} + H_2O_{ad}$ ➔ $2OH_{ad}$ (E_a = 0.81eV for Pt_3Ni and 0.50eV for Pt)
- $OH_{ad} + H_{ad}$ ➔ H_2O_{ad} (E_a = 0.11eV for Pt_3Ni and 0.11eV for Pt)

In solution O hydration is the RDS for both Pt_3Ni and Pt, quite different than for gas phase. Hence the overall barrier becomes 0.81eV for Pt_3Ni and 0.50eV for Pt. Thus our results would suggest that Pt_3Ni would not out perform Pt, which does not agree with the experimental result[63] that Pt_3Ni is more efficient than Pt.

Higher coverage, solution phase

The above analysis was based on the assumption that the reactants are each at the preferred sites, that is, all reactants are within the orange region in Figure 9-1. In contrast, at higher coverage reactants might end up in the blue region, even though not preferred at low coverage. The adsorbate coverage on the catalyst surface can be as high as 2/3 monolayer, making the blue region accessible for binding. To consider the changes that might occur at higher coverage, we calculated the corresponding barriers for the blue region.

For O_2 dissociation, starting from h_{1b}, O_2 can easily dissociate to form O_{ad} in the f_{1a} and f_{1b} sites, with a barrier of 0.24eV with solvation and 0.92eV without solvation.

For f_{1a} and f_{1b} O_{ad}, the corresponding O hydration reaction with nearby H_2O has a barrier of 0.44eV in solution but is barrierless in the gas phase.

The following step of H_2O formation also has a low barrier of 0.43 eV with solvation and 0.36eV without solvation.

Hence, when the preferred region is covered with O_{ad}, O_2 can start to bind to the unfavored h_{1b}, and then dissociate to form f_{1a} and f_{1b}. This allows a lower barrier for hydration into 2 OH. This might avoid the high O hydration (0.81eV barrier) and OH formation (1.09eV). The mechanism is as follows O_2-diss-hydr-high.

- O_{2ad} ➔ $2O_{ad}$ (E_a = 0.00 at low coverage and 0.25 at high coverage)
- O_{ad} + H_2O_{ad} ➔ $2OH_{ad}$ (E_a = 0.81eV at low coverage and 0.38eV at high coverage)
- OH_{ad} + H_{ad} ➔ H_2O_{ad} (E_a = 0.11eV at low coverage and 0.43eV at high coverage)

The overall mechanism has O hydration as the RDS with a barrier of 0.43eV, smaller than the 0.50eV for Pt. This mechanism for the reaction on Pt_3Ni happens at higher coverage.

Summarizing the above discussion, in gas phase the preferred mechanism is OOH-form-hydr with a RDS barrier of 0.34eV for Pt_3Ni and 0.29eV for Pt. With solvation at low coverage, where all intermediates can bind to the preferred region, we predict that Pt_3Ni would have slower kinetics than Pt with an overall barrier of 0.81eV. However, at higher coverage, the less preferred (blue) region leads to a RDS barrier of 0.43 eV, smaller than the Pt barrier of 0.50eV. This would be consistent with experiment.

Conclusion

We studied systematically the binding site preference of all reaction intermediates involved in ORR on Pt_3Ni. The binding energy of adsorbates on the alloy surface show strong sublayer dependence. Compared with the pure Pt surface, the binding sites are partitioned into two regions, the preferred (orange) and the less-preferred (blue) region. The mechanism of ORR on Pt_3Ni is similar to that of Pt. In solvent O_2 first dissociates into O_{ad}. O_{ad} then reacts with H_2O to produce OH_{ad}, which finally reacts with H_{ad} to form H_2O.

Due to the substantial difference in binding sites, ORR shows different kinetics on the preferred and not-preferred regions. The overall barrier for ORR in the preferred region is 0.81eV, while the barrier for the non-preferred region is 0.54eV. Thus ORR should be strongly coverage-dependent. At low coverage, all reactants and intermediates adsorb only onto the preferred region, generating a slower reaction rate than with pure Pt. At higher coverage, O_2 begins to react on the non-preferred region, leading to a better rate as compared with pure Pt.

Tables and Figures

BE	BE	H	O	OH	O_2	OOH	H_2O	H_2O_2
	t_{1a}	-2.70	-2.48	-2.29		-1.05	-0.20	
	t_{1b}	-2.60	-2.37	-2.22		-0.97	-0.18	
	t_2	-2.44	-2.16	-2.00		-0.98	-0.18	
	b_0	-2.60	-3.09	-2.42	-0.59			-0.23
	b_{1a}	-2.57	-2.98	-2.25	-0.47			-0.29
	b_{1b}	-2.48	-2.95	-2.10	-0.39			-0.29
	b_{3a}	-2.39	-2.67	-1.96	-0.26			-0.29
	b_{3b}	-2.39	-2.62	-1.85	-0.24			-0.29
Pt_3Ni	b_{2a}	-2.46	-2.76	-1.98	-0.27			-0.31
	b_{2b}	-2.52	-2.75	-2.01	-0.25			-0.31
	f_2	-2.55	-3.47	-2.29	-0.33	-0.93		
	f_{1a}	-2.45	-3.17	-1.92	0.04	-0.77		
	f_{1b}	-2.49	-3.08	-1.89	0.00	-0.78		
	h_{1a}	-2.48	-2.96	-1.90	-0.18			
	h_{1b}	-2.47	-2.94	-1.87	-0.09			
	h_2	-2.53	-3.06	-2.32	-0.15			
	best	-2.70	-3.47	-2.42	-0.59	-1.05	-0.20	-0.31
Pt	t	-2.80	-2.50	-2.23		-1.06	-0.22	
	b	-2.70	-3.10	-2.25	-0.40			-0.27

	f	-2.72	-3.66	-2.22	-0.46		
	h	-2.70	-3.28	-2.28	-0.35		
	best	-2.80	-3.66	-2.28	-0.46	-1.06	-0.22	-0.27

Table 9-1. Binding energies of various species on various sites on Pt_3Ni and Pt without solvation

BE	sites	H	O	OH	O_2	OOH	H_2O	H_2O_2
	t_{1a}	-2.78	-3.10	-2.83		-1.55	-0.61	
	t_{1b}	-2.70	-2.95	-2.73		-1.46	-0.57	
	t_2	-2.48	-2.66	-2.47		-1.45	-0.58	
	b_0	-2.70	-3.70	-2.74	-0.75			-0.58
	b_{1a}	-2.83	-3.82	-2.64	-0.66			-0.63
	b_{1b}	-2.69	-3.79	-2.55	-0.62			-0.64
	b_{3a}	-2.48	-3.25	-2.30	-0.36			-0.64
Pt_3Ni	b_{3b}	-2.54	-3.50	-2.24	-0.37			-0.63
	b_{2a}	-2.57	-3.35	-2.32	-0.39			-0.66
	b_{2b}	-2.63	-3.38	-2.33	-0.40			-0.67
	f_2	-2.74	-4.49	-2.75	-0.76	-1.42		
	f_{1a}	-2.55	-3.80	-2.27	-0.20	-1.24		
	f_{1b}	-2.77	-4.28	-2.28	-0.34	-1.32		
	h_{1a}	-2.69	-3.69	-2.25	-0.38			
	h_{1b}	-2.74	-3.89	-2.31	-0.30			

	h_2	-2.68	-3.66	-2.66	-0.38		
	best	-2.83	-4.49	-2.83	-0.76	-1.55	-0.61	-0.67
	t	-2.87	-3.09	-2.77		-1.52	-0.58	
	b	-2.82	-3.73	-2.63	-0.73			-0.61
Pt	f	-2.85	-4.36	-2.57	-0.87			
	h	-2.81	-3.92	-2.64	-0.70			
	best	-2.87	-4.36	-2.77	-0.87	-1.52	-0.58	-0.61

Table 9-2. Binding energies of various species on various sites on Pt_3Ni and Pt with solvation

Reaction Barriers	Pt	Pt_3Ni	alternative
H_2 Dissociation	0.00	0.05	
O_2 Dissociation	0.58	1.02	0.92
OH Formation	0.72	0.57	0.67
H_2O Formation	0.11	0.11	0.36
OOH Formation	0.28	0.32	
OOH Dissociation	0.14	0.04	
H-OOH dissociation	0.18	0.20	
O hydration	0.29	0.34	0.00

Table 9-3. Reaction barriers for Pt_3Ni in gas phase

* The O hydration on Pt is from 3x3 calculations because the c(2x2) cell is not large enough.

** For Pt_3Ni, to keep the correct periodic condition, we used c(4x2) and c(2x4).

Reaction Barriers	Pt	Pt_3Ni	alternative
H_2 Dissociation	0.00	0.01	
O_2 Dissociation	0.00	0.00	0.24
OH Formation	1.09	1.02	0.80
H_2O Formation	0.17	0.25	0.43
OOH Formation	0.19	0.17	
OOH Dissociation	0.00	0.00	
H-OOH dissociation	0.04	0.22	
O hydration	0.50*	0.81**	0.44

Table 9-4. Reaction barriers on Pt_3Ni with solvation

* The O hydration on Pt is from 3x3 calculations because the c(2x2) cell is not large enough.

** For Pt_3Ni, to keep the correct periodic condition, c(4x2) and c(2x4) were used.

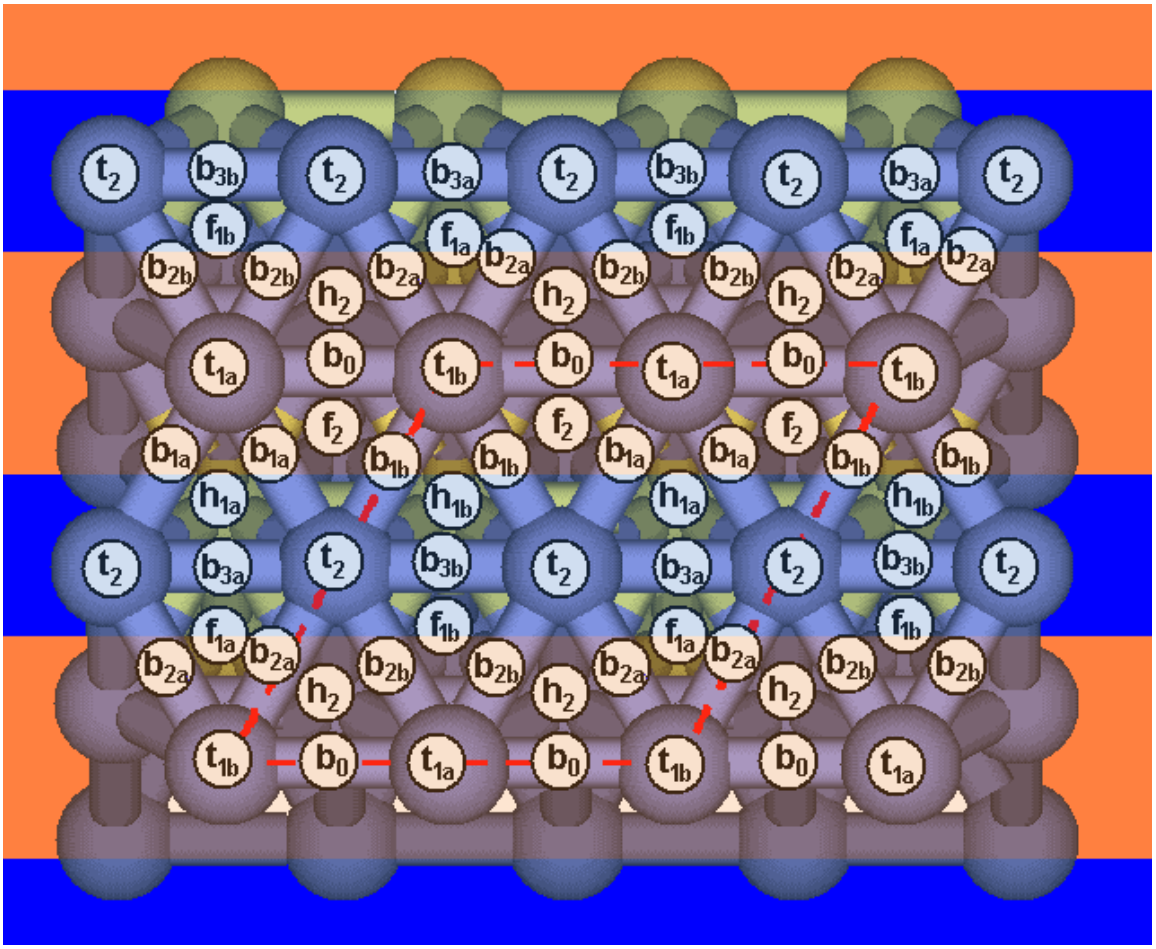

Figure 9-1. Binding sites on Pt_3Ni surface. The blue and orange stripes indicate the partitioning of the Pt surface into two regions induced by the sublayer Ni. The O_2, O, H, OH, and OOH species prefer to move only within the blue stripes.

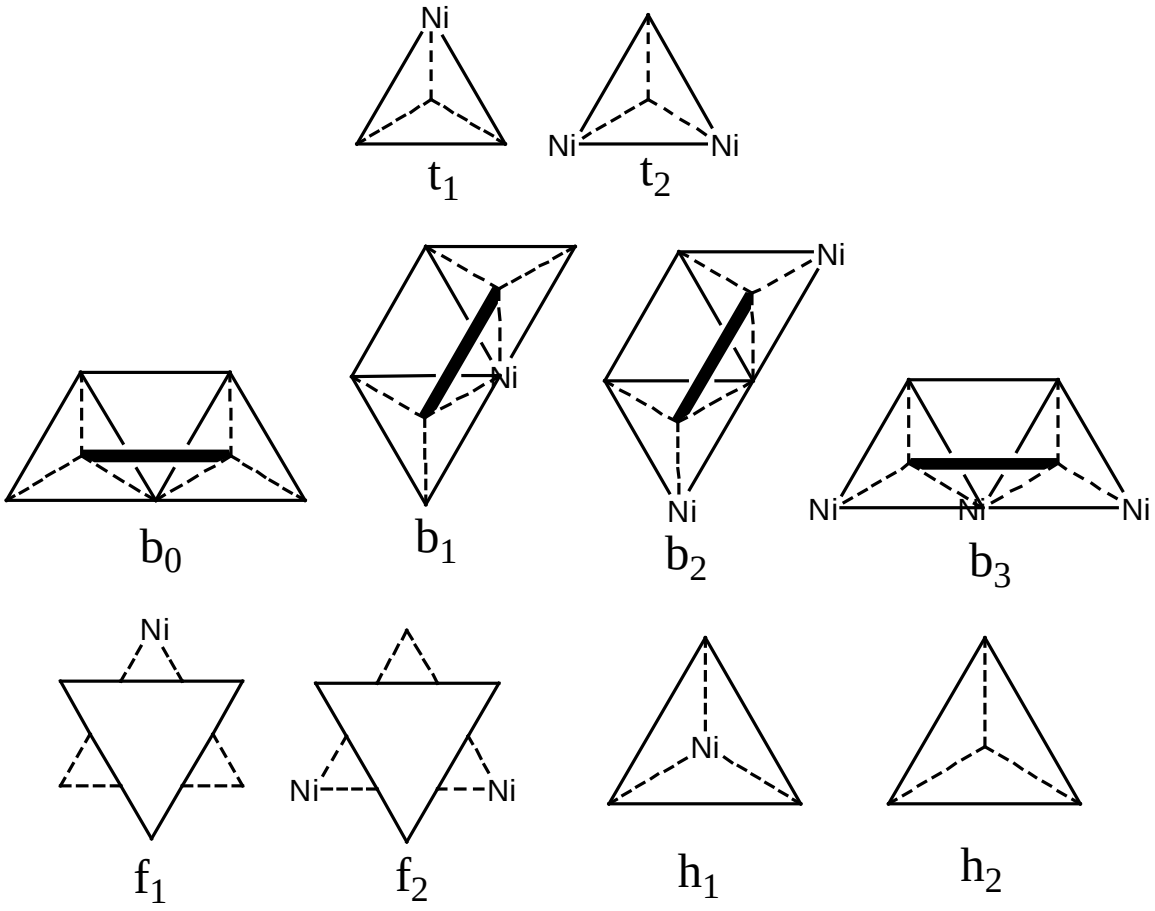

Figure 9-2. Illustration of various binding sites on Pt_3Ni surface. For top sites t_1 and t_2, the triangle indicates the sublayer atoms. t_1 has one Ni atom beneath it, while t_2 has two. For bridge sites, the bridge itself is shown as the thick black line while the two termini of the black line connect the two surface atoms forming the bridge site. The trapezoid beneath are sublayer atoms. b_0-b_3 has 0-3 Ni atoms in this sublayer. An fcc site is in the center of a surface triangle (shown as solid triangle). f_1 and f_2 differ in the sublayer triangle beneath the surface triangle. f_1 has one Ni beneath it while f_2 has two. hcp sites are also in the center of a surface triangle. hcp sites have one sublayer atom beneath it. For h_1 it is Ni, while for h_2 it is Pt.

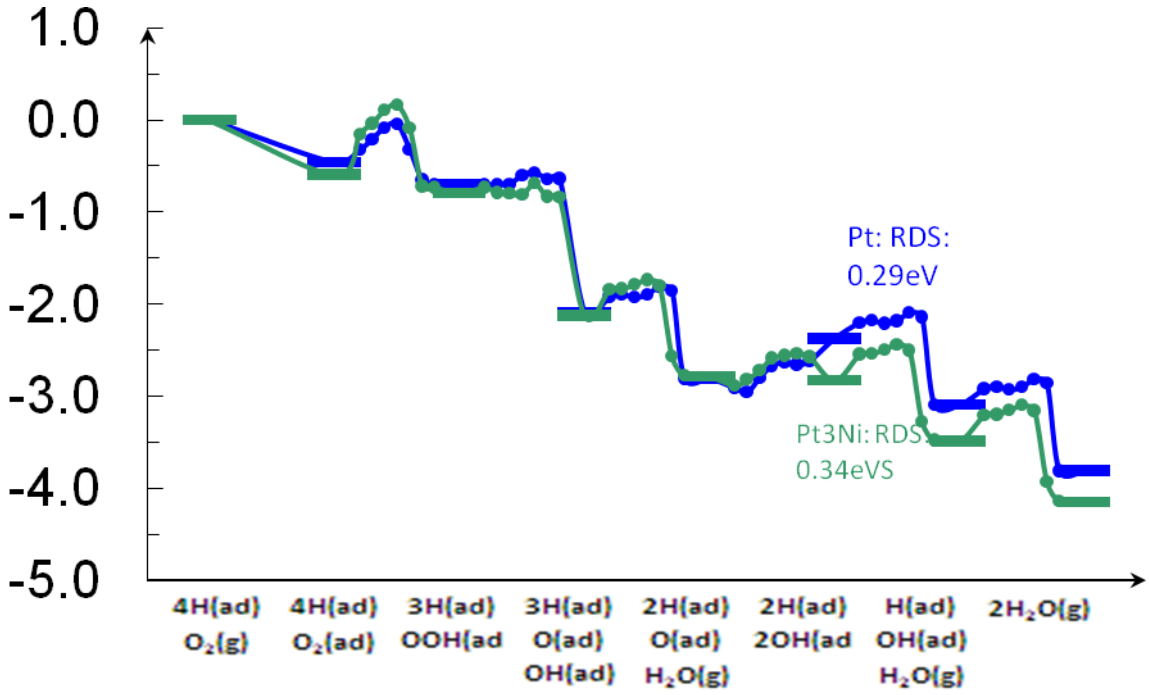

Figure 9-3. Potential energy surface, including barriers, for the OOH-form-hydr mechanism preferred for both Pt and Pt_3Ni in gas phase

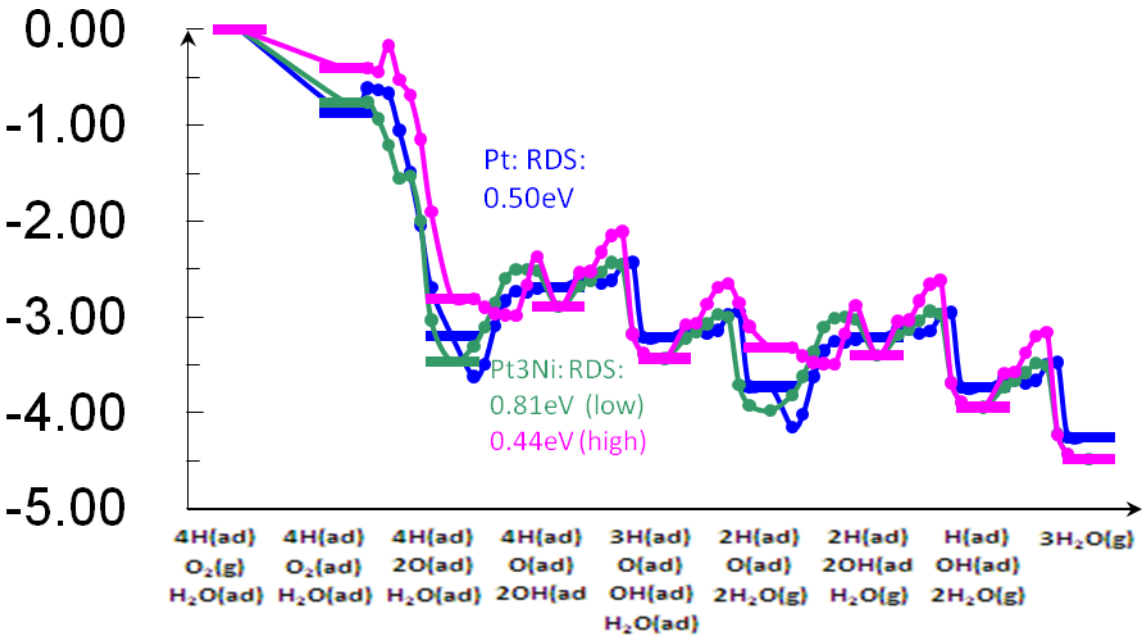

Figure 9-4. Potential energy surface, including barriers, for the O_2-diss-hydr mechanism preferred by both Pt_3Ni and Pt in solution. The purple line shows the alternative mechanism at higher coverage.

Chapter 10 Predictions of the Oxygen Reduction Reaction on Copper-Palladium Alloys

Abstract

Based on the Norskov d-band center hypothesis, we considered that Pd-Cu catalysts might have increased activity over pure Pd for the oxygen reduction reaction (ORR) in fuel cells. To serve as a basis for comparing with experiments on these catalysts and on the d-band structures, we used density functional theory calculations to determine the structural preference and ORR activity as a function of composition and structure. Five PdCu alloy structures are considered and the layered $L1_1$ structure showed promising ORR kinetics.

Introduction

There is great interest in cathode catalysts for proton electrolyte membrane fuel cell (PEMFC) that maintain or improve the high performance for the oxygen reduction reaction (ORR) exhibited by Pt, while dramatically reducing material costs[1–4]. The Norskov d-band center hypothesis suggested that Pd-Cu alloys might have improved oxygen reduction reaction (ORR) in fuel cells compared to Pd[107]. This led to a DOE-BES funded project in which experiments were carried out by Deborah Myers at Argonne National Labs and by John Regalbuto at U. Illinois Chicago Circle. In addition, experiments on the d-band centers for these alloys were carried out by Christian Heske at U. Nevada, Las Vegas. Comparisons of the theory to these d-band experiments will be

discussed in a separate paper. Here we will discuss the crystals and surface structures for PdCu alloys and the predicted ORR raters for these systems.

Methodology

The ORR studies on the PdCu catalysts modeled the system as a slab infinite in two directions (a and b) and finite in the third direction (c). We consider a 3x3 supercell of the (111) surface (4 atoms per layer) that is six layers thick (24 atoms). The top two layers are allowed to relax, representing the active surface, while the bottom four layers are fixed, representing the bulk side of the surface. The same model was applied in previous studies on Pt[66].

All calculations employed the kinetic and exchange-correlation DFT functional developed by Perdew, Burke, and Ernzerhof (PBE) [30]. We used the Seqquest[29] implementation with an optimized double-zeta plus polarization Gaussian-type basis set contracted from calculations on the most stable unit cell of the pure elements. We used the small-core, angular-momentum-projected, norm-conserving, nonlocal effective core potentials[34–37] (pseudopotentials) to replace the core electrons. Thus, the neutral Cu atom was described with 17 explicit electrons (six 3p, one 4s, and ten 3d in the ground state), while Pd included the 4p, 4d, 5s electrons so neutral Pd has 16 electrons.

The real space grid density was 5 points per angstrom, while the reciprocal space grid was 5×5×0 for slab calculations. All calculations allowed the up-spin orbitals to be optimized independently of the down-spin orbitals (spin-unrestricted DFT).

The periodic cell parameters are based on the optimized bulk structure with all possible fcc-type binary alloys.

The solvation of the water phase employed a continuum model[66] based on the Poisson-Boltzmann approximation[23–25,38]. All reaction pathways were determined using the nudged elastic band[55–56] method and solvent effects were included for each point along the path.

For the ordered bulk structures, we use FCC and BCC cubic unit cells with 4 and 2 atoms per cell, respectively, relaxing both the atom and cell parameters. The resulting lattice parameters are tabulated in Table 10-1. The reciprocal space grid was 12×12×12.

For the solid solution (disordered) bulk structures, we randomly placed Pd and Cu atoms in a 2x2x1 16-atom FCC cell. The atoms and volume of the cells were allowed to relax. The resulting lattice parameters are tabulated in Table 1. The reciprocal space grid was 6×6×12.

Table 10-1 shows the predicted lattice parameters of Pd, Cu, Pt, and alloys from DFT compared with experiment. The predicted results are within 2% of experiment.

Results and Discussion

Bulk structures and energetics

The phase diagram, Figure 10-1, shows the following structures:

- A distinct PdCu phase with CsCl type structure stable below 598 C. The composition ranges from 34 to 48 at% Pd at 400°C.
- A Cu_3Pd phase stable below 490°C with $L1_2$ structure (Cu_3Au), with a range of comparison from 20 to 27 at% Pd at 400°C. Two slightly distorted $L1_2$ structures. Cu composition in the range of 23–30 at% Pd at 400°C. The structure deviates from $L1_2$ and has a long-period superstructure (LPS) [108].

- Outside of these ranges the Cu and Pd give a single solid solution phase for 0 to 100%Pd. The structure is fcc-type with Cu randomly replaced by Pd.

Table 10-1 compares the DFT calculated cell parameters and cohesive energies to experiment where we see that for the pure phases the cell parameter is in general systematically larger than the experimental value. The pure Cu, Pd, and Pt lattice parameters are 1.23%, 1.37%, and 1.45% larger than the experimental value. For the PdCu alloys, PdCu (CsCl), $PdCu_3$ ($L1_2$), and PdCu ($L1_0$ and $L1_1$) are 1.40%, 1.21%, and 1.58% larger than the experimental value. All agree well with experiments.

For ORR catalyst particle, it is difficult to generalize the catalytic activity for a solid solution because of the numerous possible structures. Instead we consider the two most common FCC-type binary alloy, $L1_1$ (CuPt type) and $L1_0$ (AuCu type). $L1_1$-type alloy is layered in the (111) direction of an FCC cell, while $L1_0$ is layered in (001) direction. $L1_1$ can be deformed in the (111) direction and becomes a B13 structure.

For the Cu_3Pd composition we considered the $L1_2$ ordered phase in which the Cu are at the faces of a cube and the Pd at the corners. The LPS structures are ignored because they are not likely to exist, or does not differ much from the $L1_2$ structure. We also considered a random alloy. $L1_2$ is the only possible fcc-type structure that keeps all Pd separated from each other. Hence we considered an alternative structure with Pd appearing in pairs. The $L1_2$ structure is more stable than the random structure by 0.20eV per Cu_3Pd unit. This agrees with the fact that at low temperature $L1_2$ is a stable phase, while at higher temperature the alloy becomes solid solution. The LPS structures are not likely to exist or to differ from the $L1_2$ structure. Hence they are ignored in our study. Of particular interest is the 1:1 PdCu composition. The experimentally reported preferred

structures at lower than 598°C are the B_2 or CsCl structure in which the cubic unit cell has Pd at the corners and Cu at the center. Thus each atom has 8 neighbors instead of 12. At temperatures higher than 600°C Cu and Pd form a continuous FCC solid solution phase changing continuously from pure Cu to pure Pd. It is difficult to generalize the catalytic activity for a solid solution because of the numerous possible structures. Considering the fact that Cu_3Pd alloys have ordered versions of FCC, we considered two PdCu might also have a stable ordered phase related to FCC. Consequently instead of a random PdCu structure, we optimized two FCC-like ordered phases for the PdCu compositions. We considered the $L1_0$ structure (see Figure 10-2) in which the Cu and Pd are ordered in the (100) direction of FCC unit cell and the $L1_1$ structure in which the Cu and Pd are ordered in the (111) direction of FCC. $L1_1$ can be deformed in the (111) direction leading to the B13 structure, which has been observed experimentally[109]. As shown in Table 10-1, we find the $L1_1$ and $L1_0$ phase are less stable than the CsCl structure by 0.26eV per PdCu unit.

We consider that the $L1_1$/B13 phase of PdCu could be a potential interesting catalyst because it has layered structure in the closed packing direction. $L1_0$ is also layered, but its closed packing surface would always have half-Cu/half-Pd and hence be subject to much faster corrosion in the desired acid environment. The $L1_1$ structure however, is layered in the closed packing direction. Thus in a catalyst, we can expect that the Cu plane could be oxidized off the surface, leaving a closest, packed Pd surface exposed to the reactants at the cathode.

Consequently we examined the ORR reaction as reported in the next section.

Surface structures and energetics

For FCC structure, it is clear that (111) is preferred. Hence for Cu_3Pd, it is a pure Cu surface, for $L1_0$ it is the closed packing (221) surface. For $L1_1$/B13, there are two unique closed packing surfaces, one with the surface Pd connecting to two sublayer Pd atoms and another with the surface Pd connecting to one Pd atom in sublayer.

For CsCl structure, it's not clear which surface is preferred. Hence we did a surface cleavage study by cleaving all possible low-index surfaces and calculating the corresponding surface energy. The six most stable surfaces are shown in Table 10-2. We can see that the most preferred surfaces are (320) and (110). (320) surface can be viewed as a tilted (110) surface or, in other words, a (110) surface with steps. So in the following calculations, we focused on the (110) surface on CsCl-structured PdCu alloy.

Binding site preferences on Cu, Pd, PdCu, and $PdCu_3$

First of all, we studied the preferred binding sites of O, H, O_2, OH, H_2O, OOH, and H2O on all the involved surfaces. Table 10-3 shows the binding energies of all the intermediates on all PdCu alloy surfaces involved. We also included the corresponding numbers for Pt, Pd, and Cu for comparison.

H prefers to bind to ccp sites on Pd, Cu, and all layered $L1_1$ PdCu, PCu_3 and CsCl-structured PdCu alloy surfaces. Similar to Pd and Cu, the top site is a stable binding site but is less preferred. Nonlayered $L1_1$ PdCu and $L1_0$ PdCu prefer top sites. This unique preference comes from the fact that they both have lines of Pd atoms on the surface. H binds much more strongly to Pd than to Cu.

O prefers to bind to fcc sites for Pd, Cu, Pt, and all alloys except CsCl-structured and $L1_0$-structured PdCu alloys. For CsCl-structured PdCu, the smaller distance between

surface atoms (2.62A as compared to 2.70A) helps improve the stability of the μ_2 site. For all mixed-metal surfaces (CsCl structured, $L1_0$ and $L1_1$ nonlayered), sites with more adjacent Cu are always preferred, mostly due to the fact that O binds more strongly to Cu.

OH prefers to bind to μ_2, μ_3-ccp, and μ_3-hcp with similar binding energies. This leads to a flat surface on the metals and high mobility for OH, given that the OH can migrate through a μ_2 site. Similar to the case of O_{ad}, OH prefers to bind to Cu on the surface rather than Pd. Hence for the stripped $L1_0$ and $L1_1$ nonlayered structure, the migration is limited to the Cu line.

O_2 prefers to bind to a ccp site, except for CsCl-structured PdCu, where a bridge site is preferred. Again, strong bond energy between O and Cu makes all sites with more connected Cu preferred ones.

OOH and H_2O can only bind to top sites for all the materials involved.

Barriers for the essential steps

Here we only discuss the two most popular mechanisms: O_2 dissociation mechanism and OOH association mechanism. The steps involved are O_2 dissociation, OH formation, H_2O formation, OOH formation, and OOH dissociation. See Table 10-5 and Table 10-6 for the barriers with and without solvation.

O_2 dissociation is easy on $PdCu_3$ surface with a low barrier of 0.15eV without solvation, mostly due to the stable O_{ad}. On B2 and $L1_0$-structured PdCu surface the reaction has a higher barrier of 0.42eV and 0.33eV. Layered $L1_1$ PdCu has a high barrier of 0.89eV due to the weak binding of O_{ad} (3.35eV as compared to > 3.93eV for other alloys).

OH formation is difficult on Pd but much easier on PdCu alloys; the direct OH formation barrier is 0.19eV, 0.09eV, and 0.12eV on $L1_0$, $L1_1$ non layered, and $L1_1$ layered. The barrier is much higher on B2-CsCl and $L1_2$-structured PdCu. Solvation greatly increases the barriers for Pt, $PdCu_3$, and CsCl-structured alloys. For others, the barriers remain low.

H_2O formation is difficult on $L1_2$-structured, CsCl-type alloys with a barrier of 0.83eV and 0.87eV without solvation. Layered PdCu has a much lower barrier of 0.46eV. With solvation, the barrier increases as solvation stabilizes OH. The only exception is layered PdCu with a barrier of 0.50eV.

OOH formation is easy on the metals with a barrier of 0.34–0.50eV, followed by its dissociation with barrier of 0.00–0.36eV.

Rate limiting steps for each alloy and possible mechanism

For $L1_2$, CsCl, $L1_0$ and $L1_1$ nonlayered alloys, the obvious rate limiting step is the formation of H_2O. The corresponding barriers are 1.11eV, 0.95eV, 0.95eV, and 0.72eV—all too high for an acceptable ORR catalyst. Since the step is essential for ORR, it necessarily blocks ORR on the four types of alloys.

For layered $L1_1$, the situation is much better; with solvation, it can go through O_2-diss mechanism as follows:

(1a) $O_{2ad} \rightarrow 2O_{ad}$ [E_a = 0.89eV without solvation and 0.31eV with solvation]

(2a) $O_{ad} + H_{ad} \rightarrow OH_{ad}$ [E_a = 0.12eV without solvation and 0.48 with solvation]

(3a) $OH_{ad} + H_{ad} \rightarrow H_2O_{ad}$. [$E_a$ = 0.46eV without solvation and 0.50eV with solvation].

The RDS is hence O_2 dissociation with a barrier of 0.89eV in gas phase, and H_2O formation with a barrier of 0.50eV with solvation. Comparing with the Pt barrier of

0.50eV and Pd barrier of 0.76eV, we can see that the PdCu-layered alloy shows a great improvement in kinetics as well as cost, compared with Pd.

Comparison with later experimental results of colloidal Pd-Cu alloy

The calculations were carried in advance of the experimental studies for PdCu alloy materials to provide some insight useful for interpreting the experiments. Figure 10-3 shows the experimental mass activity of various Pd-Cu colloidal catalysts reported recently[107]. The mass activity was much higher for Pt (~ 1450 mA/mg) than Pd (~ 200 mA/mg), as expected. However, the mass activity of Pd-Cu alloys is higher than pure Pd (~ 800 mA/mg for PdCu and ~ 600 mA/mg for $PdCu_3$). This is consistent with the results from our computational studies.

In the analysis of the Pd-Cu catalysts by X-ray diffraction, the structures were determined to be disordered FCC rather than the BCC-like (B2) phase observed experimentally to be the stable phase for this composition. This is probably due to the heat treatment above the order/disorder transition temperature. Indeed, as shown above, the BCC structure would have poor performance, whereas the ordered $L1_1$ phase is predicted to have good performance. This suggests that the heat treatment might have facilitated the formation of the ORR favorable phase. Probably the acid treatment helped by removing the disordered components.

Analysis of d-band centers

Norskov proposed a simple model that correlates the d-band center of the surface metal to catalytic activity[110]. Indeed, he found the adsorption energy of simple adsorbates (O, CO, H) correlated well with the center of the surface metal d-band[17,110]. We will publish elsewhere a detailed description of the band structures for these PdCu alloys with

a comparison with the XPS DOS[111]. These results show that the d-band center of Pd (-2.31 eV) is lower than that of Pt (-3.15 eV). However, alloying with Cu moves the Pd d-band center more negatively, putting it closer to Pt for $L1_0$ $PdCu_3$ (-2.41), disordered $PdCu_3$ (-2.72), and disordered PdCu (-2.50). Based on this analysis, we see that the d-band center of the disordered PdCu and $PdCu_3$ alloys in the experimental study[107] is closer to Pt. However, the mass activity of $PdCu_3$ is lower than that of PdCu, even though its d-band center is closer to Pt than PdCu. This suggests that the Norskov band-center idea may provide some useful guidance in selecting alloys for ORR.

Conclusion

In this research we studied systematically the possible phases and preferred surfaces at different atomic concentrations. Five unique surfaces, namely B2 (110), PdCu3, layered and non-layered $L1_1$, and $L1_0$, were considered for further ORR mechanism investigations. We decided the binding preference, reaction barriers, and preferred reaction pathway on the PdCu alloy surfaces using first principle calculations. The high H_2O formation barrier for $L1_2$, B2, $L1_0$, and $L1_1$-nonlayered PdCu surface (1.04eV, 0.83eV, 0.87eV, and 0.69eV) makes them bad catalyst for ORR. As comparison, layered $L1_1$ PdCu alloy has a low H2O formation barrier of 0.50eV. This, combining with the O_2 dissociation and OH formation with barriers of 0.31eV and 0.48eV, leads to O_2-diss mechanism with an overall barrier of 0.50eV. Hence we predicted that layered PdCu alloy would have similar performance as pure Pt surface. One would need to maximize the $L1_1$ layered surface in the catalyst. This agrees with later experiment where PdCu has

improved performance as compared to Pd. And it also explains why heat and acid treatment could boost the ORR performance for PdCu alloy.

Tables and Figures

	Structure	cell parameters (Å) DFT	Cell parameters (Å) Experiment	Cohesive energy (eV) QM, per atom
Cu (FCC)		3.66	3.615[112]	3.63
Pd (FCC)		3.954	3.90[113]	4.27
Pt (FCC)		3.980	3.97[113]	
$PdCu_3$ ($L1_2$, FCC)		3.734	3.676[114]	3.96
$PdCu_3$ (FCC solid solution)		N/A	3.765[109]	3.91
PdCu (B1, BCC)	Pm3m	3.020	2.981[109]	4.17
PdCu ($L1_0$, FCC)		3.820*	N/A	4.04
PdCu ($L1_1$/B13, FCC)	R3m	2.706**	2.700[109]	4.04
PdCu (FCC solid solution)		N/A	3.765[109]	

Table 10-1. Calculated lattice parameter as compared to experimental value

* For $L1_0$ structure has a tetragonal cell containing a PdCu unit, to make comparison easier, convert that to a fcc-type cell instead of the tetragonal cell.

** For $L1_1$, the unit cell contains 32 atoms which is beyond the range that we can handle. Instead we used the triclinic cell with three-fold rotational symmetry forced. The number represents the Pd-Cu distance.

Surface (hkl)	Energy (eV/A^2)	Energy (erg/cm^2)
PdCu(320)	0.270	4.32×10^3
PdCu(110)	0.271	4.35×10^3
PdCu(100)	0.290	4.65×10^3
PdCu(210)	0.294	4.72×10^3
PdCu(310)	0.301	4.83×10^3
PdCu(332)	0.303	4.86×10^3

Table 10-2. Six most table surfaces of B2 PdCu

Binding Energy (eV)	Binding Site	Pt	Pd	Cu	$PdCu_3$-$L1_2$	PdCu-CsCl	PdCu-$L1_0$	PdCu-$L1_1$-non-layered	PdCu-$L1_1$-layered
M		0.00	0.00	0.00	0.00	0.00	0.00	0.00	0.00
M-H	μ_1	-2.90	-2.37	-2.03	-2.03	-2.24	-2.64	-2.81	-2.06
	μ_2	-2.75	-2.68	-2.40*	-2.49	-2.79	-2.62	-2.72	-2.52
	μ_3-ccp	-2.75	-2.78	-2.50	-2.60	-2.82	-2.66	-2.79	-2.65
	μ_3-hcp	-2.75	-2.76	-2.51	-2.58	-2.67	-2.63	-2.58	-2.68
M-O	μ_1	-2.70	-2.52	-2.79	-2.54	-2.46	-2.27	-2.41	-2.05
	μ_2**	-3.33	-3.38	-4.05	-3.99	-3.93	-3.80	-3.76	-2.91
	$\tilde{\mu}_3$-ccp	-3.89	-3.82	-4.40	-4.43	-3.93	-3.75	-3.96	-3.35
	μ_3-hcp	-3.38	-3.63	-4.29	-3.98	-3.78	-3.94	-3.82	-3.19
M-OH	μ_1	-2.42	-2.52	-2.23	-2.27	-1.95	-2.42	-2.52	-2.23
	μ_2	-2.67	-2.76	-2.53	-2.70	-2.16	-2.67	-2.76	-2.53
	μ_3-ccp	-2.69	-2.72	-2.42	-2.66	-2.12	-2.69	-2.72	-2.42
	μ_3-hcp	-2.68	-2.74	-2.81	-2.55	-2.12	-2.68	-2.74	-2.81
$M-O_2$	bridge	-0.45	-0.63	-0.46	-0.71	-0.35	-0.45	-0.63	-0.46
	ccp	-0.61	-0.71	-0.36	-0.61	-0.25	-0.61	-0.71	-0.36
	hcp	-0.47	-0.62	-0.31	-0.54	-0.26	-0.47	-0.62	-0.31
M-OOH	μ_{1b}	-1.20	-1.10	-1.27	-1.03	-1.18	-0.96	-0.94	-0.76
	μ_{1c}	-1.07	-1.05	-1.20	-0.90	-0.99	-0.92	-0.93	-0.77

M-H_2O_2	bridge	-0.30	-0.35	-0.22	-0.24	-0.30	-0.26	-0.30	-0.28
M-H_2O	μ_1	-0.29	-0.26	-0.19	-0.24	-0.16	-0.24	-0.22	-0.25

Table 10-3. Binding energies for the intermediates involved in ORR on Pt, Pd, Cu, and PdCu alloys

*H is not stable on μ_2 bridge site on Cu, $PdCu_3$ ($L1_2$).

** O is not stable on μ_2 bridge site, serves as the transition state of surface diffusion.

Binding Energy (eV)	Binding Site	Pt	Pd	Cu	$PdCu_3$-$L1_2$	PdCu-CsCl	PdCu-$L1_0$	PdCu-$L1_1$-non-layered	PdCu-$L1_1$-layered
M		0.00	0.00	0.00	0.00	0.00	0.00	0.00	0.00
M-H	μ_1	-2.97	-2.47	-2.05	-2.25	-2.37	-2.90	-3.22	-2.20
	μ_2	-2.88	-2.82	-2.43	-2.61	-3.05	-2.87	-2.92	-2.67
	μ_3-ccp	-2.88	-2.94	-2.54	-2.67	-2.98	-2.74	-2.88	-2.77
	μ_3-hcp	-2.87	-2.90	-2.54	-2.65	-2.70	-2.77	-2.85	-2.87
M-O	μ_1	-3.28	-3.13	-3.35	-3.04	-2.97	-2.90	-2.96	-2.78
	μ_2**	-3.96	-3.88	-4.51	-4.92	-4.88	-4.60	-4.18	-3.57
	μ_3-ccp	-4.60	-4.36	-4.90	-5.58	-4.85	-4.77	-5.10	-4.02
	$\mu_{3\text{-hcp}}$	-4.02	-4.15	-4.78	-4.90	-4.29	-4.55	-4.31	-3.90
M-OH	μ_1	-2.92	-2.79	-3.08	-2.87	-2.86	-2.69	-2.80	-2.58
	μ_2	-2.83	-2.90	-3.36	-3.04	-3.17	-2.96	-3.18	-2.69

	μ_3-ccp	-2.75	-2.81	-3.33	-3.02	-3.16	-2.92	-3.19	-2.55
	μ_3-hcp	-2.86	-2.82	-3.31	-3.16	-3.15	-2.92	-2.87	-2.57
	bridge	-0.95	-0.89	-0.83	-0.70	-0.88	-0.73	-0.93	-0.60
M-O_2	ccp	-1.16	-1.05	-1.10	-1.17	-1.18	-0.65	-0.89	-0.52
	hcp	-0.93	-0.97	-1.09	-1.00	-1.16	-0.79	-0.81	-0.57
M-OOH	μ_{1b}	-1.66	-1.50	-1.73	-1.44	-1.62	-1.36	-1.36	-1.31
	μ_{1c}	-1.54	-1.48	-1.68	-1.38	-1.57	-1.29	-1.36	-1.35
M-H_2O_2	bridge	-0.64	-0.66	-0.51	-0.58	-0.66	-0.53	-0.61	-0.67
M-H_2O	μ_1	-0.67	-0.60	-0.52	-0.61	-0.63	-0.56	-0.58	-0.70

Table 10-4. Binding energies for intermediates involved in ORR on Pt, Pd, Cu, and PdCu alloys with solvent effect

Reaction Barriers	Pt	Pd	Cu	$PdCu_3$-$L1_2$	PdCu-CsCl	PdCu-$L1_0$	PdCu-$L1_1$-nonlayered	PdCu-$L1_1$-layered
H_2 Dissociation	0.00	0.00	0.16	0.66	0.19	0.30	0.30	0.43
O_2 Dissociation	0.51	0.72	0.12	0.15	0.42	0.44	0.66	0.89
OH Formation	0.82	0.27	0.00	0.46	0.47	0.19	0.09	0.12
H_2O Formation	0.12	0.53	0.84	1.04	0.83	0.87	0.69	0.46
OOH Formation	0.34	0.50	0.37	0.42	0.75	0.46	0.36	0.40
OOH Dissociation	0.01	0.32	0.49	0.04	0.09	0.28	0.61	0.65

Table 10-5. Barriers for the reaction steps involved in ORR without solvation

Reaction Barriers	Pt	Pd	Cu	PdCu3-$L1_2$	PdCu-CsCl	PdCu-$L1_0$	PdCu-$L1_1$-nonlayered	PdCu-$L1_1$-layered
H_2 Dissociation	0.00	0.00	0.04	0.59	0.00	0.25	0.10	0.21
O_2 Dissociation	0.00	0.31	0.00	0.00	0.07	0.20	0.23	0.31
OH Formation	1.23	0.42	0.14	0.84	1.00	0.27	0.23	0.48
H_2O Formation	0.24	0.76	0.94	1.11	0.95	0.95	0.72	0.50
OOH Formation	0.25	0.65	0.43	0.50	0.86	0.65	0.50	0.56
OOH Dissociation	0.00	0.04	0.31	0.00	0.00	0.00	0.36	0.22

Table 10-6. Barriers for the reaction steps involved in ORR with solvation

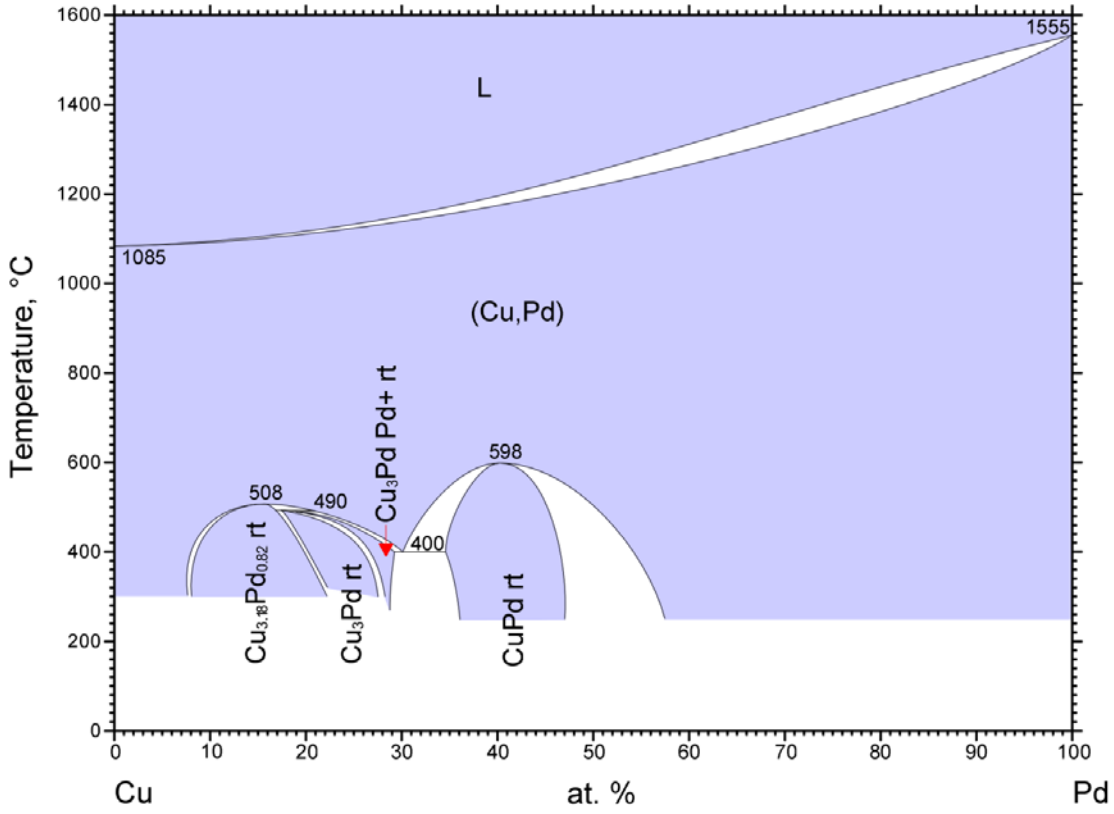

Figure 10-1. Phase diagram of PdCu system. Three unique phases exists in the diagram. A bcc type phase at around 45% atomic ratio, an FCC type Cu_3Pd ($AuCu_3$ structure), and a FCC-type solid solution phase. (From ASM[115])

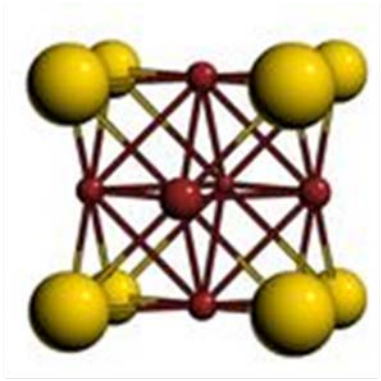

$L1_2$

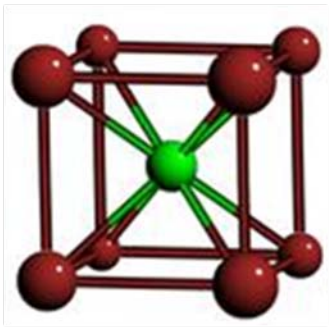

β(CsCl)

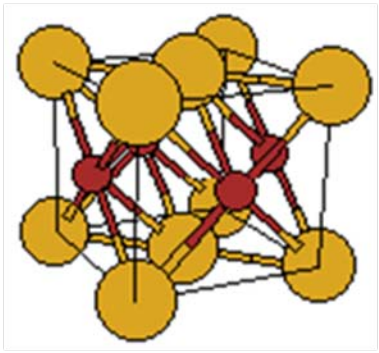

$L1_0$

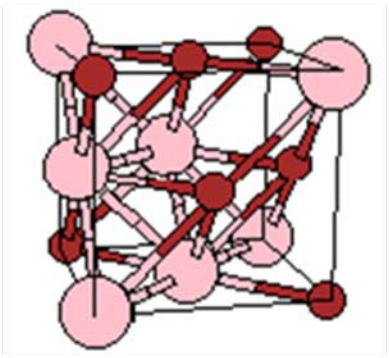

$L1_1$

Figure 10-2. Four type of bulk structures considered in this research. (Images taken from http://en.wikipedia.org/)

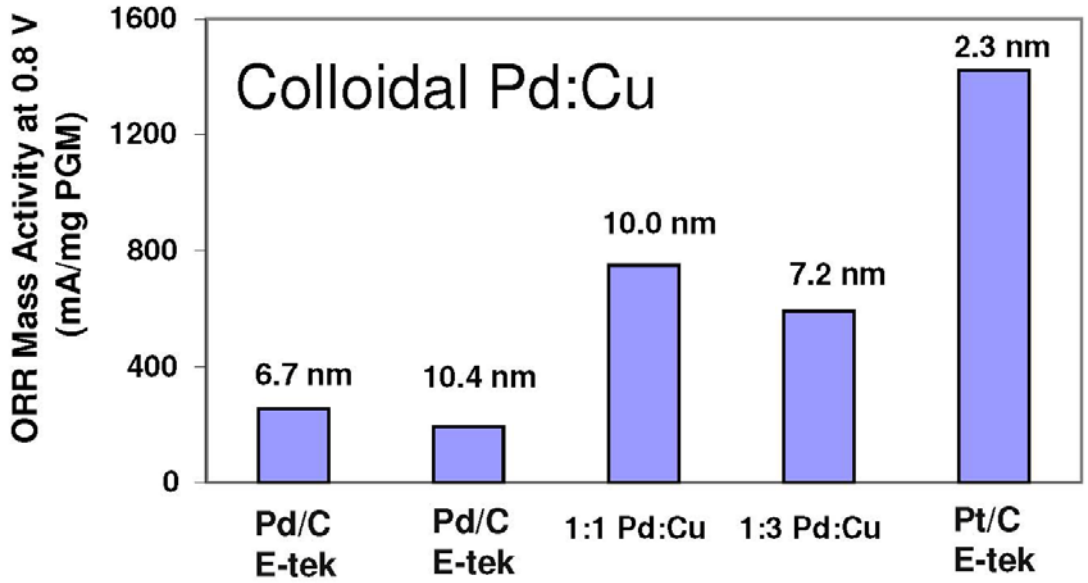

Figure 10-3. Mass activity of Pt, Pd, and Pd-Cu alloy catalysts. This shows that the 1:1 PdCu catalyst has a performance about half as good as Pt, and over twice as good as Pd. Based on the results of Deborah J. Myers, etc.[107]

References

(1) Kordesch, K.; Simader, G. *Fuel Cells and Their Applications*; VCH: New York, 1996.

(2) Appleby, A.; Foulkes, F. *Fuel Cell Handbook*; Van Nostrand Reinhold: New York, 1989.

(3) Brandon, N. P.; Skinner, S.; Steele, B. C. H. *Annu. Rev. Mater. Res.* **2003**, *33*, 183.

(4) Mehta, V.; Cooper, J. S. *J. Power Sources* **2003**, *114*, 32.

(5) Baturina, O. A.; Garsany, Y.; Zega, T. J.; Stroud, R. M.; Schull, T.; Swider-Lyons, K. E. *J. Electrochem. Soc.* **2008**, *155*, B1314.

(6) Neophytides, S. G.; Murase, K.; Zafeiratos, S.; Papakonstantinou, G.; Paloukis, F. E.; Krstajic, N. V.; Jaksic, M. M. *J. Phys. Chem. B* **2006**, *110*, 3030.

(7) Shim, J.; Lee, C. R.; Lee, H. K.; Lee, J. S.; Cairns, E. J. *J. Power Sources* **2001**, *102*, 172.

(8) Xiong, L.; Manthiram, A. *Electrochim. Acta* **2004**, *49*, 4163.

(9) Wang, B. *J. Power Sources* **2005**, *152*, 1.

(10) Michaelides, A.; Hu, P. *J. Am. Chem. Soc.* **2001**, *123*, 4235.

(11) Hyman, M. P.; Medlin, J. W. *J. Phys. Chem. B* **2006**, *110*, 15338.

(12) Qi, L.; Yu, J. G.; Li, J. *J. Chem. Phys.* **2006**, *125*, 8.

(13) Zhang, T.; Anderson, A. B. *Electrochim. Acta* **2007**, *53*, 982.

(14) Jacob, T.; Goddard, W. A. *ChemPhysChem* **2006**, *7*, 992.

(15) Nilekar, A. U.; Mavrikakis, M. *Surf. Sci.* **2008**, *602*, L89.

(16) Janik, M. J.; Taylor, C. D.; Neurock, M. *J. Electrochem. Soc.* **2009**, *156*, B126.

(17) Norskov, J. K.; Rossmeisl, J.; Logadottir, A.; Lindqvist, L.; Kitchin, J. R.; Bligaard, T.; Jonsson, H. *J. Phys. Chem. B* **2004**, *108*, 17886.

(18) Wang, Y.; Balbuena, P. *J. Phys. Chem. B* **2005**, *109*, 14896.

(19) Ogasawara, H.; Brena, B.; Nordlund, D.; Nyberg, M.; Pelmenschikov, A.; Pettersson, L.; Nilsson, A. *Phys. Rev. Lett.* **2002**, *89*, 276102.

(20) Hamada, I.; Morikawa, Y. *J. Phys. Chem. C* **2008**, *112*, 10889.

(21) Xu, X.; Muller, R. P.; Goddard, W. A. *Proc. Natl. Acad. Sci. U. S. A.* **2002**, *99*, 3376.

(22) Keith, J. A.; Oxgaard, J.; Goddard, W. A. *J. Am. Chem. Soc.* **2006**, *128*, 3132.

(23) Tomasi, J.; Persico, M. *Chem. Rev.* **1994**, *94*, 2027.

(24) Cramer, C.; Truhlar, D. *Chem. Rev.* **1999**, *99*, 2161.

(25) Tannor, D. J.; Marten, B.; Murphy, R.; Friesner, R. A.; Sitkoff, D.; Nicholls, A.; Ringnalda, M.; Goddard, W. A.; Honig, B. *J. Am. Chem. Soc.* **1994**, *116*, 11875.

(26) Rogstad, K. N.; Jang, Y. H.; Sowers, L. C.; Goddard, W. A. *Chem. Res. Toxicol.* **2003**, *16*, 1455.

(27) Jones, C. J.; Taube, D.; Ziatdinov, V. R.; Periana, R. A.; Nielsen, R. J.; Oxgaard, J.; Goddard, W. A. *Angew. Chem. Int. Edit.* **2004**, *43*, 4626.

(28) Nielsen, R. J.; Goddard, W. A. *J. Am. Chem. Soc.* **2006**, *128*, 9651.

(29) Schultz, P. *SeqQuest Code Project;* Sandia National Laboratories, (http://www.cs.sandia.gov/~paschul/Quest/).

(30) Perdew, J.; Burke, K.; Ernzerhof, M. *Phys. Rev. Lett.* **1996**, *77*, 3865.

(31) Ceperley, D. M.; Alder, B. J. *Phys. Rev. Lett.* **1980**, *45*, 566.

(32) Perdew, J. P.; Zunger, A. *Phys. Rev. B.* **1981**, *23*, 5048.

(33) Kohn, W.; Sham, L. J. *Physical Review* **1965**, *140*, A1133.

(34) Melius, C. F.; Goddard, W. A. *Phys. Rev. A* **1974**, *10*, 1528.

(35) Melius, C. F.; Olafson, B. D.; Goddard, W. A. *Chem. Phys. Lett.* **1974**, *28*, 457.

(36) Redondo, A.; Goddard, W. A.; Mcgill, T. C. *Phys. Rev. B.* **1977**, *15*, 5038.

(37) Hamann, D. R. *Phys. Rev. B.* **1989**, *40*, 2980.

(38) Baker, N.; Sept, D.; Joseph, S.; Holst, M.; McCammon, J. *Proc. Natl. Acad. Sci. U. S. A.* **2001**, 181342398.

(39) Holst, M.; Saied, F. *J. Comb. Chem.* **1993**, *14*.

(40) Holst, M.; Saied, F. *J. Comb. Chem.* **1995**, *16*, 337.

(41) Goddard, W. A.; Jaramillo-Botero, A.; Liu, Y.; Duin, A. v.; Buehler, M.; Meulbroek, P.; Dodson, J. *The Computational Materials Design Facility (CMDF) Project;* (http://www.wag.caltech.edu/multiscale/multsicale_computations.htm).

(42) Parker, D.; Bartram, M.; Koel, B. *Surf. Sci.* **1989**, *217*, 489.

(43) Nolan, P. D.; Lutz, B. R.; Tanaka, P. L.; Davis, J. E.; Mullins, C. B. *Phys. Rev. Lett.* **1998**, *81*, 3179.

(44) Puglia, C.; Nilsson, A.; Hernnas, B.; Karis, O.; Bennich, P.; Martensson, N. *Surf. Sci.* **1995**, *342*, 119.

(45) Gland, J. L.; Sexton, B. A.; Fisher, G. B. *Surf. Sci.* **1980**, *95*, 587.

(46) Eichler, A.; Hafner, J. *Phys. Rev. Lett.* **1997**, *79*, 4481.

(47) Li, T.; Balbuena, P. B. *Chem. Phys. Lett.* **2003**, *367*, 439.

(48) Michaelides, A.; Hu, P. *J. Chem. Phys.* **2001**, *114*, 513.

(49) Meng, S.; Xu, L. F.; Wang, E. G.; Gao, S. W. *Phys. Rev. Lett.* **2002**, *89*.

(50) Bădescu, C.; Salo, P.; Ala-Nissila, T.; Ying, S.; Jacobi, K.; Wang, Y.; Bedürftig, K.; Ertl, G. *Phys. Rev. Lett.* **2002**, *88*, 136101.

(51) Parker, S. F.; Frost, C. D.; Telling, M.; Albers, P.; Lopez, M.; Seitz, K. *Catal. Today* **2006**, *114*, 418.

(52) Graham, A. P.; Menzel, A.; Toennies, J. P. *J. Chem. Phys.* **1999**, *111*, 1676.

(53) Olsen, R.; Kroes, G.; Baerends, E. *J. Chem. Phys.* **1999**, *111*, 11155.

(54) Walch, S.; Dhanda, A.; Aryanpour, M.; Pitsch, H. *J. Phys. Chem. C* **2008**, *112*, 8464.

(55) Mills, G.; Jonsson, H.; Schenter, G. K. *Surf. Sci.* **1995**, *324*, 305.

(56) Mills, G.; Jonsson, H. *Phys. Rev. Lett.* **1994**, *72*, 1124.

(57) Karlberg, G. S.; Olsson, F. E.; Persson, M.; Wahnstrom, G. *J. Chem. Phys.* **2003**, *119*, 4865.

(58) Zimbitas, G.; Gallagher, M. E.; Darling, G. R.; Hodgson, A. *J. Chem. Phys.* **2008**, *128*, 12.

(59) Meng, S.; Wang, E. G.; Gao, S. W. *Phys. Rev. B.* **2004**, *69*.

(60) Rossmeisl, J.; Norskov, J. K.; Taylor, C. D.; Janik, M. J.; Neurock, M. *J. Phys. Chem. B* **2006**, *110*, 21833.

(61) Skulason, E.; Karlberg, G. S.; Rossmeisl, J.; Bligaard, T.; Greeley, J.; Jonsson, H.; Norskov, J. K. *Phys. Chem. Chem. Phys.* **2007**, *9*, 3241.

(62) Beard, B. C.; Ross, P. N. *J. Electrochem. Soc.* **1990**, *137*, 3368.

(63) Stamenkovic, V. R.; Fowler, B.; Mun, B. S.; Wang, G. F.; Ross, P. N.; Lucas, C. A.; Markovic, N. M. *Science* **2007**, *315*, 493.

(64) Jang, S. S.; Molinero, V.; Cagin, T.; Goddard, W. A. *J. Phys. Chem. B* **2004**, *108*, 3149.

(65) Jang, S. S.; Molinero, V.; Cagin, T.; Goddard, W. A. *Solid State Ionics* **2004**, *175*, 805.

(66) Sha, Y.; Yu, T. H.; Liu, Y.; Merinov, B. V.; Goddard, W. A. *J. Phys. Chem. Lett.* **2010**, *1*, 856.

(67) Hyman, M. P.; Medlin, J. W. *J. Phys. Chem. B* **2005**, *109*, 6304.

(68) Ford, D. C.; Nilekar, A. U.; Xu, Y.; Mavrikakis, M. *Surf. Sci.* **2010**, *604*, 1565.

(69) Anderson, A. B.; Sidik, R. A.; Narayanasamy, J.; Shiller, P. *J. Phys. Chem. B* **2003**, *107*, 4618.

(70) Völkening, S.; Bedürftig, K.; Jacobi, K.; Wintterlin, J.; Ertl, G. *Phys. Rev. Lett.* **1999**, *83*, 2672.

(71) Sachs, C.; Hildebrand, M.; Volkening, S.; Wintterlin, J.; Ertl, G. *J. Chem. Phys.* **2002**, *116*, 5759.

(72) Wang, X. G.; Fisher, G. B. *Phys. Rev. Lett.* **2007**, *99*.

(73) Zhang, T.; Anderson, A. **2007**.

(74) Rai, V.; Aryanpour, M.; Pitsch, H. *J. Phys. Chem. C* **2008**, *112*, 9760.

(75) Greeley, J.; Norskov, J. K. *J. Phys. Chem. C* **2009**, *113*, 4932.

(76) Cai, Y.; Anderson, A. *J. Phys. Chem. B* **2005**, *109*, 7557.

(77) Mejias, J. A.; Lago, S. *J. Chem. Phys.* **2000**, *113*, 7306.

(78) Thalinger, M.; Volmer, M. *Z. Phys. Chem. a–Chem. T.* **1930**, *150*, 401.

(79) Marcus, R. A.; Sutin, N. *Biochim. Biophys. Acta* **1985**, *811*, 265.

(80) Peremans, A.; Tadjeddine, A. *J. Chem. Phys.* **1995**, *103*, 7197.

(81) Cai, Y.; Anderson, A. B. *J. Phys. Chem. B* **2004**, *108*, 9829.

(82) Tawa, G. J.; Topol, I. A.; Burt, S. K.; Caldwell, R. A.; Rashin, A. A. *J. Chem. Phys.* **1998**, *109*, 4852.

(83) Dang, L. X. *J. Chem. Phys.* **2003**, *119*, 6351.

(84) Sha, Y.; Yu, T. H.; Merinov, B. V.; Shirvanian, P.; Goddard, W. A. *The Journal of Physical Chemistry Letters* **2011**, *2*, 572.

(85) Wasileski, S. A.; Janik, M. J. *Phys. Chem. Chem. Phys.* **2008**, *10*, 3613.

(86) Karlberg, G. S.; Jaramillo, T. F.; Skulason, E.; Rossmeisl, J.; Bligaard, T.; Norskov, J. K. *Phys. Rev. Lett.* **2007**, *99*.

(87) Sha, Y.; Yu, T. H.; Merinov, B.; Goddard, W. A. *In preparation.* **2010**

(88) Sha, Y.; Yu, T. H.; Merinov, B. H.; Goddard, W. A. *In preparation.* **2011**

(89) Barton, D. G.; Podkolzin, S. G. *J. Phys. Chem. B* **2005**, *109*, 2262.

(90) Mavrikakis, M.; Stoltze, P.; Norskov, J. K. *Catal. Lett.* **2000**, *64*, 101.

(91) Saliba, N.; Parker, D. H.; Koel, B. E. *Surf. Sci.* **1998**, *410*, 270.

(92) Miller, J. T.; Kropf, A. J.; Zha, Y.; Regalbuto, J. R.; Delannoy, L.; Louis, C.; Bus, E.; van Bokhoven, J. A. *J. Catal.* **2006**, *240*, 222.

(93) Barrio, L.; Liu, P.; Rodriguez, J. A.; Campos-Martin, J. M.; Fierro, J. L. G. *J. Phys. Chem. C* **2007**, *111*, 19001.

(94) Michaelides, A. *Appl. Phys. A.* **2006**, *85*, 415.

(95) Huang, S. C.; Lin, C. H.; Wang, J. H. *J. Phys. Chem. C* **2010**, *114*, 9826.

(96) Xu, Y.; Mavrikakis, M. *J. Chem. Phys.* **2002**, *116*, 10846.

(97) Krekelberg, W. P.; Greeley, J.; Mavrikakis, M. *J. Phys. Chem. B* **2004**, *108*, 987.

(98) Sha, Y.; Yu, T. H.; Merinov, B. H.; Goddard, W. A. *In preparation.* **2011**

(99) Sha, Y.; Yu, T. H.; Merinov, B. H.; Goddard, W. A. *In preparation.* **2011**

(100) Stamenkovic, V.; Schmidt, T. J.; Ross, P. N.; Markovic, N. M. *J. Phys. Chem. B* **2002**, *106*, 11970.

(101) Stamenkovic, V. R.; Mun, B. S.; Arenz, M.; Mayrhofer, K. J. J.; Lucas, C. A.; Wang, G. F.; Ross, P. N.; Markovic, N. M. *Nat. Mater.* **2007**, *6*, 241.

(102) Yang, H.; Vogel, W.; Lamy, C.; Alonso-Vante, N. *J. Phys. Chem. B* **2004**, *108*, 11024.

(103) Gauthier, Y.; Joly, Y.; Baudoing, R.; Rundgren, J. *Phys. Rev. B.* **1985**, *31*, 6216.

(104) Gauthier, Y. *Surf. Rev. Lett.* **1996**, *3*, 1663.

(105) Yu, T.; Sha, Y.; Merinov, B.; Goddard III, W. *The Journal of Physical Chemistry C* **2010**, *114*, 11527.

(106) Loukrakpam, R.; Luo, J.; He, T.; Chen, Y.; Xu, Z.; Njoki, P. N.; Wanjala, B. N.; Fang, B.; Mott, D.; Yin, J.; Klar, J.; Powell, B.; Zhong, C.-J. *The Journal of Physical Chemistry C* **2011**, *115*, 1682.

(107) Wang, X. P.; Kariuki, N.; Vaughey, J. T.; Goodpaster, J.; Kumar, R.; Myers, D. J. *J. Electrochem. Soc.* **2008**, *155*, B602.

(108) Takeda, S.; Kulik, J.; Defontaine, D. *J. Phys. F. Met. Phys.* **1988**, *18*, 1387.

(109) Yusenko, K. V.; Filatov, E. Y.; Vasilchenko, D. B.; Baidina, I. A.; Zadesenez, A. V.; Shubin, Y. V. *Zeitschrift Fur Kristallographie* **2007**, 289.

(110) Hammer, B.; Norskov, J. K. *Surf. Sci.* **1995**, *343*, 211.

(111) Yu, T.; Sha, Y.; Merinov, B.; Goddard, W. A. *In preparation.* **2011**

(112) Otte, H. M. *J. Appl. Phys.* **1961**, *32*, 1536.

(113) Haglund, J.; Guillermet, A. F.; Grimvall, G.; Korling, M. *Phys. Rev. B.* **1993**, *48*, 11685.

(114) Guymont, M.; Gratias, D. *Phys. Status Solidi A* **1976**, *36*, 329.

(115) Villars, P.; Okamoto, H.; Cenzual, K.; Center, A. A. P. D. ASM International, Materials Park, OH. **2006**